Asymmetrical modulation of fear expression via $GABA_B$ receptors in the mouse medial habenula

by

Hüseyin Cihan Önal

January, 2025

A thesis submitted to the
Graduate School
of the
Institute of Science and Technology Austria
in partial fulfillment of the requirements
for the degree of
Doctor of Philosophy

Committee in charge:
Jozsef Csicsvari, Chair
Ryuichi Shigemoto
Maximilian Joesch
Hitoshi Okamoto

The thesis of Hüseyin Cihan Önal, titled *Asymmetrical modulation of fear expression via $GABA_B$ receptors in the mouse medial habenula*, is approved by:

Supervisor: Ryuichi Shigemoto, ISTA, Klosterneuburg, Austria

Signature: _____

Committee Member: Maximilian Joesch, ISTA, Klosterneuburg, Austria

Signature: _____

Committee Member: Hitoshi Okamoto, RIKEN Center for Brain Science, Saitama, Japan

Signature: _____

Defense Chair: Jozsef Csicsvari, ISTA, Klosterneuburg, Austria

Signature: _____

Signed page is on file

ISTA Thesis, ISSN: 2663-337X

I hereby declare that this thesis is my own work and that it does not contain other people's work without this being so stated; this thesis does not contain my previous work without this being stated, and the bibliography contains all the literature that I used in writing the dissertation.

I accept full responsibility for the content and factual accuracy of this work, including the data and their analysis and presentation, and the text and citation of other work.

I declare that this is a true copy of my thesis, including any final revisions, as approved by my thesis committee, and that this thesis has not been submitted for a higher degree to any other university or institution.

I certify that any republication of materials presented in this thesis has been approved by the relevant publishers and co-authors.

Signature: _____

Hüseyin Cihan Önal

January, 2025

Signed page is on file

Abstract

The medial habenula (MHb) is implicated in regulating emotional responses to aversive events. Studies in zebrafish have identified a remarkable morphological left-right asymmetry in the dorsal habenula (zebrafish equivalent of mammalian MHb)-to-interpeduncular nucleus (IPN) pathway and its left-side specific role in modulating fear responses. However, there is little evidence for structural or functional lateralization in the mammalian MHb-IPN pathway.

Here, I investigated the synaptic properties of the left and right MHb afferents to the IPN in mice and addressed whether these synaptic connections selectively influence the expression of conditioned fear in mice. My findings reveal that each individual IPN neuron receives inputs from both left and right MHb. Electrophysiological recordings from the same postsynaptic IPN neurons demonstrate that the left MHb-originating synapses exhibit lower release probability and higher γ-aminobutyric acid type B receptor ($GABA_BR$)-mediated potentiation compared to the right MHb-originating synapses. Interestingly, chemogenetic inhibition of cholinergic neurons in the left but not the right MHb significantly attenuated cue-dependent fear recall. Furthermore, conditional deletion of $GABA_BR$ in the left MHb interfered with the recall of cued fear memory, whereas that in the right MHb neurons spared fear memory expression.

Collectively, I demonstrate a functional asymmetry of the MHb in mice, revealing a predominant role for $GABA_BR$-mediated signaling in the left MHb-IPN pathway in the modulation of fear memories. These findings suggest that lateralized pathways could represent a fundamental principle in the neural regulation of emotion across species.

Acknowledgments

First and foremost, I would like to express my deep gratitude to Prof. Ryuichi Shigemoto, who trusted me from the beginning and granted me the freedom to pursue my ideas, even when they diverged from his own. His belief in my perspective has shaped this thesis more than words can convey. I am equally thankful to Prof. Max Joesch for his guidance, patience, and valuable insights, all of which allowed me to mature both scientifically and personally.

A heartfelt thank you goes to Dr. Peter Koppensteiner, whose scientific rigor and friendship served as a constant source of inspiration. His support during challenging times and his readiness to discuss everything were integral to my growth as a scientist. I am also deeply grateful to Dr. Mary Muhia, who taught me to approach research from fresh angles and encouraged me to keep an open mind. I also would like to thank Elodie Le Monnier, who not only helped me scientifically but became a dear friend throughout these years.

I would like to acknowledge the friendship and support of my cohort friends, my IST colleagues, and friends in Vienna. Their warmth and encouragement helped me stay centered and motivated during difficult moments, and I feel incredibly lucky to have shared so many experiences with them.

I would like to thank the European Research Council and European Commission, under the European Union's Horizon 2020 research and innovation program (ERC grant agreement no. 694539 to Ryuichi Shigemoto and the Marie Skłodowska-Curie grant agreement no. 665385 to Cihan Önal), and the Austrian Neuroscience Association for providing financial support and opportunities, which were important in allowing me to present my work. I also wish to thank the Preclinical Facility, especially Michael Schunn, for always welcoming me from my earliest days as an intern. My gratitude goes as well to the Miba Machine Shop, in particular Todor Asenov, Astrit Arslani, and Thomas Menner, whose technical expertise often saved the day.

A very special mention goes to Roshan, a dear friend who has been by my side, sharing in both the high points and the low throughout this journey. I will always be grateful for his unwavering kindness and humor.

Finally, and perhaps most importantly, I wish to thank my family, whose enduring support and encouragement provided me with the resilience needed to see this work through. Their belief in me has been a guiding light, propelling me forward when challenges intensified.

Thank you to all of you for helping me reach this milestone. Your collective contributions made this PhD possible, and I will forever be grateful.

About the Author

Hüseyin Cihan Önal completed his undergraduate studies in Biology in 2016 in Istanbul, Turkey. During his studies, he developed a growing interest in neuroscience and academic research. This interest took him to Ryuichi Shigemoto's laboratory at IST Austria for an Erasmus internship, where he investigated the parabrachial nucleus to amygdala nociceptive pathway in rats. In 2017, he joined the Shigemoto group at IST Austria as a PhD student, focusing on brain circuits and their role in shaping behavior. His research explored the lateralization of the habenula in mice and its influence on fear memory. Over the course of his PhD, Cihan supervised master's students, collaborated on various projects, and published a part of his findings in the Proceedings of the National Academy of Sciences (PNAS). He presented his work at several international conferences, including FENS, SfN, and the Austrian Neuroscience Association, and Japanese Neuoroscience meetings, delivering both oral and poster presentations.

List of Collaborators

Dr. Peter Koppensteiner
Performed initial electrophysiological recordings, developed the thick slice cutting method and gave advice on the project.

Dr. Yukihiro Nakamura
Performed simulation of Ca^{2+} dynamics.

Dr. Mary Muhia
Assisted the behavioral experiments, the related data analysis and gave advice on the project.

Publications

Koppensteiner, P.*, *Bhandari*, P.*, Önal, C.*, Borges-Merjane, C., Le Monnier, E., Roy, U., Nakamura, Y., Sadakata, T., Sanbo, M., Hirabayashi, M., Rhee, J., Brose, N., Jonas, P., & Shigemoto, R. (2024). GABAB receptors induce phasic release from medial habenula terminals through activity-dependent recruitment of release-ready vesicles. *Proceedings of the National Academy of Sciences of the United States of America*, 121(8), e2301449121.

* co-authorship with equal contribution. Önal, C. performed the stereotaxic virus injections, built and consolidated the acute slice calcium imaging.

- A part of this publication has been used in the section 3.5, titled as 'Role of Presynaptic Ca^{2+} in $GABA_BR$-Mediated Enhancement of Neurotransmitter Release

Bhandari, P., Vandael, D., Fernández-Fernández, D., Fritzius, T., Kleindienst, D., Önal, C., Montanaro, J., Gassmann, M., Jonas, P., Kulik, A., Bettler, B., Shigemoto, R., & Koppensteiner, P. (2021). $GABA_B$ receptor auxiliary subunits modulate Cav2.3-mediated release from medial habenula terminals. *eLife*, 10, 1–28.

Table of Contents

List of Figures

List of Abbreviations

AAV	Adeno-associated Virus
ACh	Acetylcholine
ACSF	Artificial Cerebrospinal Fluid
AMPA	α-amino-3-hydroxy-5-methyl-4-isoxazole propionic acid
ANOVA	Analysis of Variance
CB_1R	Cannabinoid Receptor 1
CeA	Central Nucleus of the Amygdala
ChAT	Choline Acetyltransferase
CNO	Clozapine N-oxide
CP-AMPAR	Calcium-permeable AMPAR
CS	Conditioned Stimulus
dHb	Dorsal Habenula
DREADD	Designer Receptor Exclusively Activated by Designer Drugs
EPSC	Excitatory Postsynaptic Current
FR	Fasciculus Retroflexus
GABA	γ-aminobutyric acid
GIRK	G-protein-activated Inwardly Rectifying Potassium Channel
GPCR	Metabotropic G-protein-coupled Receptor
Hb	Habenula
IPN	Interpeduncular Nucleus
IQR	Interquartile Range
ISI	Inter-stimulus-interval
LHb	Lateral Habenula
LTD	Long-term Depression
LTP	Long-term Potentiation
LV	Lentivirus
MHb	Medial Habenula
NMDA	N-methyl-D-aspartate
PB	Phosphate Buffer
PBS	Phosphate-buffered Saline
PFA	Paraformaldehyde
PFC	Prefrontal Cortex
PPR	Paired-pulse Ratio
Pr	Release Probability
rIPN	Rostral Interpeduncular Nucleus

RMTg	Rostromedial Tegmental Nucleus
RRP	Readily Releasable Pool
VGCC	Voltage-gated Calcium Channel
VGluT	Vesicular Glutamate Transporters
vHb	Ventral Habenula
VTA	Ventral Tegmental Area

1 Introduction

1.1 *The Habenula: Structure, Connectivity, and Function*

1.1.1 Anatomical and neurochemical architecture of the habenula and MHb-IPN pathway

The habenula (Hb) is a small, bilateral structure located in the epithalamus, forming a part of the dorsal diencephalic conduction system that connects forebrain regions to midbrain and hindbrain targets (Herkenham and Nauta 1977; Sutherland 1982; Hikosaka 2010) (**Fig. 1a, c**). Early anatomical tracing studies showed its general position and connectivity, demonstrating that the habenula receives most of its inputs via the stria medullaris and in return sends efferent projections primarily through the fasciculus retroflexus (FR) to midbrain nuclei, including dopaminergic and serotonergic centers implicated in reward and aversion (Nishikawa, Fage, and Scatton 1986; Geisler and Trimble 2008; Herkenham and Nauta 1977) (**Fig. 1b**).

Broadly, the Hb is subdivided into two major nuclei: the medial (MHb) and the lateral habenula (LHb). These subnuclei differ in their cytoarchitecture, neurochemistry, connectivity and function (Namboodiri, Rodriguez-Romaguera, and Stuber 2016). The LHb, generally larger in mammals, projects robustly to midbrain regions such as the ventral tegmental area (VTA) and the raphe nuclei (Matsumoto and Hikosaka 2007; Lammel et al. 2012; Kim and Chang 2005). The MHb is further divided into the ventral (vMHb) and dorsal (dMHb) subdivisions. vMHb neurons co-express choline acetyltransferase (ChAT) and vesicular glutamate transporters (VGluT), enabling cholinergic/glutamatergic co-transmission. These neurons project predominantly to the rostral, central, and intermediate subnuclei of the interpeduncular nucleus (IPN), while dorsal MHb neurons send substance P-ergic/glutamatergic projections to the lateral subnucleus of the IPN (Aizawa et al. 2012; Qin and Luo 2009; Ren et al. 2011) (**Fig. 2a**).

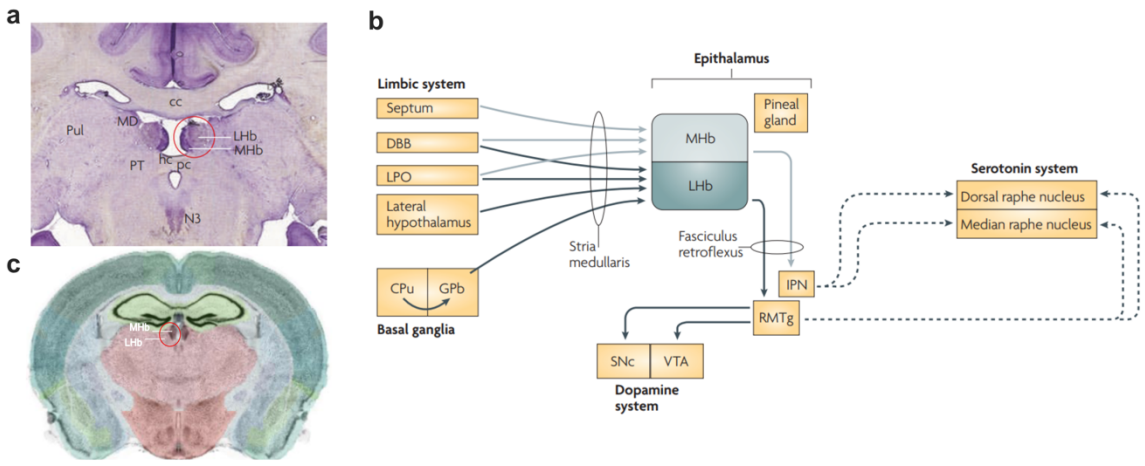

Figure 1: Position of the Hb complex and its input-output pathways.

a) Position of Hb complex including MHb and LHb in human brain. **b)** Afferent and efferent pathways of MHb and LHb with their respective brain regions. **c)** Hb complex in mouse brain. Adapted from Allen Brain Atlas and Hikosaka 2010 (Hikosaka 2010).

The MHb-IPN pathway forms a central axis through which forebrain signals influence midbrain and hindbrain neuromodulatory centers. The IPN, situated at the ventral midline of the midbrain, serves as the principal target of MHb efferents (Herkenham and Nauta 1977; Sutherland 1982; Hikosaka 2010). MHb neurons innervate the IPN in a topographically organized manner, and the IPN's subnuclei (rostral, central, intermediate, lateral) possess distinct receptor repertoires and connectivity patterns (Shibata, Suzuki, and Matsushita 1986; Morley 1986; Ren et al. 2011; Ables, Park, and Ibañez-Tallon 2023). Within these subnuclei, heterogeneous neuronal populations express markers for predominantly GABA, glutamate, and various neuropeptides, establishing intricate local microcircuits. Notably, ventral MHb terminals release both acetylcholine (ACh) and glutamate, conferring substantial chemical versatility on their synapses with IPN neurons (Qin and Luo 2009; Ren et al. 2011; Aizawa et al. 2012; Hashikawa et al. 2020). This dual-excitatory drive, coupled with auxiliary peptides (e.g., substance P), permits fine-tuned modulation of postsynaptic excitability and synaptic plasticity across multiple IPN subdomains. Functional specialization emerges as distinct MHb neuronal populations selectively target IPN subnuclei, recruiting ionotropic and metabotropic glutamate receptors, muscarinic and nicotinic ACh receptors, and in some cases, non-canonical excitatory $GABA_BRs$ (Ichijo and Toyama 2015; Koppensteiner et al. 2024; Ables, Park, and Ibañez-Tallon 2023; Hikosaka 2010; Zhang et al. 2016).

The LHb is likewise glutamatergic as MHb. It predominantly projects to regions such as the rostromedial tegmental nucleus (RMTg), the VTA, and the raphe nuclei (Matsumoto and Hikosaka 2007; Bromberg-Martin and Hikosaka 2011;

Ables, Park, and Ibañez-Tallon 2023) (**Fig. 2b**). These parallel but distinct output pathways of the MHb and LHb underscore the habenula's broad capacity for modulating midbrain and hindbrain circuits.

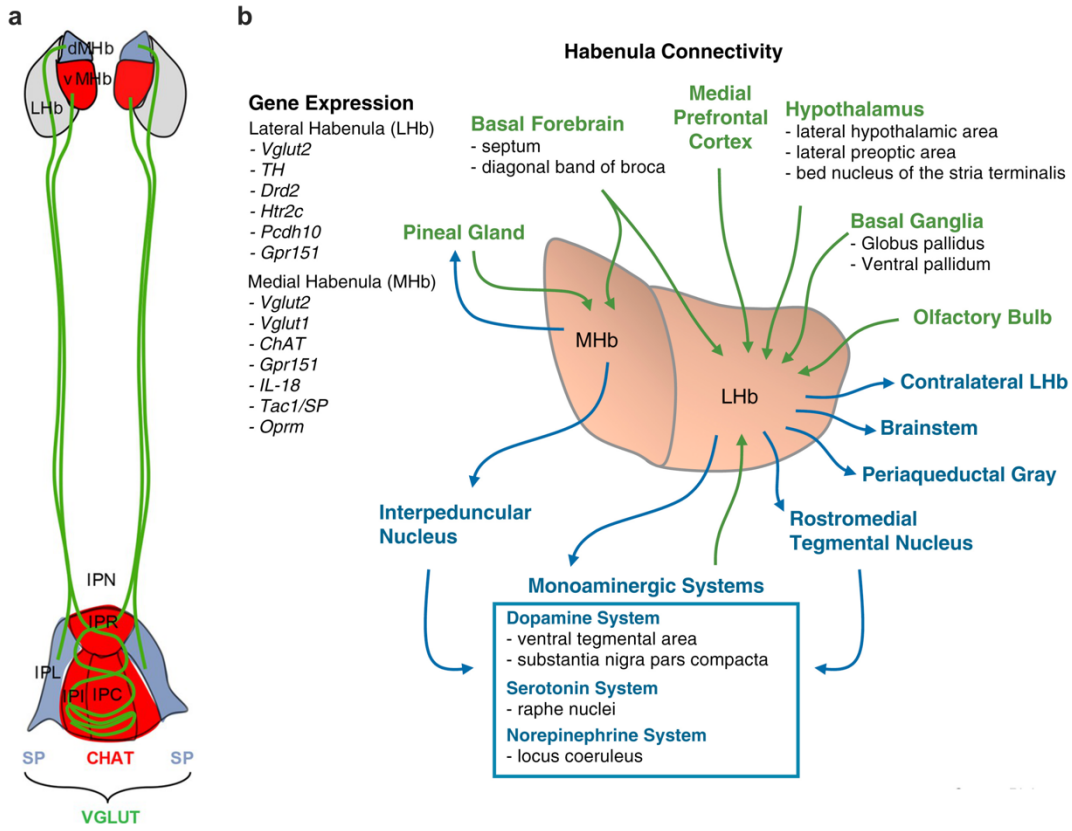

Figure 2: Neurochemical architecture of mouse Hb complex and MHb-IPN pathway.

a) vMHb and dMHb neurons targeting different subnuclei of IPN via FR and releasing different neurotransmitters and peptides. **b)** Neurochemical landscape and connectivity of mouse Hb along with expressed genes. Adapted from Frahm 2015 and Namboodiri 2016 (Frahm et al. 2015; Namboodiri, Rodriguez-Romaguera, and Stuber 2016).

Evolutionary conservation of the Hb's core architecture is observed across vertebrates, although species-specific differences exist. In zebrafish, for example, the dorsal habenula (dHb, homologous to the mammalian MHb) exhibits marked left-right asymmetries in morphology, gene expression, and connectivity, whereas in mammals such pronounced asymmetry is less overt (Duboué et al. 2017; Hüsken et al. 2014; Dreosti et al. 2014; Aizawa et al. 2005; Concha and Wilson 2001). Despite these variations, the fundamental anatomical framework of the Hb and the MHb-IPN circuit remains consistent, providing a conserved substrate upon which more nuanced modulatory mechanisms have evolved (Hsu et al. 2013; Lima et al. 2017).

Overall, the habenula and its main efferent route via the MHb-IPN pathway constitute an evolutionarily maintained architecture. This network integrates signals from forebrain areas and modifies dopaminergic and serotonergic systems

through a sophisticated blend of neurochemical inputs and subnucleus-specific projections.

1.1.2 Functional roles in behavior and emotional regulation

Seminal physiological and lesion studies showed the involvement of Hb in processing aversive stimuli and guiding motivated behavior, establishing it as a regulator of negative valence (Sutherland 1982; Herkenham and Nauta 1977). Electrophysiological and behavioral experiments, primarily focusing on the LHb, further consolidated this view. LHb neurons respond to negative prediction errors by increasing their firing rates in scenarios where an expected reward fails or an aversive event occurs. Through indirect projections, the LHb inhibits dopaminergic and serotonergic systems in the midbrain, including regions such as the VTA and raphe nuclei (Matsumoto and Hikosaka 2007; Bromberg-Martin and Hikosaka 2011; Lawson et al. 2014). Such LHb driven inhibition of reward related circuitry contributes to the experience of negative valence, discouraging unrewarded or harmful behaviors.

Beyond the LHb's established role in aversion and avoidance, accumulating evidence points to the MHb as another critical modulator of negative affective states. The MHb's cholinergic and glutamatergic projections to the IPN influence affective modulation, including responses to stress, nicotine withdrawal, and fear conditioning (Salas et al. 2009; McLaughlin, Dani, and De Biasi 2017; Dao et al. 2014; Fore et al. 2018; Yamaguchi et al. 2013; Zhang et al. 2016; Zhang et al. 2018). By adjusting IPN activity and indirectly modulating monoaminergic transmission, the MHb-IPN circuit refines learned avoidance and the expression of negative emotional valence.

Comparative work in non-mammalian species, notably zebrafish, supports the evolutionary importance of the Hb in encoding negative valence. In zebrafish, lateralized dHb neurons exhibit hemisphere-specific responses to aversive cues, facilitating adaptive avoidance behaviors (Agetsuma et al. 2010; Duboué et al. 2017; Choi et al. 2021). This evolutionary conserved evidence reinforces the notion that the Hb complex contributes fundamentally to evaluating adverse conditions, adjusting an organism's actions and affective states accordingly.

Recent chemogenetic, optogenetic, and knockout studies have further stressed MHb-IPN pathway's role in emotional regulation. Disruptions to this pathway impair fear memory extinction and recall, implicating MHb-IPN signaling in the expression and modulation of learned fear (Zhang et al. 2016; Ren et al. 2022; Soria-Gómez et al. 2015). Moreover, this circuit influences anxiety-like behavior, stress responses, and motivational states related to reward and withdrawal (Salas et al. 2009; Lee et al. 2019; Fowler and Kenny 2014; Okamoto et al. 2021). By modulating serotonergic and dopaminergic activity, the MHb-IPN

pathway integrates internal states, environmental cues, and learned experiences, thereby orchestrating appropriate emotional and behavioral responses (Hikosaka 2010; Viswanath et al. 2013; Meye et al. 2016).

Together, these findings position the Hb as a crucial hub in the broader network controlling emotional behavior and motivational processes across vertebrate species.

1.2 *Brain Lateralization and the Habenula*

1.2.1 Principles of hemispheric specialization in the brain

Hemispheric lateralization refers to the phenomenon in which the left and right sides of the brain play distinct or dominant functional roles. Laterality has been recognized for over a century, initially, from clinical studies of patients with unilateral brain lesions that showed differences in language and perceptual functions between the cerebral hemispheres (Gazzaniga 2000). Early work on language lateralization in humans established a framework for understanding how one hemisphere can dominate a particular cognitive domain, creating space for further research into a wide array of lateralized functions, including spatial processing, emotional regulation, and attention (Corballis 2014).

In both humans and non-human vertebrates, hemispheric lateralization is believed to confer evolutionary advantages. Lateralization can enhance neural efficiency by reducing redundancy, allowing parallel processing of distinct tasks in each hemisphere, which in return can potentially increase an organism's cognitive capacity (Vallortigara and Rogers 2005). Such advantages might be especially beneficial for complex behaviors like predator avoidance. The presence of lateralization across diverse taxa from invertebrates to birds, fish, and mammals suggests that this foundation emerged early in evolutionary history and has been maintained since then as a core feature of the nervous system (Robins and Rogers 2002; Güntürkün and Ocklenburg 2017).

However, lateralization is not uniform across species or brain regions. Its manifestation can range from macroscopic size asymmetries in brain structures to subtle differences. Understanding the molecular and cellular substrates of lateralization remains a frontier in neuroscience (Concha, Bianco, and Wilson 2012).

1.2.2 Evidence for lateralization in the zebrafish dorsal habenula

The dHb of the zebrafish has emerged as a model for exploring brain lateralization in vertebrates. The zebrafish dHb homologous to the mammalian MHb, displays remarkable left-right asymmetries in gene expression, morphology, and connectivity patterns (Concha & Wilson, 2001; Aizawa et al., 2005; Bianco & Wilson, 2009; Hong et al., 2013; Chen et al., 2019) (**Fig. 3a-b**). Functionally, these

anatomical and molecular asymmetries correspond to differences in how each hemisphere processes aversive stimuli and responds to environmental cues. For instance, the left and right dHb subnuclei project differentially to the IPN, establishing lateralized circuits that influence behavior, sensory integration, and stress responses (Concha and Wilson 2001; Agetsuma et al. 2010; Duboué et al. 2017).

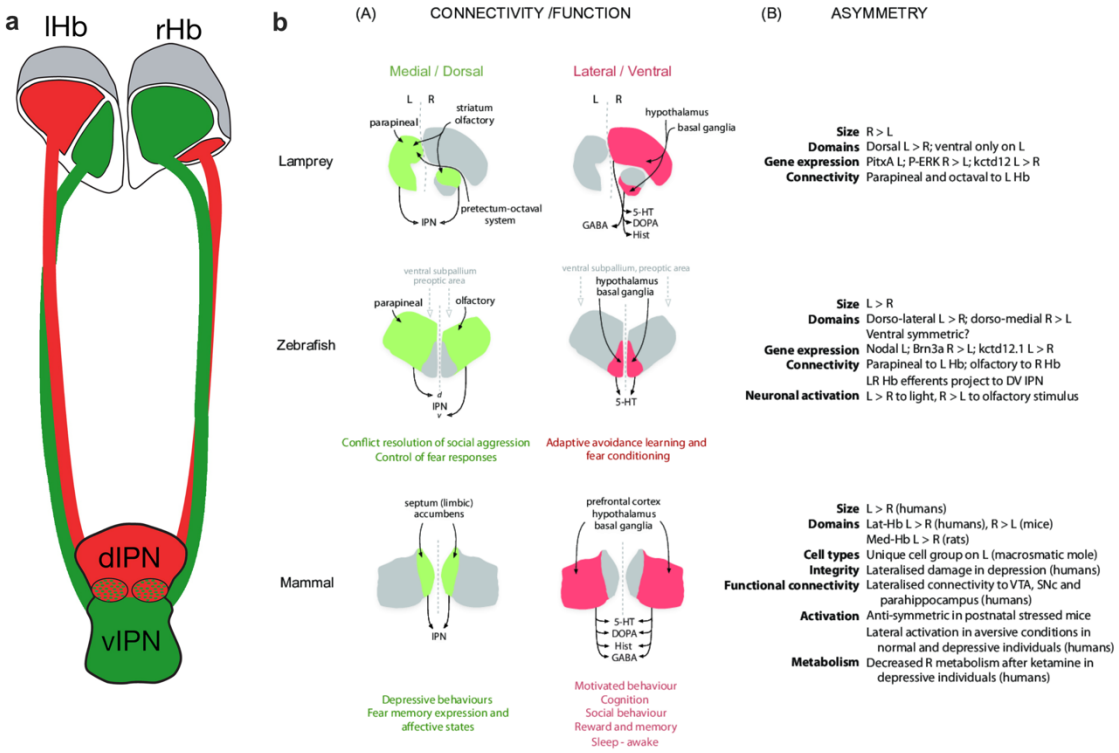

Figure 3: Zebrafish lateralized Hb-IPN pathway and hemispheric differences in other species.

a) Zebrafish Hb-IPN pathway showing macroscopic lateralization including its subnuclei size and connectivity. **b)** Structural and connective organization of Hb complex in different species showing hemispheric lateralization in both size, function and gene expression pattern. Adapted from Aizawa 2007 and Concha 2016 (Aizawa et al. 2007; Concha 2016).

Behavioral studies have reinforced the importance of these asymmetries. Perturbations that disrupt left-right differences in the dHb alter avoidance behaviors, stress coping strategies, and learning processes (Okamoto, Agetsuma, and Aizawa 2012; Dreosti et al. 2014). For example, Duboué and colleagues (2017) demonstrated that severing the left dHb projections to the IPN prolongs the duration of freezing after a mild shock. Moreover, zebrafish with left dHb isomerisms, where typical lateralization patterns are lost, fail to exhibit normal freezing responses, suggesting that left dHb activity modulates fear behavior and attenuates fear responses in larval zebrafish. In addition, Dreosti et al. (2014) showed that sensory responses to light and odor are lateralized in zebrafish Hb. They found that most Hb neurons responding to light are located on the left side, whereas neurons responding to odor are ubiquitous on the right side. These

lateralized sensory responses are essential for normal sensory processing, as manipulations that generate either double-left or double-right sided brains resulted in the alterations of responsiveness to either light or odor, respectively. (Dreosti et al. 2014).

The source of these asymmetries in zebrafish is rooted in early developmental processes. The emergence of lateralization in the dHb is influenced by left-biased embryonic signals, such as nodal flow and the positioning of the parapineal organ, which imparts asymmetry onto the epithalamus (Regan et al. 2009; Concha, Bianco, and Wilson 2012; Facchin et al. 2009). These signaling events lead to differential gene expression and activation of transcription factors on the left and right sides, establishing and maintaining stable asymmetries in dHb patterning (Aizawa et al. 2005; Hong et al. 2013). Such findings underscore that lateralization is not a mere byproduct of brain development but a robust, genetically regulated attribute of the habenular circuit.

By providing an example of how hemispheric differences in a subcortical structure can influence behavior, the zebrafish dHb presents a valuable framework for understanding lateralization in other vertebrate species. The evolutionary conservation of habenular connectivity and function suggests that the knowledge from zebrafish will help future investigations in the mammalian MHb.

1.2.3 Morphological and molecular asymmetries in vertebrates

Brain lateralization extends beyond the zebrafish Hb. Across a diverse array of vertebrate species, hemispheric specializations manifest in multiple forms, such as morphological, molecular, and functional. Differences in the size or shape of brain regions, the distribution of particular cell types, or gene expression patterns have been documented in amphibians, birds, and reptiles, where asymmetric visual processing pathways and vocalization-related nuclei exemplify how anatomical asymmetries can underpin specialized behavioral functions (Robins and Rogers 2002; Vallortigara and Rogers 2005; Ocklenburg et al. 2018; Güntürkün and Ocklenburg 2017) (**Fig. 3b**).

These principles also extend into the mammalian forebrain. The hippocampus a structure central to learning and memory exhibits lateralized features in rodents, with mice and rats showing hemispherical differences in synaptic plasticity, receptor composition, and even network oscillations (Shinohara et al. 2008; Shinohara, Hosoya, and Hirase 2013; Kohl et al. 2011; Kawakami et al. 2003). For instance, Kawakami et al. (2003) and Kohl et al (2011) demonstrated that pyramidial cell synapses receiving inputs from the left CA3 region exhibit more robust long-term potentiation (LTP) compared to those receiving right-sided inputs. Shinohara et al. (2013) further showed that rats in enriched environment exhibit enhanced gamma oscillations in the CA1 region of

the hippocampus, particularly on the right side (Shinohara 2013). Such hippocampal asymmetries can influence how spatial information is processed and how memories are formed or retrieved, demonstrating that lateralization contributes to cognitive functions beyond those related to sensory or motor specialization.

Within the epithalamus, asymmetries are not confined to teleost fish. Smaller vertebrates display subtle left-right differences in the habenula as well, potentially indicating an evolutionarily conserved blueprint for lateralization (Gugliemotti and Fiorino 1998; Concha and Wilson 2001; Aizawa et al. 2005). These variations may result from early developmental events, including asymmetric gene expression and morphogen signaling gradients (Bianco and Wilson 2009; Hong et al. 2013) (**Fig. 4**). Although such structural and molecular differences may be less pronounced in mammals than in zebrafish, their existence suggests that hemispheric specialization is a fundamental organizational principle.

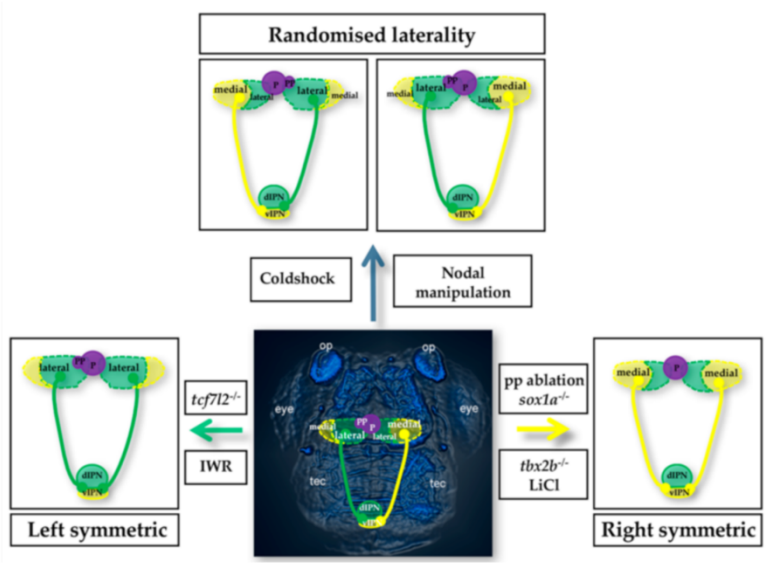

Figure 4: Differential lateralization of zebrafish Hb following different manipulations.

Nodal flow manipulation causing a randomized lateralization. Tcf7l2 knock out leading to a left sided symmetry, meanwhile, parapineal ablation leading to a right sided symmetry in the zebrafish Hb. Adapted from Bühler 2021 (Bühler and Carl 2021).

1.2.4 i.v. (inversus viscerum) mutations and brain lateralization

i.v. (inversus viscerum) mutations in mice provide an example of how early left-right patterning can affect both visceral and neural asymmetries. Under typical development, situs solitus (s.s.) describes the normal arrangement of internal organs along the left-right axis, whereas situs inversus (s.i.) denotes a reversal of this arrangement (Supp et al. 1999; Nonaka et al. 2002; Okada et al. 1999). In i.v. mutants, nodal signaling is disrupted, leading to reversed internal organ

arrangement. Some *i.v.* mutant mice exhibit s.s., others show s.i., organ orientation. This embryonic perturbation often extends to subtle changes in the nervous system, including hippocampal connectivity and synaptic plasticity (Kawakami et al. 2008). When lateralized features in the brain such as those in the hippocampus become disorganized in *i.v.* mice, it underscores a shared embryonic mechanism linking visceral and neural asymmetry.

The presence of morphological and molecular asymmetries across a range of vertebrates, including hippocampal differences in rodents and subtle epithalamic variations in smaller vertebrates, highlights lateralization as a prevalent and evolutionarily significant feature of the brain. Mutant studies, particularly those involving *i.v.* mutant mice, further demonstrate how disruptions to global left-right patterning can cause alterations in neural circuits and functions (Ukai et al. 2017; Goto and Ito 2017; Kawahara et al. 2013).

1.2.5 Outstanding questions on lateralization in the mammalian MHb-IPN pathway

Although the mammalian MHb-IPN pathway has recently received growing attention for its role in emotional regulation and aversive learning (Hikosaka 2010; Zhang et al. 2016; Okamoto and Aizawa 2013; Yamaguchi et al. 2013), its hemispheric specializations remain unclear. A question comes to mind: could more subtle molecular and synaptic-level asymmetries exist in mammals, influencing the MHb-IPN pathway's function in fear and stress responses?

Addressing such a question requires a systematic approach to analyze side-dependent differences in neurotransmitter release probability, receptor composition, and short-term or long-term synaptic plasticity mechanisms. For instance, do left and right MHb terminals differ in their response to action potentials or modulatory signals like $GABA_BR$ activation? If lateralization exists at a synaptic scale, how does it play a role in downstream neural activity and particularly during fear-related behaviors?

Uncovering these key points could eventually provide novel insights into how lateralization contributes to the complex orchestration of emotional behaviors.

1.3 *Synaptic Transmission in the MHb-IPN Pathway*

1.3.1 Fundamentals of chemical synaptic transmission

Chemical synaptic transmission is a fundamental part of intercellular communication in the vertebrate nervous system. It enables neurons to transmit information quickly and precisely across synapses (Katz and Miledi 1965; Krnjević 1974). Primarily, chemical neurotransmission involves the release of chemical messengers from a presynaptic terminal and their subsequent detection by

postsynaptic receptors, thus leading to changes in the postsynaptic neuron's membrane potential and intracellular signaling cascades.

The very first model of neurotransmission was established through pioneering electrophysiological studies at the neuromuscular junction and central synapses (Katz 1969). Action potentials at the presynaptic terminal trigger the opening of voltage-gated calcium channels (VGCC), leading to an influx of Ca^{2+} ions into the neuron. An increase in intracellular calcium concentration primes the fusion of synaptic vesicles at the presynaptic terminal membrane, releasing their contents into the synaptic cleft (Kaeser and Regehr 2014; Südhof and Rizo 2011).

Afterwards, neurotransmitters in the synaptic cleft diffuse through the extracellular space, to eventually target specific postsynaptic receptors, mainly known as ionotropic and metabotropic receptors. Ionotropic receptors, such as AMPA and NMDA receptors, are ligand-gated ion channels, which mediate rapid postsynaptic responses. On the other hand, metabotropic receptors, i.e. G-protein-coupled receptors (GPCRs) (e.g. $GABA_BRs$) including glutamate and acetylcholine receptors, act via rather slower pathways, modulating postsynaptic excitability and synaptic plasticity over longer timescales (Betke, Wells, and Hamm 2012; Pinheiro and Mulle 2008).

The strength, timing, and reliability of chemical synaptic transmission can be fine-tuned by different presynaptic and postsynaptic mechanisms. Presynaptic mechanisms include regulation of the probability of neurotransmitter release (P_r), the size of the readily releasable vesicle pool, and short-term synaptic plasticity processes (facilitation, depression), which can dynamically adjust synaptic transmission (Zucker and Regehr 2002; Jackman and Regehr 2017). Postsynaptically, the density, subunit composition, and phosphorylation of receptors, as well as the morphology and molecular composition of the postsynaptic density, modulate the strength and the duration of the postsynaptic response (Newpher and Ehlers 2008; Kennedy 2000).

Non-canonical features of synaptic transmission, like the co-release of neurotransmitters and synaptic gain control relying on neuromodulation, have expanded our understanding of synaptic function (Hnasko and Edwards 2012). Lately, advanced imaging, genetic, and computational techniques have provided further insights into the molecular machinery of vesicle docking, priming, and fusion, as well as the nanoscale organization of postsynaptic receptors and scaffolding proteins (Südhof and Malenka 2008; Kusick et al. 2020). Collectively, these studies have shown that synapses are dynamic structures, capable of structural remodeling and functional plasticity throughout development and in response to experience, thus placing synaptic transmission at the apex of mechanisms related to learning, memory, and behavior (Citri and Malenka 2008; Choquet and Triller 2013).

1.3.2 Mechanisms regulating release probability and short-term plasticity

The probability of neurotransmitter release at a given synapse is not a fixed constant. Neurotransmitter release is dynamically modulated by a range of presynaptic factors that govern both the probability and timing of vesicular fusion. Seminal electrophysiological studies at the neuromuscular junction and central synapses showed that changes in intracellular calcium concentration in presynaptic terminals is the primary and immediate determinant of P_r (Katz 1969; Katz and Miledi 1967a, 1967b)). Various works on different neural circuits have expanded our understanding, demonstrating that P_r can vary between synapses, within the same synapse, and in response to recent activity of the synapse, altogether shaping the information processing of neural networks (Zucker and Regehr 2002; Jackman and Regehr 2017).

One of the major determinants of the P_r is the coupling distance between presynaptic voltage-gated calcium channels and the neurotransmitter release machinery, comprising vesicle-associated proteins such as synaptotagmins, SNARE complexes, and active zone scaffolding molecules (Rizo and Rosenmund 2008; Kaeser et al. 2011; Ackermann, Waites, and Garner 2015). Differences in the spatial arrangement and molecular composition of the active zone influence how efficiently calcium ions trigger the vesicle fusion. Active zone related proteins like RIM, Munc13, and Bassoon organize the defined release sites and further secure the proper priming of synaptic vesicles. Furthermore, different synaptotagmin isoforms equip the synapse for distinct kinetics and calcium sensitivity to the release process (Kaeser and Regehr 2014; Schoch et al. 2002).

Short-term synaptic plasticity takes place when prior activity alters P_r on a millisecond to second timescale, thus, modulating synaptic strength transiently and providing rapid control over the synaptic transmission. Two major forms of short-term plasticity are facilitation and depression, reflecting the interplay between calcium dynamics, readily releasable pool (RRP) size, and number of release sites (Zucker and Regehr 2002; Jackman and Regehr 2017; Schneggenburger, Meyer, and Neher 1999). Facilitation occurs when consecutive action potentials arrive in close temporal proximity, causing residual intracellular calcium to accumulate and increase P_r. Facilitation can enhance signal transmission during bursts of activity, improving the reliability of synaptic communication.

In contrast, synaptic depression takes place when sustained or high-frequency stimulation depletes the RRP, reducing P_r and subsequently diminishing postsynaptic responses (Schneggenburger, Meyer, and Neher 1999; Thanawala and Regehr 2013). Depression can be useful for gain control, preventing overexcitation and maintaining synaptic homeostasis. Changes in presynaptic calcium buffering,

vesicle replenishment rate, or coupling tightness can also contribute to the strength and duration of short-term plasticity (Neher and Sakaba 2008; Regehr 2012).

1.3.3 Postsynaptic receptor composition (AMPA, NMDA, and CP-AMPARs)

Excitatory synapses majorly consist of the two main families of ionotropic glutamate receptors, AMPA (α-amino-3-hydroxy-5-methyl-4-isoxazolepropionic acid) receptors and NMDA (N-methyl-D-aspartate) receptors. They differ in biophysical and pharmacological properties. The heterogeneity in receptor composition and subunit assembly creates a high degree of functional versatility, allowing synapses to adjust their strength, kinetics, and plasticity in response to activity (Malenka and Bear 2004; Huganir and Nicoll 2013).

AMPA Receptors (AMPARs):

AMPARs are the primary mediators of fast excitatory postsynaptic currents (EPSCs). Typically composed of GluA1–GluA4 subunits arranged as tetramers, AMPARs are permeable to sodium and potassium ions, exhibiting rapid activation and deactivation kinetics that allow synaptic signaling in milliseconds (Isaac, Ashby, and McBain 2007; Dingledine et al. 1999; Chater and Goda 2014). Insertion, removal and phosphorylation of AMPARs are key components of synaptic plasticity. For example, the LTP of synaptic strength involves an increase in the number or conductance of AMPAR, whereas internalization leads to long-term depression (Malinow and Malenka 2002; Shepherd and Huganir 2007).

NMDA Receptors (NMDARs):

NMDARs are glutamate gated ion channels that also require postsynaptic depolarization to relieve a voltage dependent magnesium block, making their activation a coincidence detector for presynaptic glutamate release and postsynaptic depolarization (Bliss and Collingridge 1993; Cull-Candy, Brickley, and Farrant 2001). NMADRs contain GluN1 and GluN2 (and sometimes GluN3) subunits, allowing the calcium influx in the postsynaptic neuron upon activation, initiating an intracellular cascade. This signaling mechanism underlies many forms of synaptic plasticity, including LTP and LTD (Malenka and Bear 2004; Paoletti, Bellone, and Zhou 2013). Utilizing synaptic activity patterns and combining with intracellular messaging cascades, NMDARs serve as a critical component for learning and memory.

Calcium-Permeable AMPA Receptors (CP-AMPARs):

Most AMPARs in the adult brain contain the GluA2 subunit, which makes them calcium impermeable. On the other hand, some AMPARs lack GluA2 and are thus calcium-permeable (CP-AMPARs) (Liu and Zukin 2007; Stuart Cull-Candy, Kelly, and Farrant 2006). CP-AMPARs differ in their biophysical properties,

exhibiting higher conductance, inward rectification, and calcium permeability. The presence of CP-AMPARs has been shown to play a role in synaptic plasticity and notably in the early stages of LTP (Plant et al. 2006; Sanderson, Gorski, and Dell'Acqua 2016). Insertion and removal of CP-AMPARs are tightly regulated, therefore, allowing the modulation of synaptic responsiveness and changes in synaptic states.

1.3.4 Distinctive synaptic modulation mechanisms in the MHb-IPN pathway

The MHb-IPN circuit stands apart from conventional excitatory synapses through its capacity for neurotransmitter co-release, atypical short-term presynaptic plasticity, reliance on a unique VGCC subtype (Cav2.3) triggering the release, and a surprising form of $GABA_BR$-mediated facilitation.

Unlike many circuits where cholinergic and glutamatergic inputs arise from distinct neuronal populations, ventral MHb terminals simultaneously release ACh and glutamate onto the IPN neurons (Qin and Luo 2009; J. Ren et al. 2011; Contestabile and Flumerfelt 1981; Contestabile et al. 1987; Aizawa et al. 2012). This co-transmission enables postsynaptic IPN cells to integrate multiple excitatory and modulatory signals from a single presynaptic source, potentially allowing for rapid and coordinated adjustments in postsynaptic excitability and response dynamics.

Recent findings have also revealed distinctive presynaptic dynamics within this pathway. MHb terminals often maintain a lower initial P_r and exhibit pronounced short-term facilitation during repetitive stimulation (Koppensteiner et al. 2024). Such characteristics could allow the MHb to emphasize bursts of firing or rhythmic activity, which may be critical for encoding and retrieving fear memories and stress related behaviors (Zhang et al. 2016; Zhang et al. 2018; McLaughlin, Dani, and De Biasi 2017).

Perhaps the most striking deviation from canonical synaptic modulation is the role of $GABA_BRs$ at MHb-IPN terminals. Traditionally, $GABA_BR$ activation suppresses neurotransmitter release by reducing presynaptic calcium influx. In contrast, in the MHb-IPN pathway, $GABA_BR$ activation paradoxically enhances synaptic transmission (**Fig. 5a-b**). In fact, MHb terminals appear to be unique in their reliance on Cav2.3 calcium channels for evoked release, rather than using Cav2.1 and/or Cav2.2 channel subtypes as observed in other brain circuits (Parajuli et al. 2012; Bhandari et al. 2021). Instead of inhibiting release, presynaptic $GABA_BRs$ in this pathway boost calcium influx through Cav2.3 and recruit additional vesicles into the RRP, converting tonic release into a more potent phasic mode. Koppensteiner et al. (2024) showed that $GABA_BR$-mediated potentiation can boost the RRP size by over four-fold and significantly augment docked vesicle numbers, effectively priming the terminal for heightened synaptic output (**Fig. 5b**).

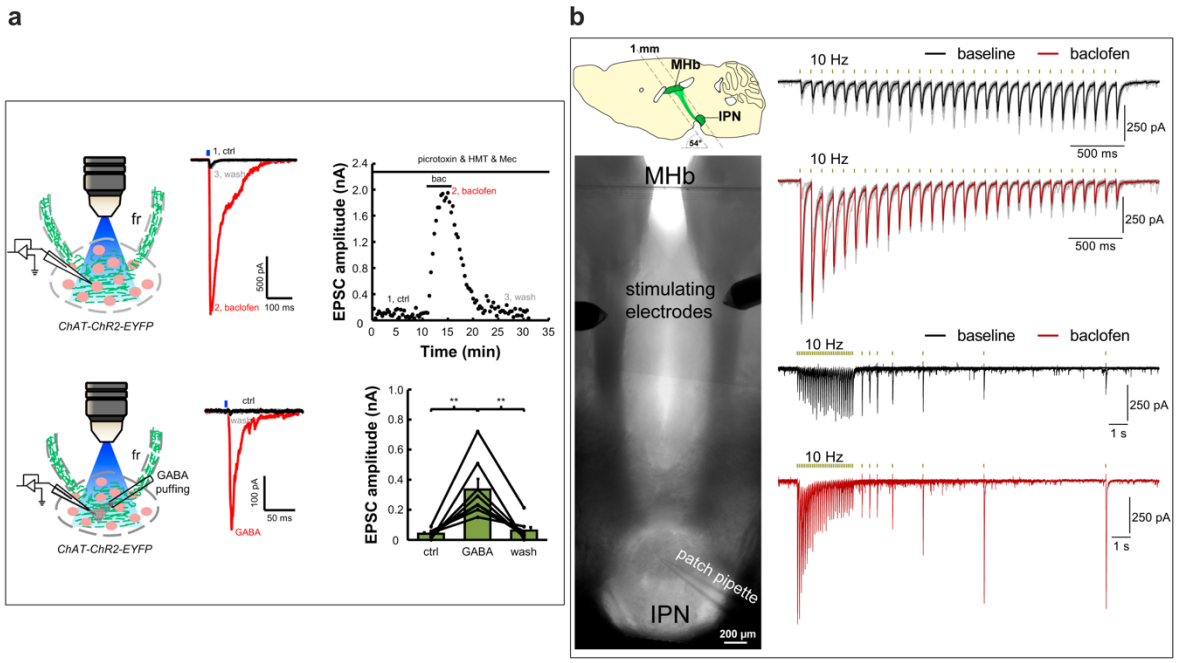

Figure 5: Presynaptic $GABA_BR$ activation potentiates neurotransmitter release in MHb-IPN pathway.

a) GABA and $GABA_BR$ agonist baclofen increase light-evoked glutamatergic postsynaptic currents in the MHb-IPN pathway. **b)** Activation of $GABA_BRs$ increases the electrically evoked post synaptic currents and causes a shift from tonic to phasic release in the MHb-IPN pathway. Adapted from Zhang 2016 and Koppensteiner 2024 (J. Zhang et al. 2016; Koppensteiner et al. 2024).

Together, these unique synaptic properties place the MHb-IPN pathway as a specialized system capable of fine tuning emotional and motivational responses. By engaging non-canonical synaptic mechanisms, the MHb-IPN circuit could rapidly adjust its output to meet the dynamic demands of behavioral states, such as fear recall, stress adaptation, and aversive learning.

1.4 $GABA_B$ Receptors and Presynaptic Modulation

1.4.1 Structure, signaling mechanisms, and subunit composition of $GABA_B$ receptors

$GABA_BRs$ are metabotropic G-protein-coupled receptors (GPCRs) for the main inhibitory neurotransmitter in the mammalian central nervous system, γ-aminobutyric acid (GABA). Unlike the fast-acting ionotropic $GABA_A$ and $GABA_C$ receptors, $GABA_BRs$ mediate slower responses, further modulating synaptic transmission (Bowery et al. 1980; Bowery 1993; Chebib and Johnston 1999). Early pharmacological and electrophysiological studies in the 1980s established the existence of $GABA_BRs$ as a distinct receptor class responsive to the selective agonist baclofen (Bowery 1989). Advances in molecular biology and structural biology have revealed the architecture, heterodimeric composition, and signal transduction

mechanisms that define $GABA_BRs$ (Kaupmann et al. 1997; Bettler and Tiao 2006; Pin and Bettler 2016).

$GABA_BRs$ are heterodimers composed of two principal subunits, $GABA_{B1}$ and $GABA_{B2}$. Each subunit contains a large extracellular Venus flytrap domain and a seven-transmembrane helical domain characteristic of GPCRs (Pin and Bettler 2016; Shaye et al. 2020) (**Fig. 6a**). The $GABA_{B1}$ subunit is responsible for ligand binding, which further undergoes a conformational change upon agonist binding. However, the $GABA_{B1}$ subunit alone is poorly trafficked to the cell surface and shows limited signaling capacity. The $GABA_{B2}$ subunit is essential for proper receptor assembly, plasma membrane localization, and G-protein coupling efficiency (Calver, Davies, and Pangalos 2002).

Upon activation, $GABA_BRs$ couple to $G_{i/o}$-type G-proteins, leading to the inhibition of adenylyl cyclase activity, reducing cyclic AMP levels and downstream modulation (Pinard, Seddik, and Bettler 2010; Pin and Bettler 2016). Activated $G_{\beta\gamma}$ subunits of the dissociated G-proteins directly interact with ion channels, resulting in the opening of G-protein-activated inwardly rectifying potassium (GIRK) channels and the inhibition of VGCCs (Lüscher and Slesinger 2010; Djebari et al. 2021) (**Fig. 6b**). Ultimately, this leads to hyperpolarization of the postsynaptic membrane and reduction in P_r at presynaptic terminals, thereby showing an inhibitory effect on synaptic function (**Fig. 6c**).

1.4.2 Distribution in the CNS and roles in modulating neurotransmitter release

$GABA_BRs$ are broadly distributed throughout the central nervous system, shaping the excitability and plasticity of diverse neural circuits. Early studies revealed that $GABA_BRs$ are present in high densities in the hippocampus, cortex, thalamus, and cerebellum, as well as various subcortical structures and spinal cord regions (Bowery 1989; Benarroch 2012). Immunohistochemical studies further confirmed that $GABA_BR$ subunits are expressed both pre and postsynaptically, and are often localized to perisynaptic domains, where they can sense extracellular spillover of GABA from neighboring synapses (Kullmann 2000; Kulik et al. 2002; Gassmann and Bettler 2012).

In the hippocampus, presynaptic $GABA_BRs$ at the Schaffer collateral-CA1 synapses modulate synaptic transmission and short-term plasticity (Davies and Collingridge 1993; Chalifoux and Carter 2011). In the cerebellum, $GABA_BRs$ at parallel fiber-Purkinje cell synapses fine-tune sensorimotor processing and motor learning by adjusting the balance between excitation and inhibition (Tabata and Kano 2006).

Beyond the canonical inhibitory role, recent studies have shown that $GABA_BR$ activation can paradoxically enhance neurotransmitter release in the

MHb-IPN pathway (Zhang et al. 2016; Koppensteiner et al. 2024). Such unconventional signaling highlights the important functional role of $GABA_BRs$ in this circuit.

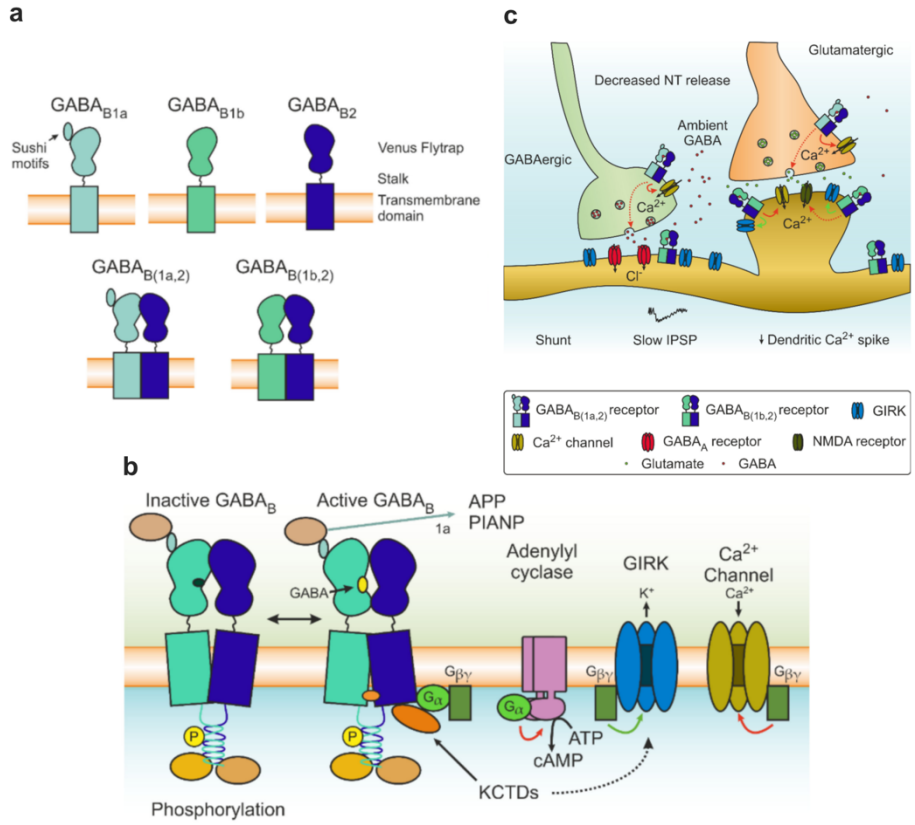

Figure 6: $GABA_BR$ composition and functions in synaptic transmission.

a) $GABA_BR$ subunit composition with its heterodimers. **b)** $GABA_BR$ activation via GABA and downstream activity cascade via inhibition of adenyl cyclase, decrease in intracellular Ca^{2+} concentration and/or activation of GIRK channels. **c)** Inhibition of vesicular release through inhibition of Ca^{2+} channels in the presynaptic terminal and shunting the postsynaptic-side through activation of GIRK channels. Adapted from Bassetti 2022 (Bassetti 2022).

1.5 *Emotional Learning and the Role of the MHb-IPN Circuit in Fear*

1.5.1 Fear as an adaptive response: acquisition, recall, and extinction

Fear is a fundamental emotional response that facilitates survival by promoting swift avoidance of potential harm. It enables organisms to detect and respond appropriately to threatening stimuli, thus increasing their survivability against predators and dangerous environments (LeDoux 2000; Stephen Maren and Quirk 2004; Tovote, Fadok, and Lüthi 2015). The adaptive value of fear lies in its capacity to rapidly modulate behavior quickly and reallocate attentional and physiological resources to deal with threats. This innate response has been assigned by the learning and memory systems to form and maintain associative

representations of previously encountered aversive events (Fanselow and Poulos 2005; Johansen et al. 2011).

The acquisition of fear involves the formation of an association between a neutral stimulus (a tone) and an aversive unconditioned stimulus (a foot shock), resulting in a conditioned stimulus (CS) that elicits a fear response even in the absence of the threat (LeDoux 2000; Maren 2001) (**Fig. 7a**). This associative learning critically depends on brain regions such as the amygdala, especially the basolateral amygdala, which integrates various sensory inputs and encodes the emotional value of the CS (Davis and Whalen 2001; Herry and Johansen 2014). The learned fear memory can be rapidly expressed in response to the CS, causing avoidance behaviors and autonomic responses.

Recall of fear memories, through the presentation of the CS alone, involves the retrieval of these associative traces and finally expression of defensive responses (Stephen Maren and Quirk 2004; Johansen et al. 2011) (**Fig. 7b**). Sometimes fear memory recall can become maladaptive if triggered inappropriately or excessively, as observed in pathological conditions such as phobias and post-traumatic stress disorder (Ressler and Mayberg 2007; Pitman et al. 2012). Understanding the neural circuits and synaptic mechanisms that control fear recall is therefore essential.

Extinction, is another key component of fear processing. When the CS is repeatedly presented in the absence of the aversive outcome, the fear response diminishes. This phenomenon shows the formation of a new memory trace that competes with the original fear association (Quirk and Mueller 2008; Herry and Johansen 2014). Structures like the ventromedial prefrontal cortex and the hippocampus work together with the amygdala to support extinction learning and the recall of extinction memories, thus reducing fear responses when there is no more threat (Myers and Davis 2007; Stephen Maren, Phan, and Liberzon 2013).

1.5.2 Core fear circuitry: amygdala, hippocampus, and prefrontal cortex

Within the mammalian brain, the processing of fear information and the formation of fear memories are majorly orchestrated by an interconnected triad of regions: the amygdala, hippocampus, and prefrontal cortex (PFC). Early lesion and recording studies in both animals and humans established the amygdala's role in detecting threats and assigning emotional valence to sensory cues (Kapp et al. 1979; LeDoux 2000). Meanwhile, subsequent research demonstrated how the hippocampus and PFC integrate contextual and regulatory information, respectively, to refine fear responses and memory retrieval (Stephen Maren and Quirk 2004; Shin, Rauch, and Pitman 2006; Herry and Johansen 2014).

The amygdala, and specifically its basolateral and central nuclei, are one of the key components of the fear circuit. Through the basolateral amygdala sensory inputs are associated with aversive outcomes, forming stable memory traces, that are otherwise neutral stimuli (Davis and Whalen 2001; Pape and Pare 2010). Once fear memory is established, the central amygdala controls the expression of conditioned fear by projecting to hypothalamic and brainstem structures, causing a cascade of autonomic and behavioral responses such as freezing, startling and changes in heart rate (Johansen et al. 2011; LeDoux 2000).

Moreover, the hippocampus provides a contextual framework for fear learning. Hippocampal networks, particularly the dorsal hippocampus, encode the spatial and situational details associated with aversive events, allowing the animal to recall not only which stimulus is dangerous but also under what circumstances the threat was encountered (Rudy, Huff, and Matus-Amat 2004; Maren 2001). Through integrating contextual information, the hippocampus ensures that fear responses remain appropriate to specific environments, preventing the generalization of fear memories to safe contexts (Hobin, Goosens, and Maren 2003; Ji and Maren 2007).

The prefrontal cortex, notably the infralimbic and prelimbic regions in rodents, plays a critical regulatory and modulatory role in fear processing. While the prelimbic region supports the maintenance and expression of conditioned fear responses, contributing to the stability of fear memories (Corcoran and Quirk 2007; Sierra-Mercado et al. 2006), the infralimbic region fosters the extinction and suppression of fear. Integrating top-down signals that can inhibit amygdala output, the infralimbic cortex enables organisms to downregulate fear responses when a previously threatening stimulus no longer causes harm (Quirk and Mueller 2008; Stephen Maren, Phan, and Liberzon 2013). Through these mechanisms, the PFC ensures that fear memories can be dynamically updated in response to changing environmental cues.

In recent years, the Hb complex, including the MHb-IPN pathway, have gained recognition as important modulators of emotional learning and stress-related behaviors (Agetsuma et al. 2010; Zhang et al. 2016; Zhang et al. 2018; Fore et al. 2018). Understanding how these additional regions work with the canonical fear circuit may offer deeper insights into the fine-tuned and multilayered regulation of fear learning, memory retrieval, and extinction.

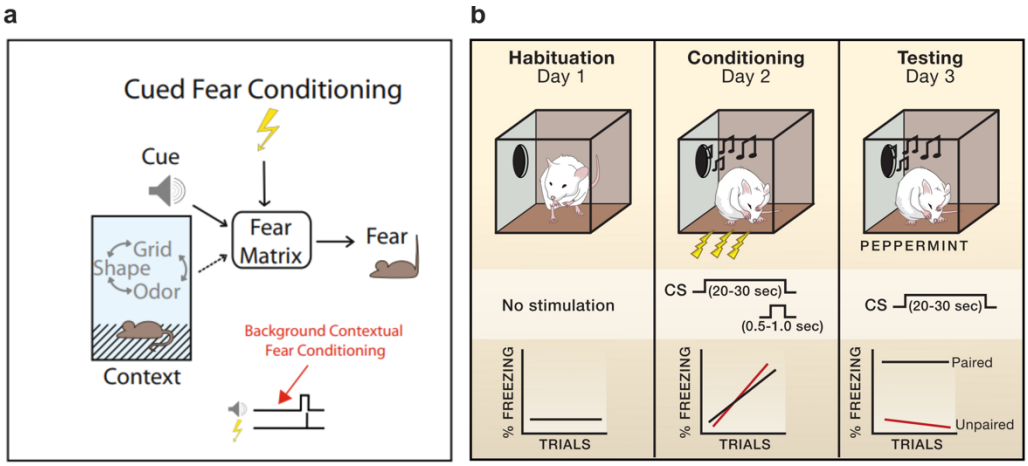

Figure 7: Cued fear conditioning paradigm.

a) Cued fear conditioning using tone (conditioned stimulus) co-terminating with foot shock (unconditioned stimulus). **b)** Three day cued fear conditioning paradigm. Day one, habituation, no apparent freezing behavior. Day two, conditioning, increased freezing levels with each tone-shock pairing. Day three, testing, elevated freezing levels to the conditioned stimulus (tone). Adapted from Johansen 2011 and Wotjak 2019 (Wotjak 2019; Johansen et al. 2011).

1.5.3 The MHb-IPN pathway's emerging role in fear conditioning

While the core neural substrates of fear learning have traditionally centered on the amygdala, hippocampus, and prefrontal cortex, accumulating evidence now points to the MHb-IPN circuit as an important modulator of fear conditioning and expression. In the past, MHb was primarily associated with behaviors related to reward avoidance, stress responses, and substance withdrawal (Lee et al. 2019; Xu et al. 2018; McLaughlin, Dani, and De Biasi 2017). However, more recent findings have begun to position the MHb-IPN pathway as a key player in the acquisition, recall, and extinction of conditioned fear memories (Koppensteiner, Melani, and Ninan 2017; Zhang et al. 2016; Soria-Gómez et al. 2015).

Previous findings hinted at the MHb-IPN pathway's involvement in aversive learning, which came from studies manipulating MHb activity during Pavlovian fear conditioning paradigms. For instance, Soria-Gómez et al. (2015) showed that deletion of CB_1Rs in MHb terminals reduced the freezing responses induced by fear conditioning, suggesting that the MHb contributes to the expression of learned fear. Further investigations using optogenetic and chemogenetic tools to selectively silence or activate MHb neurons have revealed that manipulations of MHb activity can profoundly influence the extinction of conditioned fear memories (Zhang et al. 2016). These approaches showed that the MHb, through its projections to the IPN, not only modulates the intensity of fear responses but may also gate the integration of fear-related cues at key retrieval phases.

Mechanistically, the MHb-IPN pathways' unique neurochemical composition provides an ideal environment for fine-tuning fear signals. By releasing both glutamate and acetylcholine, along with various neuropeptides,

MHb terminals in the IPN can create a dynamic and plastic synaptic milieu that is well suited to encoding and updating emotional memories (Frahm et al. 2015; Qin and Luo 2009; Ren et al. 2011).

The MHb-IPN circuit appears to integrate with other modulatory systems known to affect fear learning. For instance, alterations in MHb-IPN signaling can impact neuromodulatory centers in the midbrain and brainstem, shaping the dopaminergic and serotonergic responses that are critical for reinforcing or inhibiting aversive associations (Hikosaka 2010; Viswanath et al. 2013; Bianco and Wilson 2009). This broader network integration helps explain how the MHb-IPN axis can subtly calibrate behavioral states to match environmental contingencies and learned expectations of threat or safety.

1.6 *Rationale, Aims, and Hypotheses of This Study*

1.6.1 Motivations for investigating lateralized synaptic properties in the MHb-IPN circuit and hypotheses

Investigating the laterality of synaptic features in the mammalian MHb-IPN pathway offers new perspectives on how asymmetries in neural circuits modulate emotional behaviors. Hemispheric lateralization has been well studied in brain regions like hippocampus, amygdala and cortex. However, the functional relevance of hemispheric asymmetries in the mammalian MHb remains poorly understood. In this study, I aim to bridge this gap by examining the synaptic properties of left and right MHb-IPN projections and their differential roles in fear modulation.

Building on the emerging literature, I hypothesize that the MHb-IPN pathway might conserve its lateralized feature in mammals throughout evolution, similar to its connectivity and functional role in zebrafish. Specifically, I hypothesize that the synaptic properties might differ between left and right MHb inputs in IPN. Furthermore, these differences in synaptic properties may distinctively contribute to fear related behaviors. To test this, I performed *in vitro* electrophysiological recordings, chemogenetic, genetical manipulations, and behavioral experiments to investigate how lateralized synaptic mechanisms influence functional outcomes. This hypothesis would not only expand our understanding of habenular function but also contribute to the general principles of hemispheric lateralization in emotional circuits.

1.6.2 Objectives and scope of the present work

The overarching goal of this dissertation is to test the hypothesis that left-right MHb-IPN pathways differ in synaptic properties and further contribute to asymmetrical fear memory expression. To achieve this, I pursued the following objectives:

Characterize Synaptic Differences Between Left and Right MHb-IPN Inputs:

I used electrophysiological recordings in acute brain slices to measure P_r using paired-pulse ratio, and high-frequency depletion responses evoked from left and right MHb axons converging onto single IPN neurons. Additionally, I examined postsynaptic properties including the presence and levels of CP-AMPARs and NMDARs ensuring that any lateralization is due to the presynaptic input side.

Examine $GABA_BR$-Mediated Potentiation Across Hemispheres:

By using $GABA_BR$ activator baclofen, I determined whether $GABA_BR$-mediated synaptic modulation differs between left and right MHb inputs. This clarifies the extent to which $GABA_BR$ activation can selectively enhance synaptic output on one side.

Link Synaptic Asymmetries to Fear Memory Expression:

Using *in vivo* chemogenetics to inhibit left or right MHb neurons and genetic manipulations of left and right MHb $GABA_BRs$, coupled with the classical fear conditioning paradigm, I explored how unilateral alteration affects fear expression. If my hypothesis holds true, unilateral inhibition of MHb output on the left and right hemispheres should differentially alter the cued fear acquisition or retrieval.

By integrating synaptic physiology, pharmacology, genetics, and behavior, the present work aims to provide a comprehensive understanding of how lateralized MHb-IPN signaling contributes to the modulation of fear memories.

2 Materials and Methods

2.1 *Experimental Models*

2.1.1 Animal research ethics, housing and handling conditions

All experiments were carried out strictly following European animal experimentation guidelines and were approved by the Bundesministerium für Wissenschaft, Forschung und Wirtschaft of Austria under the license number "BMWFW-66.018/0005-WF/V/3b/2015". Replacement, reduction, and refinement (3R) were applied if possible. Mice were housed together and only single-caged after an operation, in a temperature and humidity-controlled environment with a 12-hour light/dark cycle, with ad libitum access to food and water.

2.1.2 Species and strains

Experiments in this study were performed using 8-16 weeks-old adult male and female C57BL/6J mice (Jackson Laboratory, #000664) as well as transgenic mouse lines engineered for Cre-dependent expression of reporter proteins or $GABA_BR$ deletion. Specifically, I used ChAT-IRES-Cre knock-in (#006410) mice to selectively manipulate cholinergic neurons in the medial habenula.

$GABA_B1^{lox511/lox511}$ floxed mice for $GABA_BR$ conditional knockout experiments (Haller et al. 2004), was kindly provided by Bernhard Bettler (University of Basel, Switzerland).

2.2 *Viral Vectors and Plasmids*

To achieve cell-type-specific inhibition of MHb cholinergic neurons, I employed Cre-dependent inhibitory DREADD (Designer Receptor Exclusively Activated by Designer Drugs) viruses expressing hM4Di-mCherry (AAV-hSyn-DIO-hM4Di-mCherry; AAV-hSyn-DIO-mCherry;) (Krashes et al. 2011). For presynaptic imaging experiments, I used Cre-dependent GCaMP variants targeted to axonal compartments (AAV-hSyn-DIO-axon-GCaMP6s; (Broussard et al. 2018). All viral vectors were obtained from Addgene or commercial vendors and were of high titer (≥10^12 vg/mL).

For the conditional knockout of $GABA_BRs$ in MHb neurons, I injected Cre-expressing lentiviruses (LV-hSyn-Cre-P2A-mCherry) into $GABA_B1^{\wedge flox/flox}$ mice, thereby enabling side-specific recombination and removal of $GABA_BR$ function in MHb neurons. Control groups received LV-hSyn-mCherry without Cre. Efficient recombination and receptor deletion were verified via immunohistochemistry.

2.3 *Surgical Procedures*

2.3.1 Stereotaxic virus injections

Stereotaxic injection of viruses and tracers was performed as previously described (Cetin et al. 2006). Mice were anesthetized by intraperitoneal injection of ketamine (100 mg/kg)/xylazine (4.5 mg/kg) and placed in a stereotaxic frame (Kopf). Metacam (5 mg/kg) and novalgin (33 mg/kg) were injected subcutaneously. The animal's head was shaved, and lidocaine 3% was applied locally. The parietal skin of the head was cut using scissors to expose the skull, then the periosteum was removed and the skull surface was cleaned. A nanoliter injector pump (World Precision Instruments, Sarasota, FL, USA) with a glass pipette was tilted 20° laterally and aligned on top of the bregma as a zero point for the injection coordinates. The injector was then moved to the coordinates of the region of interest respective to the brain atlas (Paxinos and Franklin 2019). For MHb, -1.45 A/P, 0.60 L, -2.65 D/V, and for IPN -3.05 A/P, 0.1 L, -4.7 D/V were used as coordinates. A small burr hole was drilled on top of the region of interest and dura mater was exposed. The glass pipette was moved to the dura, and the brain surface was taken as a zero point for the dorsoventral coordinates. 200-500 nL virus solution was loaded into the pipette and then the pipette was lowered to the injection site. The total volume was injected with a 50 nL/min flow rate, and the pipette was left in place for an additional 10 minutes. After infusion, it was slowly removed and the skin was closed using surgical glue.

2.4 Electrophysiological Recordings

2.4.1 Thick acute slice preparation preserving MHb-IPN projections

Mice were anesthetized by intraperitoneal injection of overdose ketamine/xylazine and transcardially perfused with ice-cold oxygenated (95% O_2. 5% CO_2) artificial cerebrospinal fluid (ACSF) containing (in mM): 118 NaCl, 2.5 KCl, 1.25 NaH_2PO_4, 1.5 $MgSO_4$, 1 $CaCl_2$, 10 Glucose, 3 Myo-inositol, 30 Sucrose, 30 $NaHCO_3$; pH = 7.4 as described previously (Bhandari et al. 2021; Koppensteiner et al. 2024). The brain was carefully removed and placed in the cutting chamber of a vibratome (DSK7, Dosaka). A 1-mm slice containing the IPN, the FR, and the two habenulae was cut at 56˚ and placed into a recovery chamber containing standard ACSF at 37 ℃ for 1 hr. Subsequently, the slice was moved to the recording chamber and continuously superfused with 2.5 mM $CaCl_2$-containing oxygenated ACSF at room temperature (RT), with 20 µM bicuculline methiodide (Tocris, Bristol, UK), 5 µM mecamylamine hydrochloride and 50 µM hexamethonium bromide (**Fig. 8a-b**).

Figure 8: Electrophysiology setup used for acute slice recording.

a) Image showing the amplifier, digitizer, perfusion pump, microscope, camera, micromanipulators, stimulating electrodes, isolators, recording chamber on a floating table and the PC. **b)** Example image of an acutely cut thick brain slice containing Hb, FR and IPN in the recovery chamber.

2.4.2 Whole-cell patch-clamp recordings from IPN neurons with bilateral MHb stimulation

Stimulating electrodes were placed on top of the MHb cell bodies or the fiber tract, allowing the selective stimulation of either the left or right side. For a reliable comparison, stimulating electrodes were placed on the same level on the MHb-IPN axis at all the experiments. To eliminate selection bias, we randomized the stimulating electrodes among the left and right sides as well as the recording protocol. Patch pipettes (3-6 MΩ) were filled with the internal solution containing,

(in mM): 130 K-Gluconate, 10 KCl, 2 $MgCl_2$, 2 MgATP, 0.2 NaGTP, 0.5 EGTA, 10 HEPES, 5 QX314-Cl; pH 7.4 adjusted with KOH. Electrophysiological signals were acquired at 10 - 50 kHz and filtered at 2.0 kHz using a Multiclamp 700B amplifier connected to a Digidata 1440A digitizer (Molecular Devices, CA, USA). Access resistance (Ra) was continuously monitored throughout all recordings and cell changes in Ra exceeding 20% were discarded.

2.4.3 Paired-pulse ratio, high-frequency stimulation and variance-mean analysis to assess release probability

Paired-Pulse Ratio (PPR) and Release Probability Measurements:

PPR experiments were performed using concentric bipolar electrodes for electrical stimulation. Electrodes were placed at the beginning of the FR at similar distances from the IPN and the stimulation protocol along with the electrodes were shuffled between sides to avoid any bias. The pulse duration of 0.2-millisecond with 50-millisecond inter-stimulus interval was used. The protocol consisted of 6-second between sides and 10-second same side stimulation interval.

Before applying the paired-pulse protocol, three to four stimuli were delivered to each side to condition the fibers and stabilize release. The PPR was calculated by dividing the amplitude of the second evoked EPSC by that of the first EPSC. If both pulses in a pair failed to elicit responses, the trace was excluded from PPR calculations.

Baclofen-Mediated Potentiation:

Baclofen (1 μM) was bath-applied, and its effect on EPSC amplitudes was assessed by comparing basal EPSCs to those recorded under baclofen treatment. The potentiation ratio was determined by dividing the average EPSC amplitude during baclofen application by the average basal EPSC amplitude and multiplying by 100 for each side.

Failure Rate Analysis:

Failure rates were calculated using the first pulse of the paired stimuli for both left and right inputs in the same trace. For each cell, the standard deviation of the baseline current (measured over a 2-s window between left and right stimulations) was computed across all traces; four times this standard deviation was used as the threshold for defining a response as a “failure.” Any EPSC below this threshold was deemed a failed release event. The failure ratio was then computed by dividing the number of failed events by the total number of traces, both under basal conditions and during baclofen treatment.

High-Frequency Vesicular Pool Depletion (50 Hz):

For 50-Hz high-frequency vesicular pool depletion experiments, the cumulative amplitude of EPSCs was plotted and a line was fitted to last 10-15 stable responses. The RRP size was estimated by extrapolating the line to the first stimuli.

P_r was estimated from the average EPSC amplitude and RRP size according to the following equation: I = p x q x N; where p is the P_r, q is the quantal size, and N is the number of release sites. Finally, P_r was calculated by dividing the average of the first EPSC amplitude by the RRP size.

Variance-Mean Analysis (V-M):

For variance-mean analysis, four different Ca^{2+} concentrations (1.5–8 mM) was used to assess the variance and mean amplitude of EPSCs at varying release probabilities. Each Ca^{2+} concentration was perfused for 5–10 minutes. Once the EPSC amplitudes reached a stable level, 15–20 EPSC responses were recorded for further calculation of mean amplitude vs variance. The order of Ca^{2+} application was 2.5 mM, 1.5 mM, 6–8 mM, and finally 4–5 mM. Synaptic noise was substantially larger than baseline noise. Release probability and quantal size were calculated using the equations $Var = Iq - I^2/N$ and $I = Nqp$, where I represents the mean EPSC amplitude, N the number of release sites, and q the quantal size.

2.4.4 Assessing AMPAR/NMDAR components and CP-AMPAR presence

EPSCs were recorded at multiple holding potentials (-60, -40, -20, 0, +20, +40, and +60 mV) using an internal solution containing spermine to generate current-voltage (I-V) relationships. The slopes from -60 to 0 mV and those from 0 to +60 mV were calculated to obtain rectification indexes for the left and right MHb-derived synapses, allowing the calculation of rectification indices indicative of CP-AMPARs (Liu and Zukin 2007; Hollmann, Hartley, and Heinemann 1991). NMDA receptor-mediated currents were isolated by recording at +40 mV and measuring the EPSC component 100-millisecond after the AMPA peak (S. G. Cull-Candy and Leszkiewicz 2004).

2.5 Calcium Imaging

2.5.1 GCaMP-based presynaptic calcium imaging in MHb terminals

Acute slice calcium imaging was performed as previously described (Koppensteiner et al. 2024) and the data in this study was reused to analyze left and right MHb input identification in the rIPN. Three weeks following the AAV9-hSynapsin1-FLEx-axon-GCaMP6s bilateral injection into the MHb, thick acute brain slices were prepared as described previously. The slice was recovered at RT for 40 min. I specifically centered the axon crossings such that the input from left and right MHb were visible on the same field of view. Using the same recording solution as I used in electrophysiological recordings, the slice was superfused with ACSF containing 2.5 mM Ca^{2+} at RT. Bilateral stimulating electrodes were placed at the beginning of the FR. Next, using a 20X 0.5 NA water-immersion objective (Olympus), MHb axons on the surface entering the rIPN were carefully focused, and the GCaMP expression was confirmed using blue led excitation (pE-300 led

light source (CoolLED) and a monochrome CCD camera (XM10, Olympus). To visualize the fluorescent signal, excitation filter 460 – 490 nm, dichroic mirror 505 nm and barrier filter 510 nm (U-MWIB2, Olympus) were used. GCaMP fluorescence in response to 10-Hz electrical stimulation (3-s duration, 0.2-ms pulse width, 0.5 – 2.5 V stimulation intensity) was recorded with a baseline period without any stimulation. The stimulation was alternated between the left and right side at 3 Hz and the illumination was turned off between sweeps to prevent photobleaching. To minimize background noise, I employed a rolling ball subtraction algorithm followed by standard deviation differentiation to identify fibers responsive to alternating stimulation from the left and right inputs.

2.6 *Behavioral Experiments*

2.6.1 Cued fear conditioning paradigm

Mice were handled three days consecutively before the experiment. For chemogenetic inhibition using ChAT-IRES-Cre knock-in mice, on the day of conditioning, were placed in a conditioning chamber (Context A) and, after three minutes, three CS (auditory tone 4 kHz, 80 dB, 30 s with 30 s interval) were presented with co-terminating unconditioned stimuli (foot shock 0.75 mA, 1 s with 1 m interval). At the end of the acquisition session, animals were removed from the conditioning chamber and returned to the home cages. Twenty-four hours later, mice were injected with CNO (Clozapine N-oxide) (3 mg/kg i.p.). 40 minutes after the injection, mice were placed in a different chamber (Context B) and received the CS without foot shock five times. Either left or right MHb cholinergic neurons were silenced using inhibitory DREADDs before the recall phase.

For LV-mediated $GABA_BR$ knock-out using $GABA_B1$ floxed mice, animals were placed in a conditioning chamber (Context A) and, after three minutes, three CS (auditory tone 4 kHz, 80 dB, 30 s with 60 s interval) were presented with co-terminating unconditioned stimuli (foot shock 0.75 mA, 1 s with 90 s interval). At the end of the acquisition session, animals were removed from the conditioning chamber and returned to the home cages. Twenty-four hours later, mice were placed in a different chamber (Context B) and received only the CS without foot shock four times (**Fig. 9a-b**). Expression of fear was indexed as the level of freezing (complete immobility) during the presentation of the discrete tones and inter-stimulus-interval ISI. Special care was taken to create distinct contexts by changing the shape, flooring, ceiling, wall accessories, and odor. Recall sessions in context B were performed in almost complete darkness.

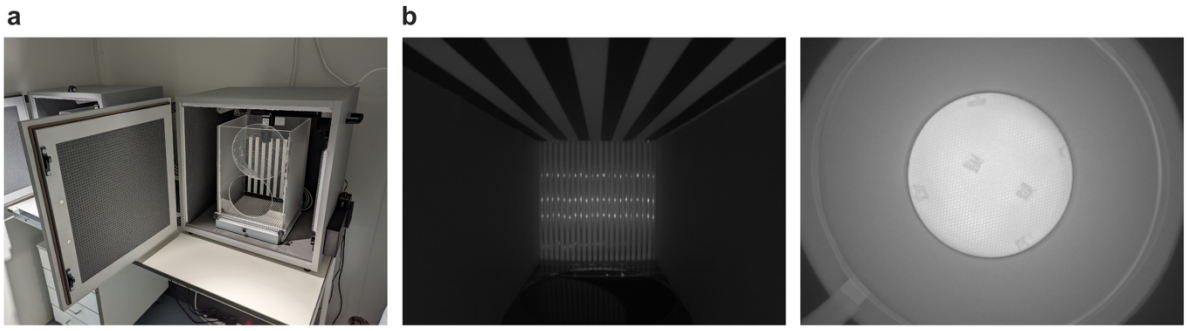

Figure 9: Behavioral setup for cued fear conditioning paradigm.

a) Sound proof chamber equipped with visible light, infrared light, speaker and a top mounted camera. **b)** A square box with a striped wall and metal grids as flooring to deliver foot shock used as a conditioning chamber on day one (left). A round drum with high walls used as a recall chamber on day two (right).

2.6.2 Behavioral scoring and statistical analysis

Behavioral videos were acquired with a video camera from the top using 20-30 frames per second. Mice were tracked using DeepLabCut (Mathis et al. 2018; Nath et al. 2019) with a custom-trained network for each arena and genotype (ChAT-IRES-Cre knock-in/C57BL/6J background, $GABA_BR1^{Flx}$/BALBc background) with five points tracking (snout, left ear, right ear, center, and tail base). Tracking data was then filtered and manually inspected for quality control. To detect the freezing events I utilized BehaviorDepot App (Gabriel et al. 2022). All acquired videos were converted to AVI and then a velocity-based freezing classifier was used with the five tracked points. Each video was pre-processed by smoothing based on the tracking quality and frame rate using Lowess method (window size 12-14) and Hampel filter (window size 6-7). The general freezing criteria for point-based tracking was less than 0.52 cm/s linear back velocity and less than 12 deg/s angular velocity of the head. Next, all the immobility events were counted starting from 200 ms to create a histogram and find the highest peak to decide a reliable freezing duration criteria based on the genotype.

Data was then used to further detect true freezing events. For ChAT-IRES-Cre knock-in mice, window size 27-32 was used based on the frame rate with a minimum threshold count of 10 and a minimum freezing duration of 0.9 s. For $GABA_BR1^{Flx}$ mice, window size 32 was used based on the frame rate with a minimum threshold count of 8 and a minimum freezing duration of 0.8 s. Using custom-written MATLAB scripts, event-related freezing time and frequency were calculated. Finally, example overlay videos of freezing events with videos were created with custom scripts for quality check. Total distance traveled, freezing time, frequency, and distribution were calculated based on those metrics.

2.7 Histological and Immunohistochemical Analysis

2.7.1 Tissue preparation and immunostaining

Mice were sacrificed by ketamine/xylazine overdose and perfused with 4% paraformaldehyde (PFA) in phosphate buffer (PB) for 12 minutes at a flow rate of 7.5 mL/min. Brains were then removed and placed in a 4% PFA in PB for an additional overnight at 4 degrees for proper fixation. To prevent tissue damage during sectioning, brains were cryoprotected in 30% sucrose in phosphate-buffered saline (PBS) solution overnight at 4 °C. 30-100 µm-thick brain slices were obtained using a sliding microtome. Slices were washed 2 times in PBS for 5 minutes each to remove any excess PFA. They were then blocked in a solution containing 10% normal goat serum and 0.1% Triton X-100 in PBS for 1 hour at RT to reduce non-specific binding. For labeling, slices were incubated with primary $GABA_BR1$ antibody (Kulik et al. 2002) (B17 made in rabbit, affinity-purified, 0.5µg/ml in PBST 2% NGS) overnight at 4 °C. After washing three times, slices were incubated with secondary antibody (Molecular probes, A11037, Goat anti-Rabbit IgG (H+L), Alexa Fluor 594, highly cross-adsorbed, 4 µg/ml) for 2 hours at RT. Slices were washed again 2 more times in PBS for 5-10 minutes each and mounted onto slides with a mounting medium (Mowiol) containing DAPI for nuclear staining.

2.7.2 Microscopy and validation of viral expression

The slides were imaged using spinning disk (Nikon CSU-W1) or confocal (Leica SP8, Zeiss LSM 900) microscopes. Quantitative image analysis was performed using ImageJ.

2.8 Data Analysis and Statistics

2.8.1 Statistical tests and significance thresholds

For the data analysis and statistics, I used GraphPad Prism (GraphPad, San Diego, CA, USA), Excel (Microsoft, Redmond, WA, USA), JASP, and Clampfit (Molecular Devices) software to perform statistical tests on the data. I first checked the normality of the data using Shapiro-Wilk or Kolmogorov-Smirnov tests. For normally distributed data, I used two-tailed student's t-test to compare the means of two groups. For non-normally distributed paired data, I used Wilcoxon singed rank test to compare pairs. I considered the p-value less than 0.05 to be statistically significant. I also performed one-way, two-way and three-way analysis of variance (ANOVA) with post-hoc Tukey's multiple comparisons test to compare the means of multiple groups for multiple factors. The error bars for parametric tests are presented as ± SEM. Box-and-whisker plots show the median, interquartile range (IQR), and whiskers extending to 1.5 times the IQR (Tukey method).

3 Results

3.1 *Bilateral Convergence and Input-side Dependent Signaling of MHb Inputs to the IPN*

3.1.1 Anatomical mapping of MHb projections to the IPN

My initial investigations focused on establishing whether the rostral subnucleus of the IPN (rIPN) neurons receive convergent yet distinguishable inputs from both the left and right MHb. Previous anatomical studies have demonstrated the prominent projections of the MHb to the IPN through the FR (Herkenham and Nauta 1977; Swanson and Cowan 1979). However, these early descriptions did not explicitly address the possibility of functional asymmetry or distinguish the terminal fields originating from the left versus right MHb. I first used the ChAT-ChR2-EGFP transgenic line and showed the ChAT^{+} vMHb neurons targeting IPN neurons. This line with channelrhodopsin set the ground for further experiments where I isolated the preserved connected pathway. Blue light delivery using angled optical fibers on the left and right MHb evoked reliable responses in the rostral IPN (**Fig. 10a-b**).

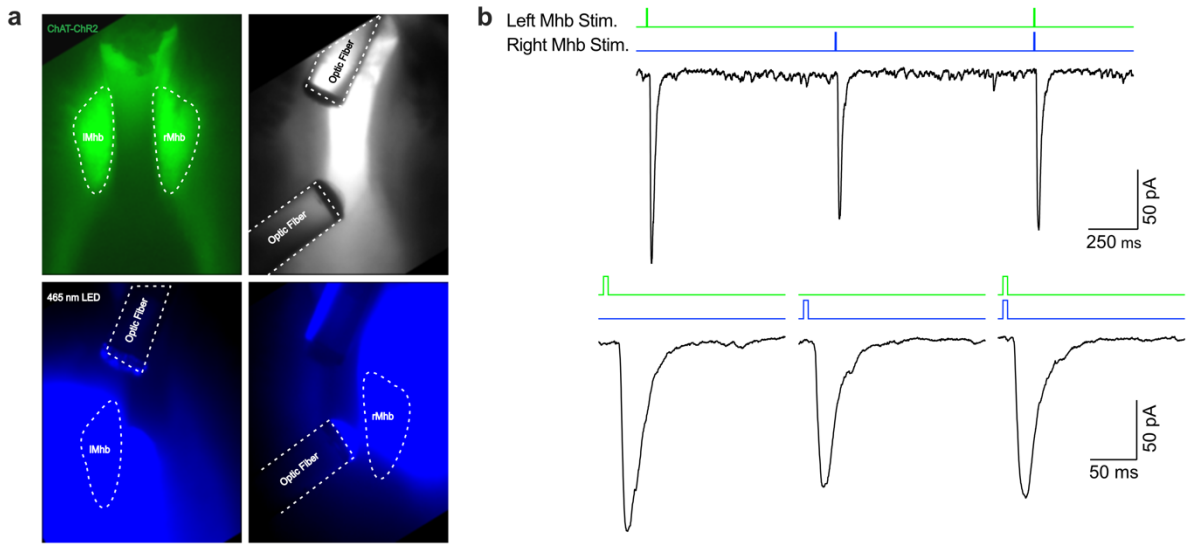

Figure 10: Optogenetic stimulation of distinct left and right MHb fiber paths using ChAT-ChR2 line.

a) Images showing ChR2 expressing MHbChAT+ neurons in green (left, top) and fiber optic placement to target only left and/or right fiber path (right, top). Blue light during the stimulation showing the condensed and targeted side dependent stimulation (bottom). **b)** Example stimulation of left and right MHb with optogenetic stimulation pattern. Light evoked post synaptic currents recorded from the same IPN neuron showing response to both side stimulations.

3.1.2 Synaptic input distribution in the IPN

To investigate the synaptic features of the left and right MHb inputs to the IPN in adult mice, I employed 1-mm thick slices cut at a 53° angle to preserve the FR fiber bundle from the MHb to the IPN (Bhandari et al. 2021; Koppensteiner et al. 2024). This preparation allows selective electrical stimulation of the left and right MHb-derived axons and recording bilateral responses in a single postsynaptic IPN neuron (**Fig. 11a**). To rule out the potential cross-stimulation, I stimulated the FR in one hemisphere with a 100-Hz train. This potentiated the excitatory postsynaptic current (EPSC) responses only on the side that received the 100-Hz stimulus without influencing the EPSCs evoked from the contralateral axons (**Fig. 11b**), thus confirming the confinement of the stimulation to the respective sides. Interestingly, I noted that all the recorded neurons in the rIPN received bilateral MHb inputs. This observation suggests that although the left and right MHb input fibers follow distinct and separate paths towards the IPN (**Fig. 11e**), MHb on both sides innervates all neurons within the rIPN. Intense dendritic arborization of IPN neurons allows them to receive bilateral inputs from both habenulae (**Fig. 11c**).

3.1.3 Presynaptic calcium activity of MHb-IPN projections

I next employed presynaptic calcium imaging to further rule out cross-communication between the left and right inputs. I injected viral vectors encoding an axon-enriched calcium indicator (AAV9-hSyn-DIO-axon-GCaMP6s-EGFP) into the bilateral ventral MHb of adult ChAT-IRES-Cre knock-in mice (**Fig. 11d**). Three weeks following the injections, GCaMP fluorescence revealed rich axons from both left and right MHb projecting to the rIPN in acute slice preparations (**Fig. 11e**). These axons traversed the midline in the rIPN, and extended across other IPN subnuclei, reaching the ventral region of the central nuclei while forming additional crossings (**Fig. 11e**). I then conducted calcium imaging in the rIPN where left and right MHb input fibers intersect while stimulating the incoming fiber paths using 10-Hz electrical stimulation. This approach provided a unique opportunity to observe both input fibers within the same field of view. I compared the presynaptic fluorescence intensity at rest and during stimulation as a metric of evoked activity in the region of interest (ROI) for each of the left and right stimuli (**Fig. 11f**). I found that stimulation of each side induced a robust increase in Ca^{2+} influx without significant overlap between the left and right inputs (**Fig. 11g**). The marginal response observed during the contralateral stimulation likely resulted from fibers running beneath the recorded surface. Overall, these data demonstrate that the left and right MHb input fibers relay non-overlapping information with minimal crosstalk, thus providing further support for the convergence of bilateral MHb synaptic inputs in the IPN.

In summary, the data presented in this section establish bilateral convergence of MHb inputs onto individual IPN neurons and confirm their functional independence. This foundation enabled me to investigate further whether and how left-right differences in synaptic probability, receptor composition, and modulatory mechanisms shape the postsynaptic response of this evolutionarily conserved pathway.

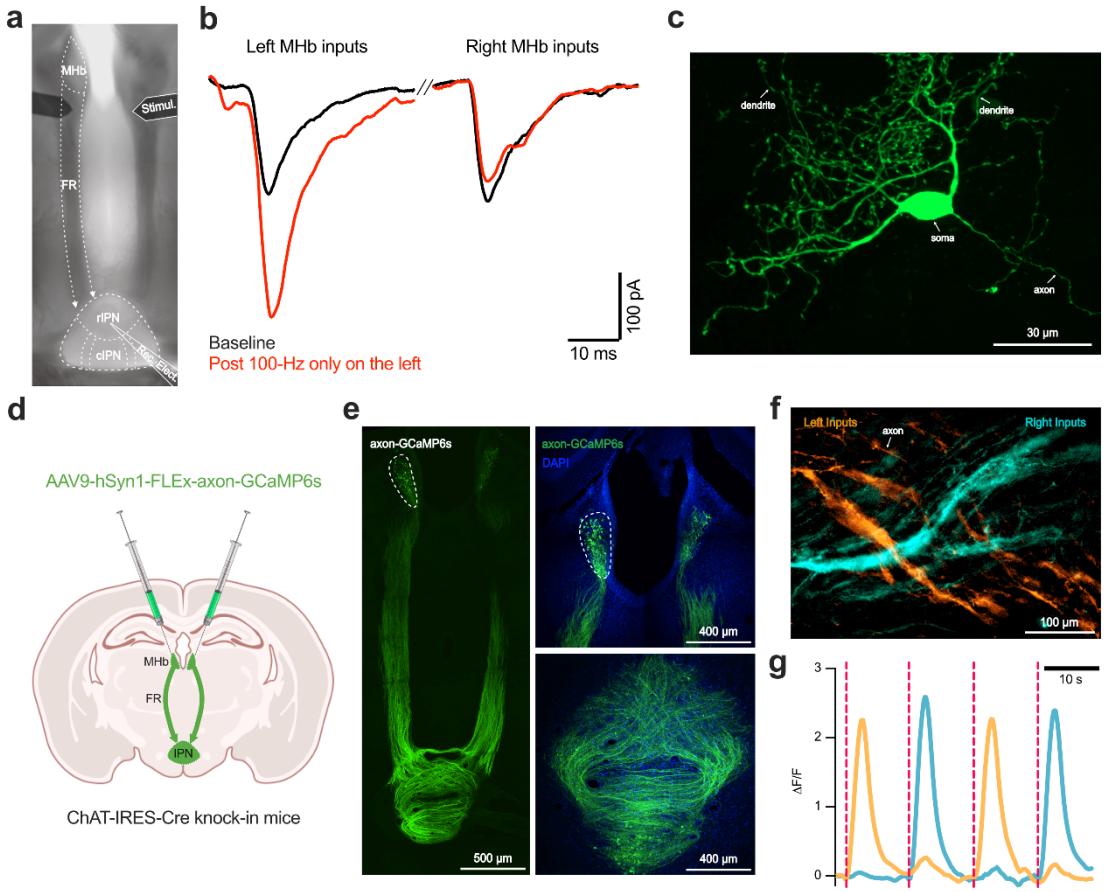

Figure 11: Selective recording from left and right MHb inputs in single IPN neurons.

a) Representative image showing the experimental setup for the selective stimulation of left and right medial habenula (MHb) inputs at the fasciculus retroflexus (FR) and recording EPSCs in the same postsynaptic neuron in the rostral interpeduncular nucleus (rIPN) using 1 mm-thick slices. Concentric bipolar electrodes (Stimul.) are placed at the beginning of the FR and a recording electrode is placed in the rIPN. **b)** First, the basal EPSCs were measured from left and right inputs on each side individually. Next, only the left inputs were stimulated using a 100-Hz high-frequency stimulation to induce potentiation on those synapses. Lastly, post stimulation EPSCs were measured. Traces show EPSCs from the left but not right inputs were potentiated, indicating that the electrical stimulation of the left and right inputs was independent without any crosstalk to the contralateral side. **c)** High magnification confocal image of a biocytin filled single IPN neuron showing the soma, single axon and the intense dendritic arborization. **d)** Schematic illustration of the experimental design for AAV-mediated calcium imaging using GCaMP6s. AAV9-hSyn1-FLEx-axon-GCaMP6s was bilaterally injected into the MHb of ChAT-IRES-Cre knock-in mice to selectively label cholinergic neurons, enabling visualization of FR and comparison of Ca^{2+} responses in left and

right MHb-derived axons. **e)** Representative confocal images of axon-GCaMP6s fluorescence in MHb cell bodies (top right), FR (left), and crossing axons in the IPN (bottom right). **f)** Rolling ball background subtracted fluorescent image showing crossing left and right MHb axons in the rIPN. Fibers were pseudo-colored for left and right inputs based on the standard deviation difference in response to 10-Hz train. **g)** Fluorescence traces showing ΔF/F in response to 10-Hz electrical stimulation of the left and right FR based on responsive regions in **e.** Quantification of the ΔF/F responses indicates distinct, side-spesific, and non-overlapping calcium responses.

3.2 *Electrophysiological Properties of MHb-IPN pathway*

3.2.1 Left MHb inputs exhibit higher paired-pulse ratios, indicating lower P_r

To address potential side-dependent synaptic differences in glutamatergic projection originating from the vMHb to the rIPN, I first focused on synaptic P_r, a crucial determinant of synaptic strength and plasticity (Dobrunz and Stevens 1997; Schulz, Cook, and Johnston 1994). I stimulated left and right MHb fibers using paired pulses with a 50-millisecond inter-stimulus interval, ensuring a 6-second interval between opposite-side stimuli and a 10-second interval between consecutive same-side stimuli (**Fig. 12a**). PPR, calculated as the ratio of the second evoked EPSC to the first EPSC, serves as an index of synaptic P_r, with higher PPR values generally reflecting lower P_r (Dobrunz and Stevens 1997). The recordings revealed significantly higher PPR in synapses derived from left vMHb terminals compared to those from the right side ($W = -689.0$, $n = 53$ *cells*, $p = 0.0019$, *Wilcoxon matched-pairs signed-rank test*; **Fig. 12b**), indicating a lower P_r in left vMHb-derived synapses. The asymmetry in PPR suggested that synaptic terminals from left vMHb neurons release neurotransmitters less readily upon stimulation. Notably, during recordings, I also observed that left vMHb synapses typically required several stimulations to achieve a stable release state, with a higher amount of failed synaptic release events ($W = -689.0$, $n = 17$ *cells*, $p = 0.0166$, *Wilcoxon matched-pairs signed-rank test*; **Fig. 12c**).

3.2.2 Release probability distribution

To determine whether the synaptic asymmetry was driven by the input side rather than the target location, I first categorized the recorded rIPN neurons based on the difference in RRPs. By normalizing the differences between the paired PPR values obtained with the left and right input stimulation and categorizing recorded neurons into three groups, I found that the majority of the rIPN cells have higher PPRs for the left input (**Fig. 12d-e**) (PPR L > R: 62.26%, L= R: 16.98%, L< R: 20.75%). To examine the location of neurons based on their PPR differences, I mapped the recorded neurons in rIPN with this categorization (**Fig. 12f**). Interestingly, the observed differences in P_r were independent of their location in rIPN. The

homogenous distribution of neurons indicates that the synaptic asymmetry is due to the input side rather than the target location.

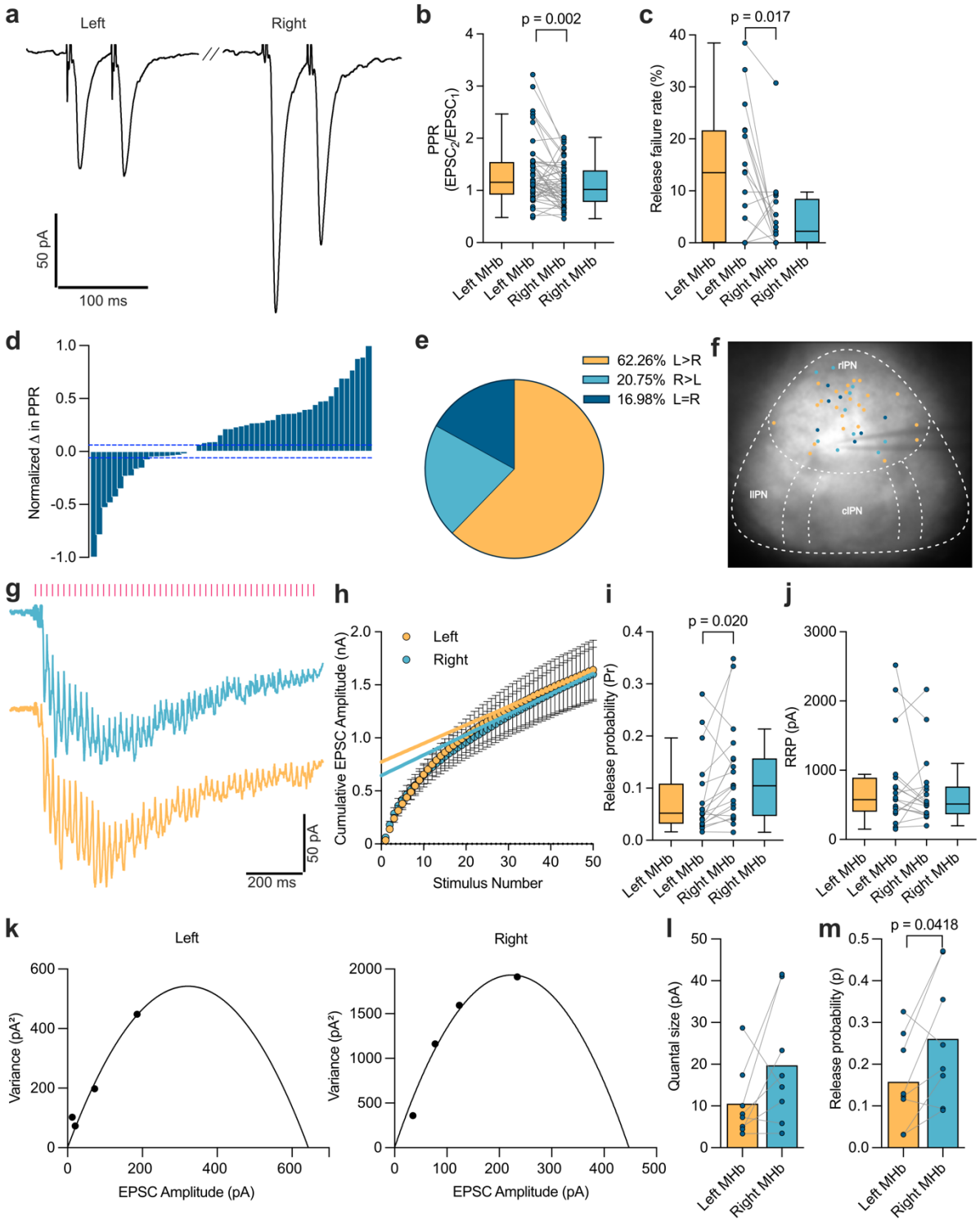

Figure 12: Asymmetrical release probability in MHb terminals.

a) Example paired-pulse trace (50 ms interval) of excitatory postsynaptic currents (EPSCs) in the rIPN, evoked by electrical stimulation of the left and right FR. **b)** The paired-pulse ratio (PPR), calculated as EPSC2/EPSC1, showed that synapses derived from the left MHb exhibit a significantly higher PPR than those from the right MHb in the same postsynaptic rIPN neurons, indicating a lower

release probability (P_r) in left than right MHb terminals; (W = -689.0, *n = 53 cells*, *p = 0.0019*, *Wilcoxon matched-pairs signed-rank test*). **c)** Synaptic release failure threshold was calculated as EPSCs lower than 4 times of the pre-stimulus baseline current's standard deviation. Paired comparison showing higher percentage of failed synaptic release events in the left MHb inputs compared to right MHb in response to electrical stimulation (W = -689.0, *n = 17 cells*, *p = 0.0166*, *Wilcoxon matched-pairs signed-rank test*). **d)** Normalized differences in PPR between left and right inputs for each cell are plotted in a sequential order from the highest PPR difference for right MHb terminals (-1.0) to the highest PPR difference for left MHb inputs (1.0). The difference values are categorized using 15% of standard deviation (blue dashed line), within which are defined as equal PPRs. **e)** Pie chart showing the categorized PPRs. The majority of the neurons in the rIPN show higher PPRs from left MHb inputs. **f)** Location of recorded neurons with their respective PPR category indicated by the same color as **e** showing a homogenous distribution. **g)** Example of averaged EPSC traces for inputs originating from the left (orange) and right (blue) MHb following a 50-Hz stimulation (pink bars), demonstrating depletion of the readily releasable vesicle pool. **h)** Cumulative mean EPSC amplitudes plotted as a function of stimulus number for left and right MHb synapses (*n = 19 cells*). The error bars are presented as ± SEM. **i)** Paired comparison showing a significantly lower P_r for left then right MHb-derived synapses based on the first EPSC amplitude divided by the readily releasable pool size (RRP) using the high-frequency depletion protocol; (W = 114.0, *n = 19 cells*, *p = 0.0204*, *Wilcoxon matched-pairs signed-rank test*). **j)** Paired comparison of RRPs showing no significant difference between left and right MHb-derived synapses; (W = -20.0, *n = 19 cells*, *p = 0.7086*, *Wilcoxon matched-pairs signed-rank test*). **k)** Representative V-M measurements of EPSC amplitudes at different Ca^{2+} concentrations. **l)** Analysis of quantal size shows no difference; (W = -22, *n = 8 cells*, *p = 0.1484*, *Wilcoxon matched-pairs signed-rank test*). **m)** Paired comparison showing a significantly lower P_r for left then right MHb-derived synapses; (*p = 0.0418*, *n = 8 cells*, *paired t-test*). Box-and-whisker plots show the median, interquartile range (IQR), and whiskers extending to 1.5 times the IQR (Tukey method).

3.2.3 High-frequency stimulation and V-M analysis confirm side-dependent differences in vesicle pool utilization

To verify further the lower P_r in left MHb-derived synapses, I utilized a high-frequency (50-Hz) stimulation protocol designed to exhaust the RRP of vesicles, thus allowing me to analyze the cumulative EPSC amplitudes over successive stimuli (**Fig. 12g-h**) (Schneggenburger, Meyer, and Neher 1999). I confirmed that left vMHb-derived synapses have significantly lower P_r relative to right vMHb-derived synapses in the rIPN (W = 114.0, *n = 19 cells*, *p = 0.0204*, *Wilcoxon matched-pairs signed-rank test*; **Fig. 12h-j**). This is consistent with a lower initial P_r: fewer vesicles are released per stimulus at the onset, preserving a larger fraction of the RRP for subsequent stimuli, thus allowing the left input to better maintain output under repetitive firing conditions.

I finally quantified the P_r concentration using variance-mean experiment. By measuring changes in both EPSC variance and mean amplitude under different Ca^{2+} concentrations (**Fig. 12k**), I found that terminals derived from the left MHb exhibited a significantly lower P_r than those from the right side (*p = 0.0418*, *n = 8 cells*, *paired t-test*; **Fig. 12m**). There was no difference in quantal size (W = -22, *n = 8 cells*, *p = 0.1484*, *Wilcoxon matched-pairs signed-rank test*; **Fig. 12l**).

These experiments support a model in which the left side's lower basal P_r is not only reflected in paired-pulse parameters but is also evident in its response to sustained high-frequency activity. Together, these data provide strong physiological evidence of asymmetry in presynaptic release dynamics between the two hemispheres.

3.2.4 Comparable postsynaptic receptor composition rules out postsynaptic contributions

Next, to test whether the synaptic asymmetry also involves postsynaptic mechanisms, I compared CP-AMPARs in synapses receiving left and right MHb inputs. These receptors have been previously reported to contribute to the long-lasting enhancement of glutamate release in the MHb-IPN pathway (Koppensteiner, Melani, and Ninan 2017). I recorded EPSCs at holding potentials of -60, -40, -20, 0, +20, +40, and +60 mV using an internal solution containing spermine (**Fig. 13a**), and plotted the current/voltage relationship (**Fig. 13b**). The slopes from -60 to 0 mV, and those from 0 to +60 mV were calculated to obtain rectification indexes for the left and right MHb-derived synapses. Inwardly rectifying currents, characteristic of CP-AMPARs, were observed in both of them (**Fig. 13c**, *main effect of slopes:* $F_{(1, 22)} = 25.10$ $p < 0.0001$, *main effect of side:* $F_{(1, 22)} = 0.5104$ $p = 0.4825$, *side and slope interaction:* $F_{(1, 22)} = 0.05207$ $p = 0.8216$), with Sidak post-hoc correction ($p = 0.0054$ *and* $p = 0.0025$ *for left and right MHb slopes, respectively*) with comparable levels of rectification indexes (**Fig. 13d**). These rectification indexes are consistent with previous findings (Koppensteiner, Melani, and Ninan 2017), and demonstrate that the thick slice-cutting method followed by long-range stimulation accurately captures the synaptic characteristics of the MHb-IPN pathway.

I also examined the AMPA/NMDA ratios by recording EPSCs at -60 mV and +40 mV holding potentials to assess potential side-dependent asymmetry. The NMDA currents were measured at 100-millisecond after the AMPA peak current (**Fig. 13e**). I observed marginal NMDAR-mediated components with no difference in the AMPA/NMDA ratios between left and right MHb-derived inputs (**Fig. 13f**). Based on the comparable levels of CP-AMPARs and AMPA/NMDA ratios between left and right inputs recorded in the same postsynaptic neurons, the input-side dependent asymmetry in synaptic transmission is ascribable to presynaptic mechanisms.

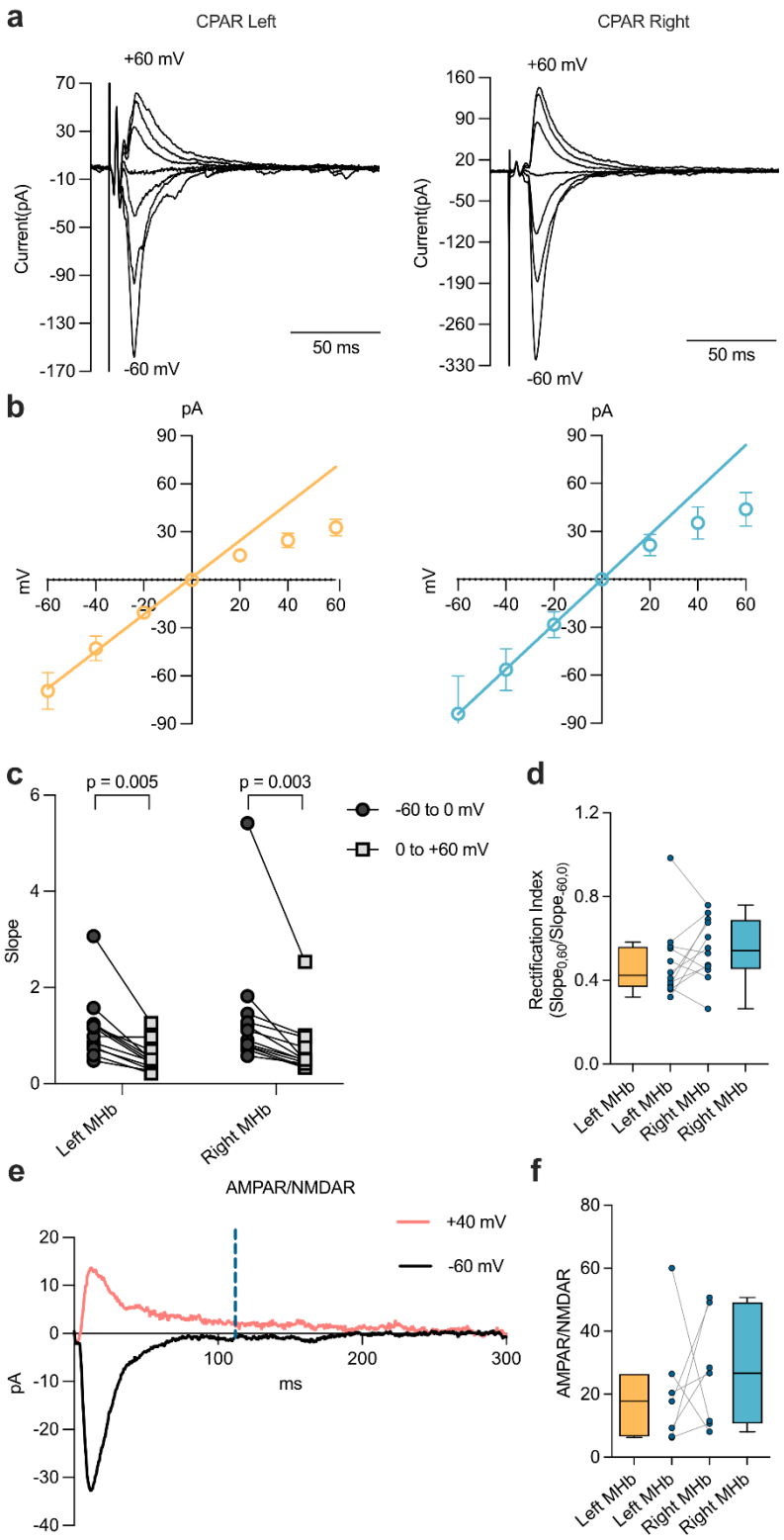

Figure 13: No difference in postsynaptic properties in left and right MHb projections.

a) Representative current-voltage (I-V) traces recorded from synapses receiving left and right MHb-derived inputs. The traces show currents evoked at different holding potentials (-60 to +60 mV) in the presence of spermine in the intracellular solution. **b)** I-V plots showing the characteristic inwardly rectifying current, indicative of calcium-permeable AMPA receptors (CP-AMPARs) for both left (orange) and right (blue) MHb terminals. **c)** Comparison of slopes from -60 mV to 0 mV and

those from 0 mV to +60 mV calculated for left and right MHb-derived inputs. The data indicates significant inward rectification in synapses from both sides, confirming the presence of CP-AMPARs. Two-way ANOVA showed a main effect of negative/positive slopes, (*main effect of slopes:* $F_{(1, 22)} = 25.10$ $p < 0.0001$, *main effect of side:* $F_{(1, 22)} = 0.5104$ $p = 0.4825$, *side and slope interaction:* $F_{(1, 22)} = 0.05207$ $p = 0.8216$), with Sidak post-hoc correction ($p = 0.0054$ *and* 0.0025 *for left and right MHb slopes, respectively*). **d)** Connected pairs showing no difference in the rectification index between synapses receiving left and right MHb terminals; (W = 34.0, $n = 12$ *cells*, $p = 0.2036$, *Wilcoxon matched-pairs signed-rank test*). **e)** Representative traces showing AMPAR current at -60 mV (black) and NMDA receptor (NMDAR) current at +40 mV holding potentials. The vertical blue dashed line indicates a time point for measuring the isolated NMDAR component. **f)** Graph depicting the AMPA/NMDA ratio in synapses receiving left and right MHb terminals. The data suggests NMDARs are present on both sides, though at a low levels with no difference between synapses receiving left and right side-derived terminals; (W = 8.0, $n = 7$ *cells*, $p = 0.5781$, *Wilcoxon matched-pairs signed-rank test*). Box-and-whisker plots show the median, interquartile range (IQR), and whiskers extending to 1.5 times the IQR (Tukey method).

3.3 *Role of $GABA_B$ Receptors in Synaptic Modulation*

3.3.1 $GABA_BR$ activation disproportionately potentiates left MHb-originating EPSCs

In most brain regions, $GABA_BR$ activation reduces neurotransmitter release probability by inhibiting presynaptic calcium channels and promoting potassium efflux, thus diminishing synaptic transmission (Bowery and Brown 1997; Chalifoux and Carter 2011; Pin and Bettler 2016). In contrast, previous studies have demonstrated that baclofen, a $GABA_BR$ agonist, potentiates synaptic transmission in the MHb-IPN pathway by increasing Ca^{2+} influx at presynaptic terminals (Zhang et al. 2016; Koppensteiner, Melani, and Ninan 2017; Koppensteiner et al. 2024). To explore whether this potentiation shows input-side dependent difference, I stimulated left and right-derived fiber paths individually and recorded EPSC amplitudes in the absence and presence of baclofen (1 μM) (**Fig. 14a**). The potentiation ratio, obtained by dividing the EPSC amplitudes after baclofen application with the basal EPSC amplitudes, showed significantly higher degree of $GABA_BR$-mediated potentiation for the left than right inputs (**Fig. 14b**, W = -272.0, $n = 27$ *cells*, $p = 0.0006$, *Wilcoxon matched-pairs signed-rank test*) despite having similar basal release amplitudes (**Fig. 14c**).

3.3.2 $GABA_BR$ activation equalizes P_r and abolishes failures in left MHb inputs

I next analyzed how $GABA_BR$ activation impacted P_r and synaptic reliability. Under control conditions, left MHb inputs displayed a lower baseline P_r and more frequent transmission failures compared to the right side. The PPRs in the presence of baclofen showed no difference, indicating an equalization of P_r between left and right MHb inputs (**Fig. 14d**). One notable observation was the complete

abolishment of failures to evoke EPSC responses during $GABA_BR$-mediated potentiation in contrast to the basal state (**Fig. 14e**, *Left MHb:* $W = -78$, $n = 17$ *cells*, $p = 0.0005$; *Right MHb:* $W = -55$, $n = 17$ *cells*, $p = 0.0020$, *Wilcoxon matched-pairs signed-rank test*). Altogether, these data indicate that the left MHb-IPN pathway may play a key role in plasticity mechanisms for emotion regulation, while the right MHb pathway dominates in the basal state.

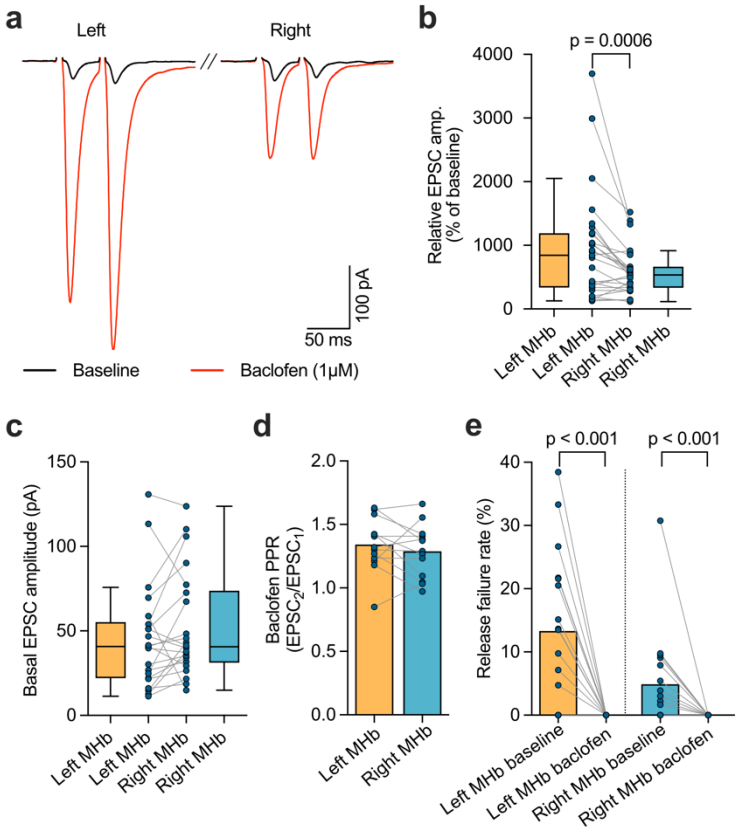

Figure 14: Asymmetrical $GABA_BR$-mediated potentiation of left and right MHb synapses.

a) Representative traces showing EPSCs recorded for left and right MHb-derived inputs before (black) and after (red) the application of baclofen (1 µM), a $GABA_B$ receptor ($GABA_BR$) agonist. The traces indicate drastic potentiation in response to $GABA_BR$ activation, with left inputs showing a greater EPSC increase compared to right inputs on the same postsynaptic neuron. **b)** Box plot with connected pairs showing the relative increase in EPSC amplitudes following baclofen treatment in left and right MHb-derived synapses in the rIPN. A significantly higher potentiation ratio was found in left than right MHb-derived synapses; ($W = -272.0$, $n = 27$ *cells*, $p = 0.0006$, *Wilcoxon matched-pairs signed-rank test*). **c)** No difference in the basal release EPSCs in the left and right MHb inputs in the same postsynaptic IPN neuron ($W = 95$, $n = 22$ *cells*, $p = 0.1289$, *Wilcoxon matched-pairs signed-rank test*). **d)** Comparison of the PPR between left and right MHb-derived synapses following baclofen application, showing similar PPRs following baclofen treatment; ($t = 1.018$, $df = 12$, $n = 13$ *cells*, $p = 0.3288$, *paired t-test*). **e)** Bar graph showing the complete abolishment of failed synaptic release events during baclofen treatment. Found decrease was much more prominent in the left inputs. No difference was found between left and right MHb inputs; (*Left MHb:* $W = -78$, $n = 17$ *cells*, $p = 0.0005$; *Right MHb:* $W = -55$, $n = 17$ *cells*, $p = 0.0020$, *Wilcoxon matched-pairs signed-rank test*). Box-and-whisker

plots show the median, interquartile range (IQR), and whiskers extending to 1.5 times the IQR (Tukey method).

3.3.3 Lateralization persists in i.v. situs solitus but not in i.v. situs inversus

To determine whether embryonic left-right patterning underlies the asymmetry in MHb-to-IPN synapses, I examined PPR ad baclofen sensitivity from i.v. mutants exhibiting either situs solitus or situs inversus. In i.v. animals with situs solitus, the PPR confirmed that left MHb terminals maintain a lower P_r than the right, mirroring wild-type (WT) results ($W = -189.0$, $n = 24$ *cells*, $p = 0.0065$, *Wilcoxon matched-pairs signed-rank test*; **Fig. 15a, left**). However, in i.v. animals displaying situs inversus, there was no significant difference in PPR between left and right terminals ($W = -102.0$, $n = 27$ *cells*, $p = 0.2268$, *Wilcoxon matched-pairs signed-rank test*; **Fig. 15a, right**).

I next examined the $GABA_BR$-mediated potentiation in these mutants. As in WT, i.v. animals with situs solitus showed a significantly higher potentiation ratio on the left side than on the right ($p = 0.0287$, $n = 5$ *cells*, *paired t-test*; **Fig. 15b, left**). In contrast, i.v. mutants with situs inversus displayed only a near-significant left-right difference ($W = -28.0$, $n = 8$ *cells*, $p = 0.0547$, *Wilcoxon matched-pairs signed-rank test*; **Fig. 15b, right**).

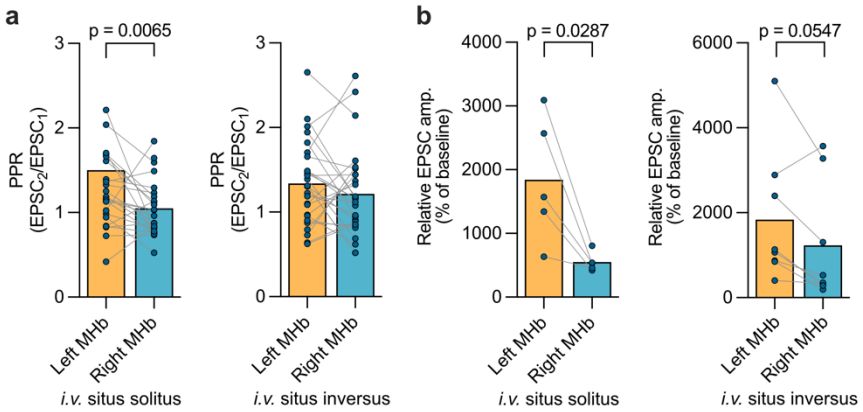

Figure 15: i.v. situs solitus follow WT P_r and $GABA_BR$-mediated potentiation pattern but not the i.v. situs inversus.

a) The Paired-pulse ratio (PPR) shows that a lower release probability (P_r) in left than right MHb terminals in i.v. situs solitus similar to WT ($W = -189.0$, $n = 24$ *cells*, $p = 0.0065$, *Wilcoxon matched-pairs signed-rank test*) but no difference in i.v. situs inversus; ($W = -102.0$, $n = 27$ *cells*, $p = 0.2268$, *Wilcoxon matched-pairs signed-rank test*). **b)** A significantly higher $GABA_BR$-mediated potentiation ratio was found in left than right MHb-derived synapses similar in i.v. situs solitus similar to WT ($p = 0.0287$, $n = 5$, *paired t-test*), *and close to significant* difference in i.v. situs inversus; ($W = -28.0$, $n = 8$ *cells*, $p = 0.0547$, *Wilcoxon matched-pairs signed-rank test*).

3.4 Role of Presynaptic Ca^{2+} in $GABA_BR$-Mediated Enhancement of Neurotransmitter Release

* This section is adapted from a part of a previous publication; $GABA_B$ receptors induce phasic release from medial habenula terminals through activity-dependent recruitment of release-ready vesicles. *Proceedings of the National Academy of Sciences of the United States of America*, 121(8), e2301449121.

To determine the contribution of presynaptic Ca^{2+} dynamics to the $GABA_BR$ induced increase in neurotransmitter release, we expressed an axon-targeted GCaMP6s sensor in cholinergic MHb neurons of ChAT-IRES-Cre mice. This was achieved through AAV-mediated transduction, enabling us to monitor presynaptic Ca^{2+} influx at MHb terminals in the IPN following stimulation of the FR.

Under control conditions, a 10 Hz, 3 s stimulation train increased presynaptic GCaMP6s fluorescence by approximately 4.0 ± 0.6-fold. In the presence of the $GABA_BR$ agonist baclofen, this response was significantly enhanced, reaching 6.5 ± 0.9-fold (n = 5 slices, 5 mice; **Fig. 16a-b**). Notably, such an increase in Ca^{2+}-dependent fluorescence is unexpected, as $GABA_BR$ activation typically inhibits presynaptic Ca^{2+} channels and no previous studies have reported GBR-mediated enhancements of Ca^{2+} influx in simplified or reconstituted model systems.

To explore potential mechanisms, we simulated the changes in presynaptic Ca^{2+} using our GCaMP6s data. We considered whether reduced buffering capacity could account for the observed increase, but simulations demonstrated that lowering Ca^{2+} buffering affinity led to prolonged decay times rather than the faster rise times we observed experimentally. Adjusting Ca^{2+} extrusion rates also failed to reproduce the baclofen-induced kinetics. Instead, a 2.3-fold increase in Ca^{2+} influx best recapitulated the enhanced peak GCaMP6s signal.

To test whether increased Ca^{2+} influx alone could induce the phasic release observed with $GABA_BR$ activation, we applied voltage-gated K^+ channel blockers (TEA-Cl and 4-AP) to boost Ca^{2+} entry. Although TEA/4-AP application increased spontaneous release and presynaptic Ca^{2+} signals, it neither induced phasic release nor occluded the baclofen effect (**Fig. 16c-g**). Thus, merely raising Ca^{2+} influx is insufficient to trigger phasic release, suggesting that $GABA_BR$-mediated enhancement involves additional molecular or positional factors.

We next considered the spatial coupling of vesicles to Ca^{2+} channels. Application of the slow Ca^{2+} chelator EGTA-AM (100 µM) after baclofen reduced the initial EPSC amplitude (EPSC1) by approximately 51.8 ± 2.1% (n = 8 cells, 4 mice; **Fig. 16h–j**), indicating that phasic release vesicles are loosely coupled to Cav2.3 channels. When EGTA-AM was applied before baclofen, it completely prevented the phasic release induction (**Fig. 16k-m**), supporting the idea that $GABA_BR$-

mediated phasic release recruits vesicles from more distant release sites, requiring Ca^{2+} diffusion away from the immediate channel vicinity. Consistent with this interpretation, Ca^{2+} imaging confirmed that EGTA-AM reduced stimulation-induced GCaMP6s fluorescence to near-baseline levels, and subsequent baclofen application failed to surpass these levels (**Fig. 16n-o**).

In summary, our results indicate that $GABA_BR$ activation in MHb terminals increases Ca^{2+} influx and mobilizes vesicles located beyond the tight coupling zone of presynaptic Ca^{2+} channels. This Ca^{2+}-dependent recruitment of loosely coupled vesicles is critical for phasic release induction. Importantly, increasing Ca^{2+} influx alone, without $GABA_BR$ activation, does not replicate these effects, suggesting that $GABA_BRs$ engage a more complex mechanism involving both altered Ca^{2+} signaling and specific vesicle recruitment strategies.

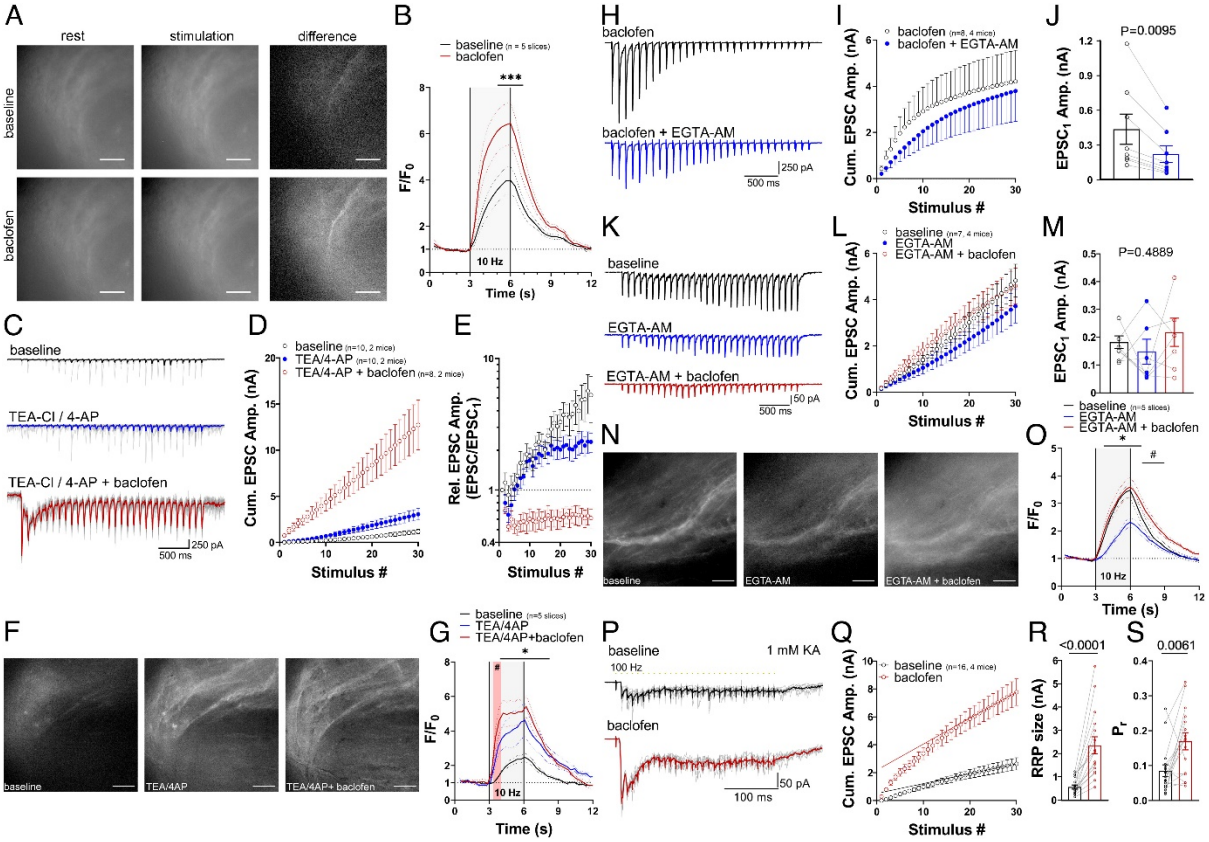

Figure 16: Role of presynaptic Ca^{2+} in tonic and phasic neurotransmission.

a) Example images of axon-GCaMP6s fluorescence at rest (Left) and at peak fluorescence during stimulation (Middle) under baseline (Top) and baclofen conditions (Bottom). Subtraction of resting fluorescence from peak fluorescence reveals stimulation-induced fluorescence increase in a subset of MHb axons (Right). (Scale bars, 50 µm.) **b)** Time course of GCaMP6s fluorescence change during stimulation under baseline and baclofen conditions in five slices from five mice. ***P < 0.001 two-way ANOVA with Bonferroni post hoc test; main effect of baclofen: $F_{(1,\ 328)} = 86.01$, P < 0.0001. **c-e)** K^+ channel blockers TEA and 4-AP did not induce phasic release and did not occlude phasic release induction by baclofen. Notice the increase in spontaneous EPSCs in the example traces **c** of TEA/4-AP and TEA/4-AP+baclofen groups before and after 10-Hz stimulation. **f)** The same as in A, at baseline

(Left), the application of TEA/4-AP (Middle) and TEA/4-AP + baclofen (Right). (Scale bars, 50 μm.) **g)** The time course of GCaMP6s fluorescence change reveals a significant increase in fluorescence by TEA/4-AP and TEA/4-AP + baclofen compared to baseline. TEA/4-AP and TEA/4-AP + baclofen groups only differed at the rising phase (red highlighted section) but not during peak fluorescence (Two-way ANOVA main factor of drug treatment: $F_{(2, 456)} = 107.4$, $P < 0.0001$; Tukey post hoc test: # indicates $P < 0.05$ between TEA/4-AP vs. TEA/4-AP + baclofen; * indicates $P < 0.05$ between baseline vs. TEA/4-AP and TEA/4-AP + baclofen). **h)** Example trace of a phasic response before and 10 min after the application of 100 μM EGTA-AM. **i)** Cumulative EPSC amplitude plot before and after EGTA-AM application. **j)** Phasic $EPSC_1$ amplitude was significantly reduced by EGTA-AM. $P = 0.0095$, calculated with the paired t test. **k-m** Application of EGTA-AM prior to baclofen prevents phasic release induction but does not significantly alter tonic $EPSC_1$ amplitudes. Repeated measures one-way ANOVA: $F_{(1.902, 11.41)} = 0.7478$, $P = 0.4889$. **n)** The same as in a, at baseline (Left), 15 min after the application of 100 μM EGTA-AM (Middle) and during the application of EGTA-AM + baclofen (Right). (Scale bars, 50 μm.) **o)** EGTA-AM significantly reduced GCaMP peak fluorescence compared to baseline (Two-way ANOVA main effect of treatment: $F_{(2, 492)} = 162.6$, $P < 0.0001$; * indicates $P < 0.05$ EGTA-AM vs. baseline and EGTA-AM + baclofen groups, Tukey post hoc test), whereas the addition of baclofen restored GCaMP peak fluorescence to baseline levels, but fluorescence decayed slower than baseline. # indicates $P < 0.05$ between EGTA-AM + baclofen vs. baseline and EGTA-AM, Tukey post hoc test. **p)** Example traces of EPSC responses during 100-Hz stimulation at baseline and after baclofen application. **q)** Baseline and baclofen cumulative EPSC amplitude plots with linear regression fit through the last 6 stimuli (#25 to #30). **r)** Paired comparison of RRP sizes before and after baclofen. $P < 0.0001$, Wilcoxon test. **s)** Paired comparison of P_r at baseline and after baclofen, $P = 0.0061$ calculated by the two-tailed paired t test. (Adapted from Koppensteiner at al. 2024)

3.5 *Behavioral Consequences of Asymmetric MHb Manipulations*

3.5.1 Chemogenetic inhibition of left MHb neurons selectively impairs fear recall

Based on my findings above showing enhanced plasticity in the left MHb-derived inputs, I hypothesized that the synaptic asymmetry may be involved in shaping behavioral functions. I focused on conditioned fear memories based on previous evidence showing a critical role for the MHb in the control of fear responses (Agetsuma et al. 2010; Zhang et al. 2016; Soria-Gómez et al. 2015; Duboué et al. 2017). To this end, I employed ChAT-IRES-Cre knock-in mice that were unilaterally injected with the Cre-dependent inhibitory DREADDs virus into the left or right MHb (**Fig. 19a-b; Fig. 17a**). This approach allowed me to achieve targeted silencing of cholinergic neurons via activation of inhibitory DREADDs with CNO. I first verified the efficacy of the inhibition by recording neuronal firing activity in acute brain slices derived from ChAT-IRES-Cre knock-in mice expressing the virus (**Fig. 17b**). Whole-cell voltage clamp and cell-attached recordings of mCherry-positive vMHb neurons showed that CNO administration significantly suppressed neural firing compared with the basal state (**Fig. 17c**), and its washout recovered the firing to the baseline state (**Fig. 17c-d**).

Next, I employed the cued fear-conditioning paradigm, in which adult ChAT-IRES-Cre knock-in mice expressing hM4Di-mCherry in the left or right vMHb were conditioned to associate a mild aversive foot shock with a discrete tone (**Fig. 19c-d**). For all groups, freezing responses increased across tone-shock trials, indicating successful acquisition of the conditioned stimulus - unconditioned stimulus (CS-US) association (*main effect of stimulus:* $F_{(3.038,\ 54.568)} = 31.857$ $p < 0.001$, *Repeated Measures* ANOVA (*Greenhouse-Geisser corrected*), (*Left MHb-vehicle*, $n = 4$; *Left MHb-CNO*, $n = 7$; *Right MHb-vehicle*, $n = 3$; *Right MHb-CNO*, $n = 8$, **Fig. 18a-b**). One day after the conditioning, CNO (i.p. 3 mg/kg) was injected into the mice 40 min before testing for cued memory recall in a different neutral context (Context B). Animals from all experimental groups showed minimal baseline freezing levels, indicating that the context itself was not aversive in itself and that the chemogenetic manipulation did not induce the generalization of fear responses. Freezing behavior increased significantly upon presentation of conditioned discrete tone stimulus in all groups (*main effect of side:* $F_{(1,18)} = 2.199$ $p = 0.155$; *main effect treatment:* $F_{(1,18)} = 3.199$ $p = 0.091$). However, the magnitude of fear responses was significantly weaker in the group expressing hM4Di in the left MHb compared with the vehicle control group (**Fig. 19e-f**; left), indicating that the acquired fear memory was not effectively expressed upon inhibition of left MHb neurons. In contrast, CS-evoked freezing levels in the group expressing hM4Di in the right MHb did not differ from those observed in the respective vehicle control group (**Fig. 19e-f**, right). Analyses of freezing levels to the CS and during ISI revealed a significant interaction between side and treatment (*side and treatment interaction:* $F_{(1,18)} = 8.217$ $p = 0.010$), which was attributed to significantly less freezing in the left MHb-CNO group (*left MHb-vehicle vs left MHb-CNO:* $p = 0.003$; *right MHb-vehicle vs right MHb-CNO:* $p = 0.472$, *Repeated measures* ANOVA *with Tukey's post-hoc comparison*). In addition, assessment of freezing levels specifically during the tone-CS indicated that inhibition of the left MHb attenuates CS-evoked fear responses (*main effect of side:* $F_{(1,18)} = 0.038$ $p = 0.848$, *main effect of treatment:* $F_{(1,18)} = 1.827$ $p = 0.193$, *side and treatment interaction:* $F_{(1,18)} = 3.404$ $p = 0.082$, *post-hoc comparison, left MHb-vehicle vs left MHb-CNO,* $p = 0.03$; *right MHb-vehicle vs right MHb CNO:* $p = 0.741$, *Two-Way ANOVA with Tukey's post-hoc comparison*, **Fig. 19g**). Taken together, the findings indicate that the vMHb is functionally lateralized in mice, and that the left MHb cholinergic neurons may exert a facilitatory role on cued fear memory recall.

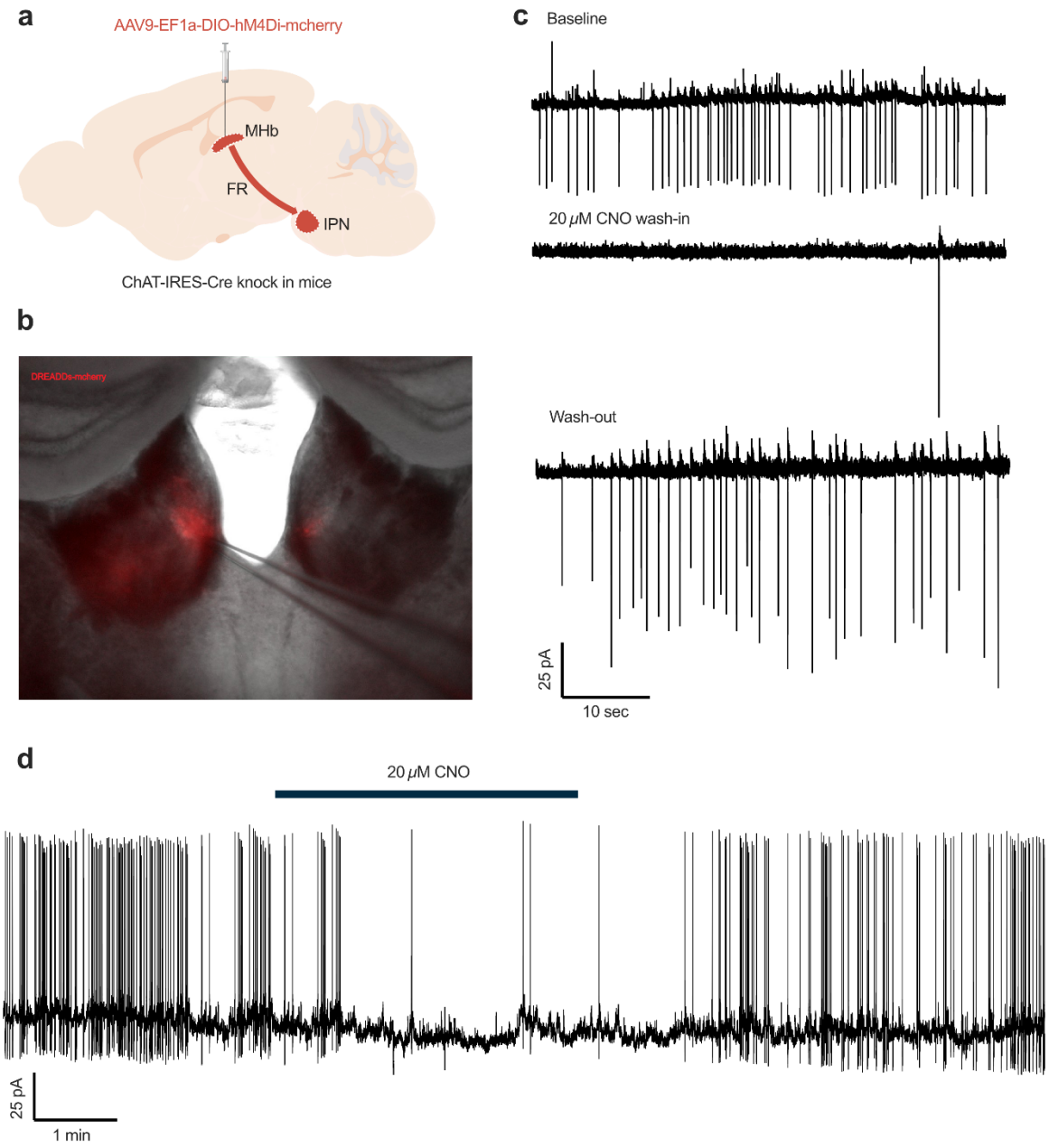

Figure 17: Activation of inhibitory DREADDs via CNO decreases the firing of MHb neurons in acute slices.

a) Schematic representation of the experimental procedure illustrating the injection of AAV9-EF1a-DIO-hM4Di-mCherry for expressing inhibitory DREADDs (hM4Di) in cholinergic neurons of the ventral medial habenula (vMHb) in ChAT-IRES-Cre knock-in mice. The targeted pathway from the MHb to the IPN via the FR is highlighted in red. **b)** A representative image of an injected acute brain slice shows that the recorded neurons express hM4Di-mCherry (red). **c)** Representative traces of neuronal firing recorded from hM4Di-mCherry-expressing MHb neurons in acute brain slices in cell-attached mode, showing firing activity during baseline, 20 µM CNO wash-in, and the subsequent wash-out period. The trace shows a robust decrease in neuronal firing upon CNO application into the bath, indicating effective activation of inhibitory DREADDs. **d)** A representative trace of an hM4Di-mCherry-expressing neuron in the whole-cell current-clamp mode showing the basal spontaneous activity, decreased firing during the CNO application, and the subsequent recovery after the wash-out period.

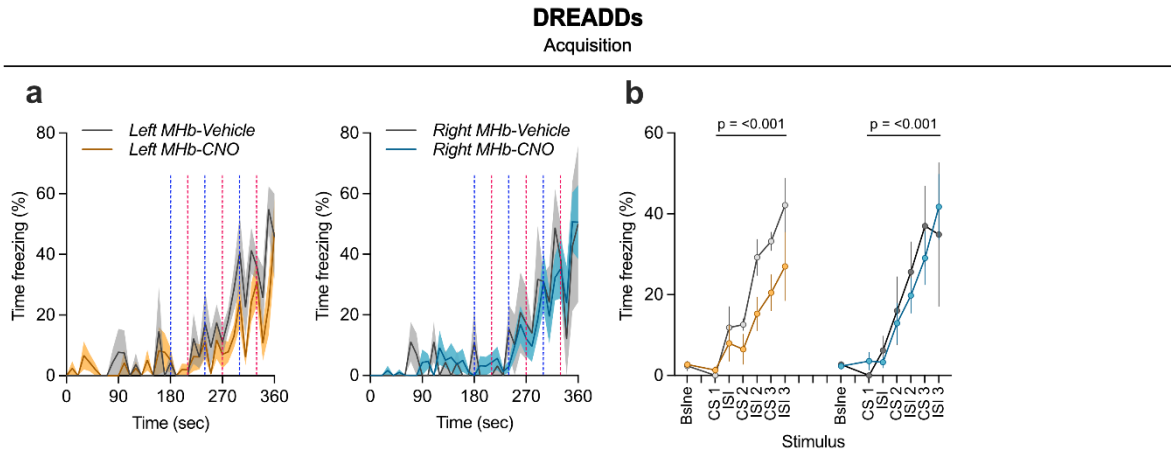

Figure 18: Intact acquisition of cued fear memory in DREADDs-injected ChAT-Cre mice.

a) Graphs showing time course of freezing behavior in 10 seconds bins during the acquisition phase of cued fear conditioning in mice injected with the hM4Di-mCherry-expressing AAV. Both vehicle-injected (gray, saline) and CNO-treated (orange, left; blue, right panel) groups show increasing freezing levels in response to co-terminating tone-shock pairings, indicating successful fear learning. **b)** The freezing time over conditioned stimuli (CS) and inter-stimulus intervals (ISI) during the fear acquisition phase. The data depicts a gradual increase in freezing with successive tone-shock pairings (CS1-ISI3) indicating similar learning curves in all the groups (*main effect of stimulus:* $F_{(3.038,\ 54.568)} = 31.857$, $p < 0.001$, *Repeated Measures ANOVA (Greenhouse-Geisser corrected)*). These results demonstrate that DREADDs-mediated inhibition in ChAT-Cre mice does not impair the acquisition of cued fear memory. Left MHb-vehicle, n = 4; Left MHb-CNO, n = 7; Right MHb-vehicle, n = 3; Right MHb-CNO, n = 8. The error bars are presented as ± SEM.

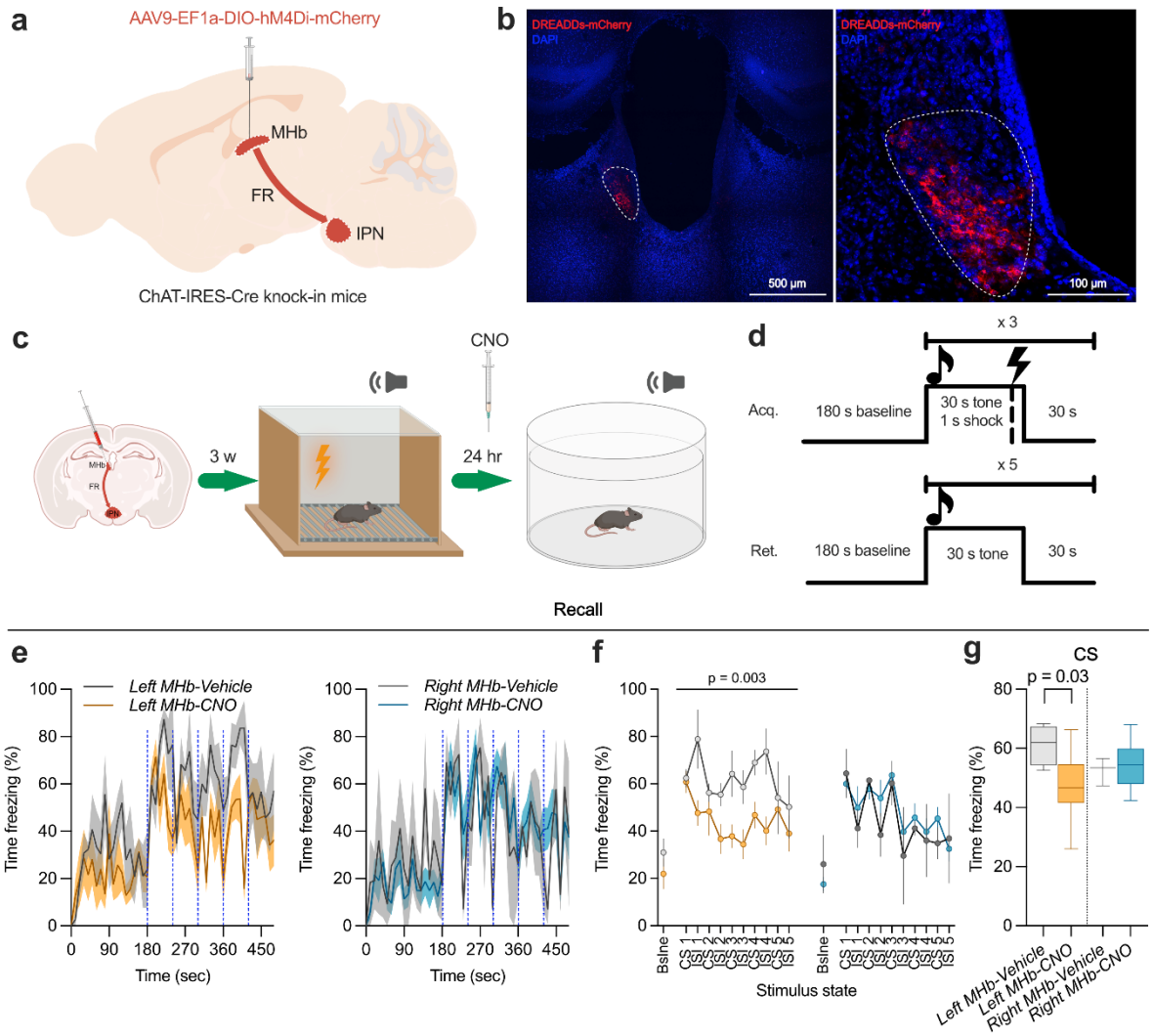

Figure 19: Chemogenetic inhibition of the left but not the right MHb cholinergic neurons attenuates fear response.

a) Schematic representation of the experimental design, showing the targeted chemogenetic inhibition of cholinergic neurons in the MHb using AAV9-EF1a-DIO-hM4Di-mCherry virus in ChAT-IRES-Cre knock-in mice. **b)** Representative confocal images of the injection site of the AAV in the vMHb, showing strong DREADD-mCherry expression (red) in the cholinergic vMHb neurons. **c)** Diagram showing the timeline of the viral injection, cued fear conditioning in context A on day 1, and retrieval in context B on day 2. CNO or vehicle (saline) was applied 24 hours after the conditioning and an hour before the recall, followed by re-exposure to the tone to assess freezing behavior. **d)** Protocol of the fear conditioning. Acquisition (Acq.) involved 3 minutes of baseline followed by five co-terminating tone-shock pairings. Recall (Ret.) was performed 24 hours later, with mice exposed to the tone without shock. **e)** Time course of freezing behavior in 10-second bins during recall following chemogenetic inhibition of the left MHb (left panel, orange) or the right MHb (right panel, blue), compared to vehicle controls. Vertical blue dashes indicate the presentation of the conditioned stimuli (CS, tone). Inhibition of the left but not right MHb reduced freezing time compared with the control. **f)** Freezing behavior across different stimulus states during fear memory recall. All groups show low freezing levels in the baseline habituation phase in context B. Over the CS and inter-stimulus intervals, left MHb inhibition (orange) shows reduced freezing compared to the control. Right MHb inhibition (blue) does not significantly alter freezing behavior (*main effect of side*: $F_{(1,18)}$ =

2.199, p= 0.155; *main effect treatment*: $F_{(1,18)}$ = 3.199, p= 0.091; *side and treatment interaction*: $F_{(1,18)}$ = 8.217 p= 0.010, *post-hoc comparison left MHb-vehicle vs left MHb-CNO*: p = 0.003; *right MHb-vehicle vs right MHb-CNO*: p = 0.472, *Repeated measures ANOVA with Tukey's post-hoc comparison*). The error bars are presented as ± SEM. **g)** Boxplot showing the freezing time percentage during the CS presentation. Inhibition of the left but not right MHb significantly reduced fear expression compared to vehicle controls (*main effect of side*: $F_{(1,18)}$ = 0.038, p = 0.848, *main effect of treatment*: $F_{(1,18)}$ = 1.827, p = 0.193, *side and treatment interaction*: $F_{(1,18)}$ = 3.404, p = 0.082, *post-hoc comparison, left MHb-vehicle vs left MHb-CNO*, p = 0.03; *right MHb-vehicle vs right MHb CNO*: p = 0.741, *Two-Way ANOVA with Tukey's post-hoc comparison*). Left MHb-vehicle, n = 4; Left MHb-CNO, n = 7; Right MHb-vehicle, n = 3; Right MHb-CNO, n = 8. The error bars are presented as ± SEM. Box-and-whisker plots show the median, interquartile range (IQR), and whiskers extending to the minimum and maximum values.

3.5.2 Conditional knockout of $GABA_BRs$ in left MHb reduces cued fear responses

Finally, given that left MHb inputs show a lower P_r but higher $GABA_BR$-mediated potentiation (**Fig. 14**), I investigated whether $GABA_BR$ signaling in the mouse MHb-IPN circuitry may be involved in the lateralized modulation of fear responses. I utilized Cre-expressing lentiviruses (LV-hSyn1-Cre-mCherry) to achieve conditional knockout of $GABA_BRs$ in the left or right MHb of adult $GABA_B1$ floxed mice (**Fig. 20a**). Three weeks following the virus delivery, I conducted immunohistochemical evaluation on brain slices derived from injected mice to verify the efficacy of the procedure. In the control group of $GABA_{B1}$ floxed mice injected with mCherry-expressing virus (LV-hSyn1-mCherry), targeted neurons co-expressed mCherry and $GABA_{B1}$ (**Fig. 20b**, left). By contrast, in the Cre-mCherry group, the complete absence of $GABA_BR$ expression in mCherry-positive cell bodies confirmed successful knockout of $GABA_{B1}$ in the targeted neurons (**Fig. 20b**, right). Visualization of MHb axonal terminals in the IPN showed that while mCherry-expressing axons in Cre-mCherry-injected mice were engulfed by $GABA_{B1}$-expressing fibers, no co-localization of the two signals was observed (**Fig. 20c**), further confirming the selective knockout of $GABA_{B1}$ in the targeted presynaptic terminals.

To address the relevance of $GABA_BRs$ in the MHb for fear memory, I employed again the cued fear-conditioning paradigm (**Fig. 21a-b**). During conditioned acquisition, all groups irrespective of the viruses or their injected side, showed a gradual increase in freezing responses with consecutive tone-shock pairings (*main effect of stimulus*: $F_{(3.318,\ 79.622)}$ = 56.174 p < 0.001, *Repeated Measures ANOVA (Greenhouse-Geisser corrected), Left MHb-mCherry*, n = 4; *Left MHb-Cre*, n = 6; *Right MHb-mCherry*, n = 6; *Right MHb-Cre* n = 12, **Fig. 20d-f**). Importantly, since targeted $GABA_BR$ knockout was conducted prior to testing, successful acquisition of the CS-US association indicated that targeted $GABA_{B1}$ knockout in the left or right MHb does not interfere with the ability to acquire fear memories. When tested for fear memory recall in a neutral context (Context B), mice that received

conditional $GABA_{B1}$ knockout in the left MHb demonstrated significantly less freezing than those in the mCherry group following the presentation of the CS (**Fig. 20g-h**, left). By contrast, conditional $GABA_{B1}$ knockout in the right MHb did not change cued fear recall compared with the mCherry control (*main effect of side*: $F_{(1, 24)} = 0.849$ $p = 0.366$; *main effect of virus*: $F_{(1, 24)} = 1.090$, $p = 0.307$, **Fig. 20g-h**, right). Analysis of freezing levels elicited by the CS and during ISI showed a near-significant interaction between the side and the virus (*Side and treatment interaction*: $F_{(1, 24)} = 3.927$, $p = 0.059$, *Left MHb-Cre vs Left MHb-mCherry*: $p = 0.068$; *Right MHb-Cre vs Right MHb-mCherry*: $p = 0.452$; *Repeated Measures ANOVA with Tukey's post-hoc comparison*). However, time freezing to the discrete tone only (**Fig. 20i**) was significantly shorter in the left MHb-Cre group compared to the control group (*main effect of side*: $F_{(1, 24)} = 0.009$, $p = 0.926$; *main effect of virus*: $F_{(1, 24)} = 1.601$, $p = 0.218$, *side and virus interaction*: $F_{(1, 24)} = 7.180$, $p = 0.013$; *Left MHb-Cre vs Left MHb-mCherry*: $p = 0.020$; *Right MHb-Cre vs Right MHb-mCherry*: $p = 0.260$; *Repeated Measures ANOVA with Tukey's post-hoc comparison*). To gain a better understanding of the fear memory phenotype, I evaluated the distribution of immobility events throughout the recall session (**Fig. 20j**). I found an increased amount of immobility events around 0.9-seconds which I then used as minimum freezing duration threshold. Additionally, I found that the decreased fear responses in left MHb-Cre mice stemmed from an overall decrease in the number of freezing episodes rather than a shortening in the duration of individual freezing bouts (*main effect of side*: $F_{(1, 24)} = 0.988$ $p = 0.330$; *main effect of virus*: $F_{(1, 24)} = 2.297$ $p = 0.143$, *side and virus interaction*: $F_{(1, 24)} = 6.055$ $p = 0.021$; *Left MHb-Cre vs Left MHb-mCherry*: $p = 0.019$; *Right MHb-Cre vs Right MHb-mCherry*: $p = 0.448$; *Repeated Measures ANOVA with Tukey's post-hoc comparison*; **Fig. 20j**, left). These outcomes support the results following chemogenetic inhibition of the left and right cholinergic MHb (**Fig. 19e-g**). Overall, our findings highlight lateralization of the mouse MHb, with the left MHb playing a key role in the modulation of conditioned fear responses via $GABA_BR$ signaling.

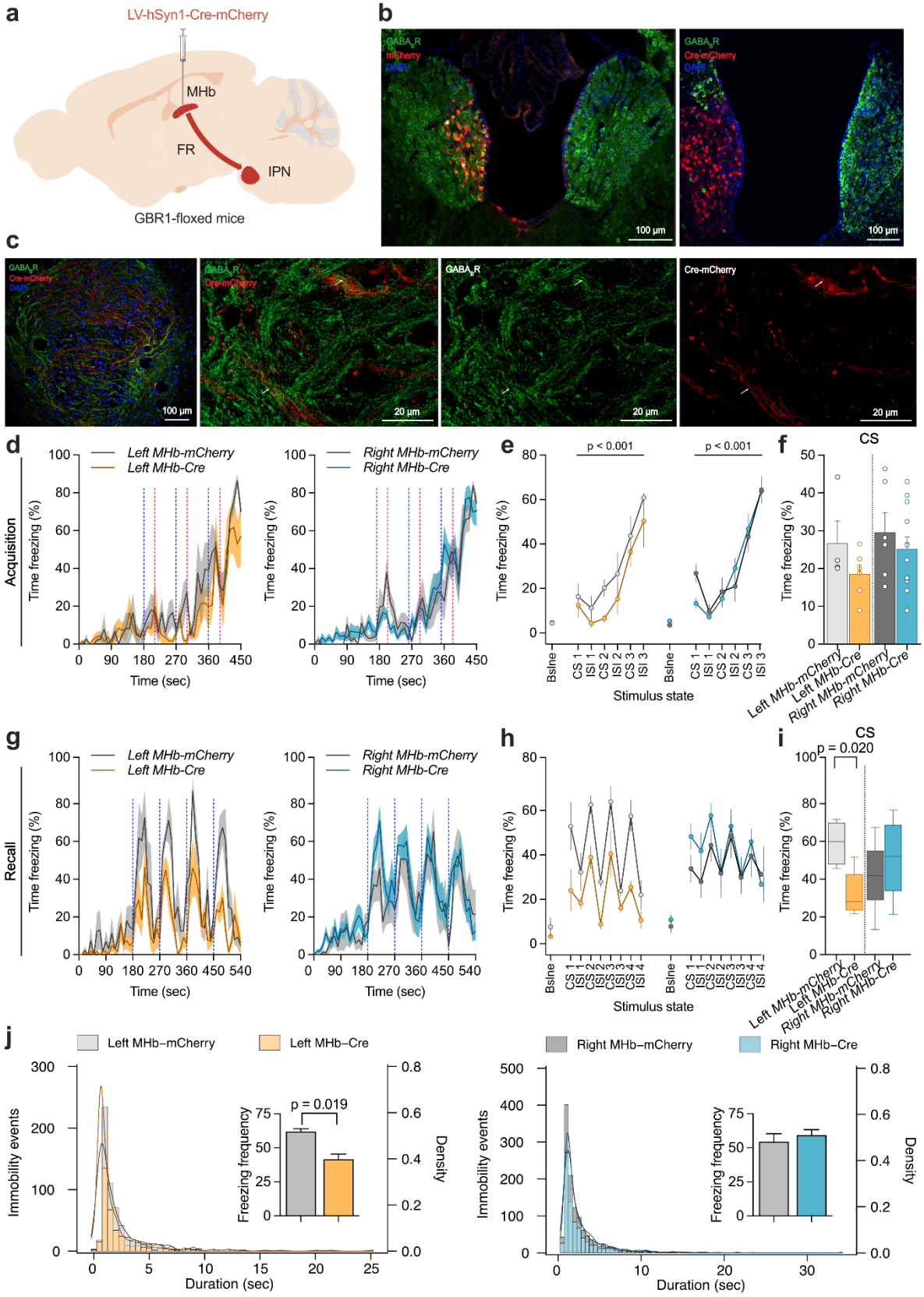

Figure 20: Conditional knock-out of $GABA_B1$ in left MHb neurons attenuates cued fear response.

a) Schematic of the experimental design for conditional $GABA_B$ receptor ($GABA_B1$) knock-out in MHb neurons using Cre-lox system and lentivirus-mediated (LV) Cre expression. Mice were injected with either a control virus (LV-hSyn1-mCherry) or a Cre-expressing virus (LV-hSyn1-Cre-mCherry) to conditionally knock-out $GABA_B1$ unilaterally in the targeted MHb neurons. The diagram illustrates the MHb projection to the IPN via the FR. **b)** Representative immunohistochemistry images showing successful knockout of $GABA_B1$ in the targeted ventral MHb neurons. In the control virus-infected MHb neurons, mCherry (red) is co-expressed with $GABA_B1$ (green) (left), whereas in Cre-expressing virus-infected neurons, no $GABA_B1$ immunoreactivity is observed in mCherry-positive cell bodies (right). **c)** Images of MHb axons and terminals in the rIPN showing no overlap of mCherry and $GABA_B1$ labeling (left). Higher magnification images demonstrate the absence of $GABA_B1$ immunoreactivity (green) in mCherry-Cre-expressing axons (red). **d)** Time course of freezing behavior in 10 seconds bins during the fear acquisition phase in $GABA_B1$ floxed (GBR1-floxed) mice injected with Cre-expressing lentivirus (LV-hSyn1-Cre-mCherry) or mCherry-expressing lentivirus (LV-hSyn1-mCherry) as a control. Both left MHb-Cre (orange, left panel) and right MHb-Cre (blue, right panel) groups show increasing freezing time over CS and ISI, indicating successful acquisition of fear memory. **e)** Analysis of freezing behavior across stimulus states for GBR1-floxed animals during fear acquisition. Both left and right Cre-injected animals exhibit increased freezing levels across successive tone-shock pairings, similar to controls, confirming effective learning (*main effect of stimulus:* $F_{(3.318, 79.622)} = 56.174$, $p < 0.001$, *Repeated Measures ANOVA (Greenhouse-Geisser corrected)*). **f)** Bar graph showing the percentage of freezing time during the conditioned stimulus (CS) presentation in the fear acquisition phase. These results demonstrate that the conditional $GABA_B1$ knock-out mice does not impair the acquisition of cued fear memory (*main effect of side:* $F_{(1, 24)} = 1.192$, $p = 0.286$; *main effect of virus:* $F_{(1, 24)} = 2.098$, $p = 0.160$, *side and virus interaction:* $F_{(1, 24)} = 0.188$, $p = 0.668$; *Left MHb-Cre vs Left MHb-mCherry:* $p = 0.245$; *Right MHb-Cre vs Right MHb-mCherry:* $p = 0.416$; *Repeated Measures ANOVA with Tukey's post-hoc comparison*). The error bars are presented as ± SEM. **g)** Time course of freezing behavior in 10 seconds bins during the cued fear recall phase. Vertical blue dashed lines indicate the conditioned stimuli (CS, tone) presentation. All groups show low levels of freezing in the baseline habituation phase in the context B. Left panel shows that conditional knock-out of $GABA_B1$ in the left MHb (orange) significantly reduced freezing behavior compared to the control mice over the conditioned stimuli (CS) and inter-stimulus intervals. Right panel shows that $GABA_B1$ knock-out in the right MHb (blue) does not significantly alter freezing behavior compared to the control. **h)** Analysis of freezing behavior across stimulus states during fear memory recall. Mice with left (orange) but not right (blue) MHb $GABA_B1$ knock-out show reduced freezing compared to respective controls (gray) (*main effect of side:* $F_{(1, 24)} = 0.849$, $p = 0.366$; *main effect of virus:* $F_{(1, 24)} = 1.090$, $p = 0.307$, *side and virus interaction:* $F_{(1, 24)} = 3.927$, $p = 0.059$; *Left MHb-Cre vs Left MHb-mCherry:* $p = 0.068$; *Right MHb-Cre vs Right MHb-mCherry:* $p = 0.452$; *Repeated Measures ANOVA with Tukey's post-hoc comparison*). **i)** Boxplot showing the average freezing time percentage across groups during CS. Knock-out of $GABA_B1$ in the left but not right MHb significantly reduced freezing behavior compared to the control (*main effect of side:* $F_{(1, 24)} = 0.009$, $p = 0.926$; *main effect of virus:* $F_{(1, 24)} = 1.601$, $p = 0.218$, *side and virus interaction:* $F_{(1, 24)} = 7.180$, $p = 0.013$; *Left MHb-Cre vs Left MHb-mCherry:* $p = 0.020$; *Right MHb-Cre vs Right MHb-mCherry:* $p = 0.260$; *Repeated Measures ANOVA with Tukey's post-hoc comparison*). **j)** All immobility event durations plotted as a histogram showing the number of immobility events per bin and the density curve (left panel, left MHb; right panel, right MHb). Density plot showing distinct freezing durations around 0.9-seconds, which is further used as freezing threshold. Bar graph showing the left but not right MHb-Cre group decreased the overall freezing episodes to CS and ISI rather than shortening individual episodes. (*main effect of side:* $F_{(1, 24)} = 0.988$, $p = 0.330$; *main effect of virus:* $F_{(1, 24)} = 2.297$, $p = 0.143$, *side and virus interaction:* $F_{(1, 24)} = 6.055$, $p = 0.021$; *Left MHb-Cre vs Left MHb-mCherry:* $p = 0.019$; *Right MHb-Cre vs Right MHb-mCherry:* $p = 0.448$; *Repeated Measures ANOVA with Tukey's post-hoc comparison*). Left MHb-mCherry, n = 4; Left MHb-Cre, n = 6; Right MHb-

mCherry, n = 6; Right MHb-Cre n = 12. Box-and-whisker plots show the median, interquartile range (IQR), and whiskers extending to the minimum and maximum values.

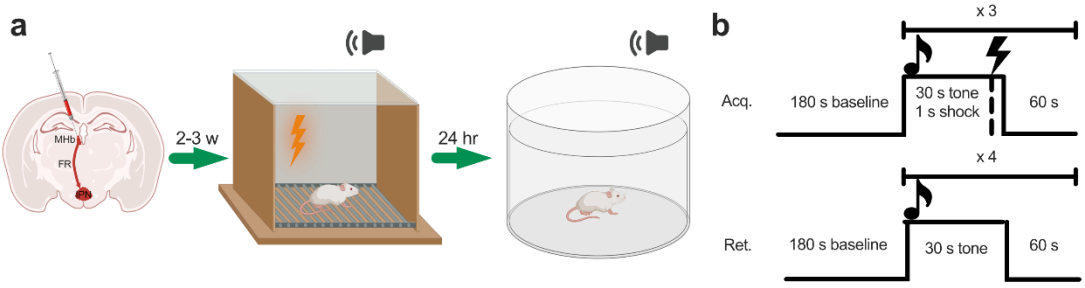

Figure 21: $GABA_BR$ knock-out experimental timeline and cued fear conditioning paradigm.

a) Diagram showing a timeline of the unilateral injection of Cre-expressing LV into the MHb with the pathway to the IPN via the FR, cued fear conditioning in context A on day 1, and memory recall in context B on day 2. **b)** The experimental protocol, including the acquisition (Acq., top) and recall (Ret., bottom) phases of cued fear conditioning, depicting 3 minutes of baseline habituation, conditioned stimuli (tone), unconditioned stimuli (foot shock), and the inter-trial interval with the number of repetitions.

4 Discussion and Conclusions

4.1 *Summary of Principal Findings*

In my project, I showed a previously unknown lateralization in the MHb-IPN pathway in the mouse. Specifically, I show that while individual rIPN neurons receive bilateral inputs from both the left and right MHb (**Fig. 11**), these inputs differ in fundamental ways. The left MHb synapses exhibit lower P_r under basal conditions (**Fig. 12**) and display a more pronounced potentiation upon $GABA_BR$ activation (**Fig. 14**), ultimately influencing fear memory expression. Chemogenetic inhibition or knocking out of $GABA_{B1}$ receptors selectively in the left MHb impairs conditioned fear responses (**Fig. 19-20**), establishing a link between these asymmetric synaptic properties and lateralized behavioral modulation.

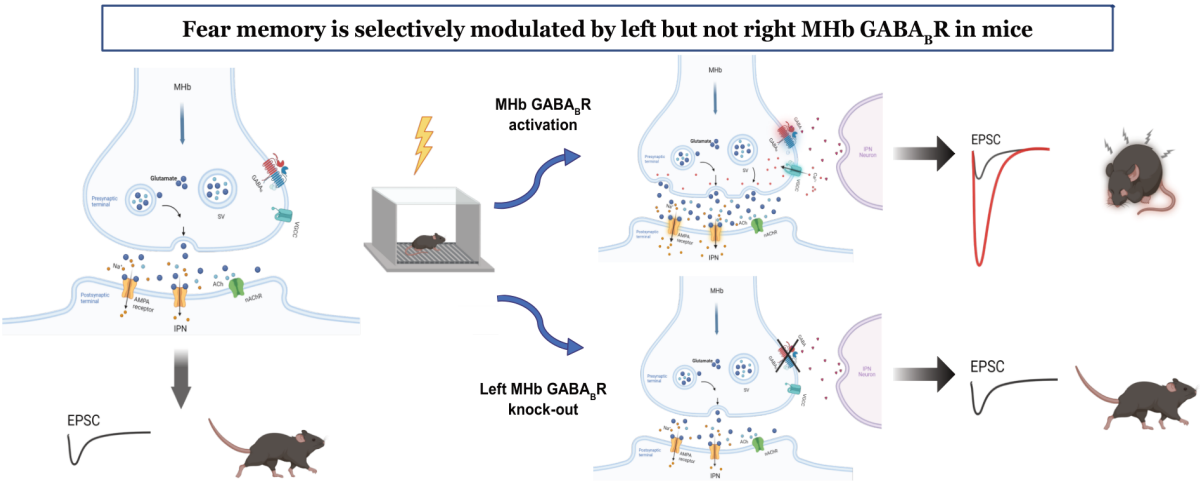

Figure 22: Schematic summary of the study.

4.1.1 Discovery of lateralized synaptic function in the mammalian MHb-IPN circuit

The major finding of my study is the identification of lateralized synaptic properties within the MHb-IPN pathway. Although the Hb has been known for its involvement in aversive behavior, stress response and anxiety (Murphy et al. 1996; E. H. Lee and Huang 1988; Hikosaka 2010), its hemispheric lateralization of anatomy and function, which is known in teleost species (Aizawa et al. 2005; Duboué et al. 2017; Dreosti et al. 2014) had not been well described in mammals. In particular, physiological lateralization at the synaptic level has never been studied. Previous research on mammalian MHb treated it as a symmetrical structure targeting it bilaterally, therefore, ignoring the possible hemispheric differences. Utilizing acute slice electrophysiology and slice calcium imaging, I provide the first evidence that the mammalian left and right MHb afferents, despite converging onto the same IPN neuron, are not functionally the same. I demonstrate that those inputs have different baseline P_r and show lateralized $GABA_BR$-mediated potentiation. Notably, no difference in postsynaptic receptor compositions such as CP-AMPAR or NMDAR was observed, indicating that the asymmetry originates solely from presynaptic mechanisms. Further analysis of P_r indicated that this lateralized synaptic function is robust across various experimental conditions (PPR, 50-Hz depletion, V-M), reflecting possible intrinsic differences in presynaptic architecture and/or local calcium dynamics. This side-dependent lateralization adds a new insight into the input-side dependent hemispheric asymmetry in synaptic connections.

4.1.2 Lower P_r and stronger $GABA_BR$-mediated potentiation on the left side

My findings indicate that the left input MHb-IPN synapses maintain a distinctly lower P_r under basal conditions compared to those originating from the right MHb (Fig. 2). Such intrinsic feature might help left MHb inputs to prevent overflooding the IPN neurons by acting as a filter. This reduced P_r under baseline conditions may translate into an increased capacity for short-term facilitation and dynamic adjustments in synaptic strength, allowing the left side to robustly respond to bursts of presynaptic activity or rhythmic firing (Zucker and Regehr 2002; Jackman and Regehr 2017).

Although $GABA_BRs$ typically inhibit VGCCs, reduce neurotransmitter release by limiting presynaptic calcium influx, enhance potassium efflux or drive presynaptic hyperpolarization (Chalifoux and Carter 2011; Pin and Bettler 2016), the MHb-IPN pathway presents a striking exception. Defying the canonical role of $GABA_BRs$ as inhibitory modulators, in this circuit, $GABA_BR$ activation paradoxically boosts vesicular release rather than suppressing it by augmenting

local calcium signaling and enhancing vesicle recruitment into the readily releasable pool (Bhandari et al. 2021; Koppensteiner et al. 2024; Zhang et al. 2016). Crucially, my findings indicate that this facilitation is more robust in the input from the left MHb, where basal P_r is lower and the presynaptic configuration is possibly more permissive to dynamic upregulation.

In effect, the stronger $GABA_BR$-mediated potentiation may serve to compensate for the lower basal P_r. My results show that during the $GABA_BR$ activation via agonist baclofen, both MHb inputs onto rIPN neurons show similar levels of PPRs, indicating equalized levels of P_r.

The observed higher level of potentiation in the left inputs could arise from differences in the influx of Ca^{2+} upon $GABA_BR$ activation. Such lateralized enhancements in local Ca^{2+} dynamics could be due to non-canonical disinhibition of Ca2.3 in the left MHb terminals by $GABA_BR$ activation. Although the precise molecular details remain to be fully determined, these results highlight an intriguing interplay between low P_r and dynamic receptor-mediated facilitation, underscoring a specialized form of presynaptic regulation in the MHb-IPN circuit.

4.1.3 Effect of *i.v.* mutation on habenular asymmetry

The observation that *i.v.* mutants with s.s. but not s.i. exhibit the same left–right differences in P_r and $GABA_BR$-mediated potentiation as WT supports the idea that normal left-sided embryonic signals are crucial for establishing normal lateralization in the MHb. Specifically, when internal organs show the typical left right arrangement, the left MHb retains its characteristic lower P_r and higher $GABA_BR$-induced facilitation. By contrast, *i.v.* mutants that display s.i. fail to show this usual or reversed left–right difference in P_r, and $GABA_BR$-mediated potentiation, implying that reversed nodal signaling can abolish the typical lateralization if the default mode of synaptic properties is asymmetric or at least cannot fully induce reversed MHb synaptic properties. One possibility is that in s.i. animals, both MHb hemispheres adopt either left-like or right-like features, showing the default mode of symmetrical synaptic properties.

Placing these findings in a broader developmental framework underscores how nodal flow and related left–right determination mechanisms influence MHb asymmetry in a manner distinct from visceral organ orientation. For example, in zebrafish carrying *i.v.* mutations, perturbations in nodal signaling and internal organ laterality can lead to reversed or randomized dHb asymmetry, with the epithalamic sidedness paralleling the internal organ arrangement (Levin 2005; Barth et al. 2005).In mammals, although left-right asymmetry of internal organs is similarly established by left–right dynein-dependent fluid flow at the embryonic node and subsequent nodal signaling (Hamada et al. 2002; Levin 2005; Nonaka et al. 2002), habenular asymmetries are comparatively subtle. The i.v. (inversus

viscerum) mouse line thus offers a unique perspective on whether disruptions in nodal flow might invert or diminish specific brain asymmetries (Kawakami et al. 2008).

Interestingly, the input side-dependent asymmetry in mouse hippocampus appears to be regulated by different mehanisms; *i.v.* mutants end up with a right-sided hippocampal phenotype, regardless of whether their internal organs are in s.s. or s.i. orientation. The MHb in mice may thus be more similar to the zebrafish dHb, where left–right patterning in this subcortical structure parallels the visceral axis at least in s.s. animals. Taken together, these results highlight how the embryonic nodal flow system can impart lateralized traits onto specific brain regions in a circuit specific manner. While one brain structure shows a fixed right-like bias in *i.v.* mutants, another circuit exhibits normal or no asymmetry following the normal or reversed nodal cues, respectively.

4.2 Mechanistic Insights into Lateralized Synaptic properties

4.2.1 Presynaptic scaffolding and active zone organization

A fundamental determinant of P_r is how presynaptic proteins assemble at the active zone. Proteins such as RIM, Munc13, Bassoon, and ELKS form a scaffold that controls vesicle docking, priming, and the precise positioning of VGCCs relative to these docked vesicles (Kaeser and Regehr 2014; Ackermann, Waites, and Garner 2015; Y. Han et al. 2011; Kaeser et al. 2011). Even slight differences in expression, phosphorylation states, or spatial distribution of these proteins between left and right MHb terminals could result in distinct P_r.

Vesicle Priming Factors:

Munc13, RIM, and related proteins govern vesicle priming, determining how readily vesicles transition into a ready to release state (Kaeser and Regehr 2014). Hemisphere specific variation, such as reduced Munc13-mediated priming on the left, could produce fewer vesicles in a readily releasable state at rest, lowering initial P_r. Simultaneously, a larger reservoir of vesicles available for rapid priming by $GABA_BR$ activation aligns well with potent facilitation observed on the left.

4.2.2 Calcium influx and Cav2.3 channels

A second key factor influencing P_r is the presynaptic calcium influx that triggers vesicle fusion. Although many brain regions employ multiple VGCC subtypes (P/Q, N and R type) to trigger exocytosis, MHb terminals uniquely and solely rely on Cav2.3 channels (Parajuli et al. 2012; Bhandari et al. 2021). This reliance underscores the impact of left-right differences in Cav2.3 channel properties, distribution, and regulation.

Reliance on a Single Channel Subtype (Cav2.3):

In circuits where multiple VGCCs contribute to release, the loss or modulation of one subtype can be partially compensated by others. However, in MHb synapses, subtle changes in Cav2.3 localization, gating properties, or associated modulatory proteins could alter basal P_r more significantly. If Cav2.3 in left MHb terminals exhibit channel properties that limit basal calcium entry, the lower P_r would remain under resting conditions since there is no other substituting channel.

Spatial Coupling to Docked Vesicles:

Even when Cav2.3 with the same channel properties is present on both the left and right input side synapses, their spatial arrangement relative to docked vesicles may differ. Active zone proteins could determine how far vesicles are located from Cav2.3 channels. For instance, if the left side has a loosely arranged organization of channels and vesicles, the local calcium microdomain around each channel may be less effective at triggering exocytosis compared to the right side, where channels and vesicles are more tightly coupled. A tight spatial coupling means that smaller changes in local calcium concentration can trigger exocytosis, whereas loose coupling makes basal P_r lower (Jackman and Regehr 2017). Under baseline conditions, this asymmetry would manifest as a lower P_r on the left side. However, under modulatory conditions that enhance calcium influx such as $GABA_BR$ activation, the left side could rapidly increase its release output, potentially matching or even surpassing the right side. This highlights how differences in calcium channel positioning, despite the presence of the same channel properties, can create functional asymmetry in synaptic release, which can be dynamically modulated by activity or $GABA_BR$ activation.

Channel Kinetics and Regulation:

Small hemisphere-dependent shifts in Cav2.3 inactivation, facilitation, or protein kinase regulation such as via phosphorylation by CaMKII or PKA could affect P_r. A Cav2.3 variant on the left side that inactivates more readily under low stimulation might minimize the basal release but may respond robustly to bursts or $GABA_BR$ activation to increase P_r.

4.2.3 Calcium sensors

Another explanation could be the molecular sensors that transduce calcium influx into vesicle fusion. Synaptotagmin isoforms, such as synaptotagmin 1, 7 or 9 differ in their calcium binding kinetics and cooperativity, thereby shaping whether release is fast and synchronous versus slow (Rizo and Rosenmund 2008; J. Xu, Mashimo, and Südhof 2007; Bacaj et al. 2013; Luo and Südhof 2017).

Synaptotagmin 1 vs. Slow Isoforms:

Synaptotagmin 1 typically drives rapid, synchronous release under brief calcium transients, whereas synaptotagmin 7 or 9 can promote asynchronous or facilitating release, especially during sustained or repetitive stimulation (Jackman and Regehr 2017). On the left side, a bias toward slower or lower affinity isoforms could decrease basal release events but amplify responsiveness during higher-frequency firing or $GABA_BR$ activation.

Isoform Interaction with Scaffolding Proteins:

Synaptotagmin isoforms exhibit distinct binding properties to presynaptic scaffolding components, shaping both vesicle docking and release probability. If the left MHb expresses isoforms that interact suboptimally at rest, baseline P_r would be lower. However, once calcium builds up via high-frequency firing or $GABA_BR$ actibation, these isoforms could achieve potentated fusion efficiency.

Taken together, differences in synaptotagmin expression or distribution could complement the organizational variations of scaffolding proteins and the reliance on Cav2.3 channels. This multifaceted interplay could establish how the left MHb maintains a lower P_r yet retains the potential for strong facilitation under $GABA_BR$ activation.

4.2.4 $GABA_BR$ Activation

Auxiliary Proteins and KCTD Subunits:

Variations in auxiliary proteins may explain why $GABA_BR$ potentiation is more pronounced on the left side. KCTD subunits, for instance, modulate $GABA_BR$ desensitization and kinetics (Rajalu et al. 2015). Differential KCTD expression or subunit composition could strengthen the receptor's facilitative effects on the left, whereas the right side might maintain modest response to $GABA_BR$ activation.

Number of $GABA_B$ Receptors:

One plausible mechanistic reason for the lateralized $GABA_BR$-mediated potentiation could be the differential number of receptors between the left and right MHb terminals. Specifically, the left MHb terminals may express a higher density of $GABA_BRs$ compared to the right side. Following the activation of the receptors via GABA, the asymmetry in receptor abundance would lead to a greater amount of calcium influx, higher amount of vesicle recruitment and eventually greater synaptic release in the left MHb terminals.

The two-pool hypothesis of vesicle dynamics:

Another possible explanation for the left MHb's enhanced facilitation is based on the two-pool hypothesis of vesicle dynamics (Koppensteiner et al. 2024). According to this model, the RRP consists of multiple subpopulations of vesicles, some tightly coupled to VGCCs and others more loosely coupled, supporting different release modes: tonic and phasic release, respectively (Koppensteiner et al. 2024). Under basal, low-frequency conditions, transmission primarily relies on a

small subset of tightly coupled vesicles within the RRP (tonic pool), and my results show that in this state, the RRP levels are similar for both left and right MHb inputs. However, the left side maintains a lower P_r, which may indicate a larger proportion of loosely coupled vesicles (phasic pool) that are recruited under normal conditions.

When $GABA_BRs$ are activated, these phasic pool vesicles become further mobilized, particularly in the left MHb terminals, leading to a pronounced potentiation of release. Koppensteiner et al. (2024) reported a four-fold increase in the RRP, supporting the idea that overall increase of the phasic pool in both sides may cancel the difference in P_r. However, $GABA_BR$ activation leads to a greater amount of potentiation in the left input compared to the right potentially because of a larger RRP recruitment in the left inputs, providing a mechanistic explanation for the observed asymmetry in synaptic facilitation.

4.3 *Developmental Mechanisms underlying Hb Asymmetry*

4.3.1 Hb asymmetry in zebrafish models

Nodal Signaling, Parapineal, and *i.v.*, *Tcf7l2* Mutants:

In zebrafish, the pronounced left-right asymmetry of the dHb, homologous to the mammalian MHb, arises from early developmental events driven by nodal signaling and the parapineal organ (Aizawa et al. 2005; Duboué et al. 2017; Dreosti et al. 2014). These embryonic processes establish differential gene expression and connectivity patterns between the left and right dHb, resulting in robust hemispheric specialization (Hüsken et al. 2014; Regan et al. 2009; Hong et al. 2013). Mutant lines provide deep insights into how this asymmetry is set:

Parapineal Knockout and Tcf7l2 Mutants:

Ablating the parapineal or disrupting *Tcf7l2* function abolishes or misdirects the usual left side bias of the dHb. In parapineal ablated zebrafish, for instance, the dHb often exhibits more right sided gene expression on both hemispheres (Duboué et al. 2017), indicating that local signals from the parapineal are crucial for establishing left-sided identity. Conversely, loss of Wnt singalling via *Tcf7l2* gene mutation leads to left isomerism (Hüsken et al. 2014; Hong et al. 2013).

4.3.2 Asymmetry in mammalian models

Mammalian Left-Right Axis and i.v. Mutant Mice:

In wild-type mice, synaptic plasticity and connectivity of pyramidal cells in the hippocampus show a left-right input bias. CA3–CA1 projections receiving the left input have distinct ionotropoic glutamate receptor compositions, size and LTP thresholds relative to those receiving the right input (Kawakami et al. 2003; Shinohara et al. 2008; Kawakami et al. 2008; Kohl et al. 2011). In *i.v.* mice, however, these normal asymmetries are disrupted, showing right-input phenotype on both

sides (right isomerism). If the MHb-IPN pathway behaves similarly, *i.v.* mice of both s.s. and s.i. phenotypes could have revealed abolished differences in P_r and $GABA_BR$–mediated potentiation between the left and right MHb. The partial loss of asymmetry in the MHb-IPN pathway suggests that, in contrast to zebrafish, the mammalian Hb likely attains its asymmetry through more indirect developmental cues. While nodal flow provides a broad left-right blueprint, region specific transcription factors or epigenetic regulators might subsequently refine lateralized features in the mouse MHb.

Implications of MHC Class I and Other Pathways:

Molecules like MHC Class I (MHCI) and their receptor PirB are involved in synaptic pruning and plasticity (Boulanger 2004; Ukai et al. 2017). It remains elusive whether hemisphere specific MHCI activity is involved in asymmetry formation in the mouse MHb-IPN circuit.

Exploring *i.v.* mutants, MHCI-related lines, or transcription factor knockouts in mice could reveal how visceral laterality is translated into the MHb asymmetry, bridging global left-right axis formation with the nuanced synaptic differences at play in the MHb-IPN axis.

4.4 Comparisons with Low P_r Synapses in Other Brain Regions

The functional significance of maintaining a low initial P_r is not unique to the MHb-IPN pathway. Similar low P_r configurations are found at multiple excitatory synapses throughout the brain, including cerebellar parallel fibers, hippocampal mossy fibers, and certain thalamocortical connections (Atwood and Karunanithi 2002; Jackman and Regehr 2017; Regehr 2012). In each of these circuits, a reduced basal P_r confers advantages for enhanced dynamic range and temporal fidelity, enabling synapses to respond robustly to short bursts of activity or to encode precise spiking patterns rather than individual action potentials.

For instance, cerebellar parallel fiber synapses rely on their low initial P_r to sustain temporal summation and short term facilitation, ultimately refining cerebellar output (Atluri and Regehr 1996; Regehr 2012). In the hippocampus, mossy fiber synapses that innervate CA3 pyramidal neurons also exhibit a low P_r, facilitating strong and frequency dependent plasticity. This allocates them as so called detonator synapses, capable of reliably eliciting postsynaptic firing once presynaptic input crosses a certain threshold (Salin et al. 1996; Vyleta, Borges-Merjane, and Jonas 2016). Thalamic inputs to cortical layer 4 neurons also often exhibit low P_r, allowing precise transmission of sensory stimuli. The facilitation profile ensures that only sustained or rhythmic activity (e.g., during attention) is amplified, filtering out sporadic noise (Béhuret, Deleuze, and Bal 2015).

In this low P_r framework, the presynaptic terminal acts as a dynamic filter, modulating incoming signals before they reach the postsynaptic terminal, which serves as a gain controller to adjust synaptic response. This highlights the importance of presynaptic plasticity in tuning synaptic transmission to neuronal activity patterns. This plasticity enhances dynamic range and adaptability, allowing synapses to respond robustly to specific activity patterns while filtering out noise (Tong, Emptage, and Padamsey 2020).

4.5 *Linking Synaptic Physiology to Behavioral Modulation*

4.5.1 MHb-IPN pathway and its role in fear behavior

Contrasts with Previous MHb Studies:

Zhang et al. (2016) performed bilateral manipulations of the MHb and observed a disruption in fear extinction (J. Zhang et al. 2016). By contrast, my unilateral approach highlights a specialized role for the left side in expressing acquired fear memory. The difference in these outcomes underscores that bilateral targeting can obscure hemisphere specific contributions, particularly in circuits where lateralization is subtle but consequential.

Soria-Gómez et al. (2015) demonstrated that indirect disinhibition of MHb terminals via bilateral CB_R1 disruption enhances the cholinergic output but not the glutamatergic signaling. This manipulation of the MHb terminals reduced the expression of fear conditioned freezing (Soria-Gómez et al. 2015), suggesting that the endocannabinoid system within the MHb modulates fear responses.

Yamaguchi et al. (2013) investigated the septo-habenular pathway's role in anxiety and fear by bilaterally ablating neurons in the triangular septum (TS) or the bed nucleus of the anterior commissure (BAC), which project to the ventral and dorsal MHb, respectively. Their findings revealed that ablation of TS-MHb projections impaired anxiety-like behaviors, while disruption of BAC-MHb pathways enhanced fear responses and learning (Yamaguchi et al. 2013). These results suggest that segregated inputs to the MHb via the septo-habenular pathway play specialized roles in modulating distinct emotional behaviors.

Lateralized Gain Control in Fear Memory Retrieval:

The left MHb plays a pivotal role in orchestrating fear memory recall by ensuring that aversive responses are expressed only when contextually appropriate. Unlike the right MHb, which does not modulate fear behavior in the same manner, the left side specifically gates the retrieval of fear-associated memories, preventing premature or exaggerated responses. This lateralization is underpinned by two key features: a low baseline P_r and a capacity for swift amplification via $GABA_BR$-mediated potentiation.

Under normal conditions, the left MHb outputs exhibit low baseline activity due to their low P_r that minimizes unnecessary excitatory output. This

conservative baseline ensures that fear responses are not inadvertently triggered in the absence of an immediate threat. However, when a fear inducing stimulus is encountered, the left MHb rapidly enhances its output. Its higher $GABA_BR$-mediated potentiation provides a swift gain, dramatically increasing synaptic release to align fear expression with the relevant cues. Such scenario highlights that the low baseline (low P_r and failed release events) and the capacity for rapid, high-gain potentiation via $GABA_BRs$ are essential for the precise regulation of fear expression.

Overall, this lateralized specialization likely offers an advantage, optimizing threat detection and ensuring that fear is manifested accurately and efficiently. It prevents the generalization of fear while enabling rapid defensive behavior in response to genuine threats, a balance that is critical for survival in unpredictable environments (Herry and Johansen 2014; Stephen Maren, Phan, and Liberzon 2013).

4.5.2 Consistency with literature on lateralization in emotion and associative learning

Hippocampal Lateralization Similarities and Differences:

Hemispheric differences also appear in other regions involved in emotion and memory, including the hippocampus and amygdala (Allen, Bobnar, and Kolber 2021; Kohl et al. 2011; Shinohara, Hosoya, and Hirase 2013). For example, left CA3 inputs to CA1 can have lower LTP thresholds and distinct receptor subunits, compared with right CA3 inputs (Kohl et al. 2011; Shinohara et al. 2008). This feature is similar to MHb-IPN lateralization where I show an input side-dependent laterization of basal P_r independent of the location of the postsynaptic IPN neuron. Another feature of hippocampal asymmetry is that synapses originating from the left CA3 contain higher GluN2B density, lower GluA1 density, and smaller postsynaptic sizes (Kawakami et al. 2003; Shinohara et al., 2008). This aspect is analogous to the greater potentiation of left MHb inputs, potentially due to a higher density of $GABA_B$ receptors in the left-originating terminals. Regarding memory formation and expression, silencing the left, but not the right, CA3 impairs working memory and spatial memory retrieval (Shipton et al. 2014; Song et al. 2020). This closely resembles the MHb-IPN pathway, where inhibition of the left MHb or knockout of $GABA_BRs$ on the left side, but not the right, reduces fear memory expression. One stark difference between the lateralization of these pathways is the site of asymmetry; postsynaptic in the hippocampus, and presynaptic in the MHb-IPN pathway.

Amygdalar Lateralization:

The amygdala is another well-described lateralized brain structure within the limbic system (Carrasquillo and Gereau 2008; Jeong Seok Han and Neugebauer

2004; G. Ji and Neugebauer 2009). It plays a key role in emotional and behavioral regulation, as well as pain processing (Neugebauer et al. 2004; Allen, Bobnar, and Kolber 2021). The right central nucleus of the amygdala (CeA) exhibits a predominantly pro-nociceptive function across different pain models (Carrasquillo and Gereau 2007; G. Ji and Neugebauer 2009). The right side plays a pivotal role in modulating pain responses, particularly in conditions of acute and chronic pain (Neugebauer and Li 2003; Jeong Seok Han and Neugebauer 2004). Activation of the right amygdala increases pain-like behaviors, with enhanced nociceptive transmission from the parabrachial nucleus to the CeA (Miyazawa et al. 2018; S. Han et al. 2015). In response to pain, right amygdala activation is consistently higher than left amygdala activation when exposed to noxious stimuli (Miyazawa et al. 2018). Neuroimaging studies further confirm that the right amygdala is more responsive to experimentally induced pain (Arimura et al. 2019). Furthermore, blocking ERK1/2 phosphorylation in the right CeA, but not the left, reduces pain-related behaviors in mice (Carrasquillo and Gereau 2008, 2007). Meanwhile, the left CeA is thought to have an anti-nociceptive role, particularly in bladder pain models, and has also been linked to the stress response (Sadler et al. 2017). This left-sided lateralization of amygdalar circuitry parallels the MHb-IPN pathway's lateralization, where I observed stark differences in P_r and greater $GABA_BR$-mediated potentiation on the left side. It is possible that as right CeA evolved to be involved in nociception and pain, the left MHb evolved to be involved in fear behavior.

4.5.3 Evolutionary and adaptive implications of hemispheric specialization

From an evolutionary standpoint, lateralization is posited to increase processing capacity and efficiency, reducing redundancy while facilitating parallel handling of emotional or cognitive tasks (Robins and Rogers 2002). Such specialization could have arisen in response to ecological pressures demanding quick predator avoidance or nuanced social interactions. Over time, these subtle asymmetries may have been maintained and refined, enabling organisms to deploy emotional responses with high specificity, minimal energy, and improved adaptive fitness.

MHb-IPN Lateralization:

By showing that presynaptic differences on the left MHb confer a heightened capacity for fear memory retrieval, my findings offer a compelling example of how lateralization can serve discrete, evolutionary relevant functions. Much as the zebrafish dHb uses left-right differences to modulate avoidance behaviors, the mammalian MHb-IPN circuit may exploit similar principles on a more subtle scale,

providing an evolutionarily conserved mechanism for precise and context-dependent emotional regulation (Aizawa et al. 2005; Duboué et al. 2017).

General Utility of Lateralization:

Taken as a whole, the evidence from mammalian subcortical structures (including the MHb-IPN pathway) and from non-mammalian models (like zebrafish) reveals that lateralization can enhance behavioral flexibility. Rather than view these asymmetries as mere coincidence, my data support the broader concept that hemispheric differences can tune synaptic output to align with cognitive and emotional demands. In so doing, they amplify the brain's capacity for rapid and complex responses, particularly vital for survival in uncertain or threatening environments.

Collectively, such hemispheric specialization likely enhances computational efficiency, assigning each hemisphere or nucleus a distinct yet complementary role. By utilizing the same structure in both hemispheres, the brain can leverage lateralization to effectively double its neural representation resources. This allows the same neuronal ensemble to encode and/or decode different memories and behaviors, optimizing information processing. As a result, the organism can process more information at a faster rate while utilizing limited neural resources efficiently.

My findings not only expand our understanding of the habenula's role in aversive learning but also illustrate how subtle hemisphere specific synaptic features can have substantial behavioral ramifications, reinforcing the broader principle that lateralization is a fundamental aspect of vertebrate brain organization.

4.6 *Limitations, Open Questions, and Future Directions*

4.6.1 Molecular determinants of synaptic asymmetry

While my findings highlight lateralized differences in P_r and $GABA_BR$-mediated potentiation in the MHb-IPN pathway, the precise molecular underpinnings remain to be elucidated. Although differences in presynaptic scaffolding proteins, synaptotagmin isoforms, Cav2.3, and active zone composition could be potentially involved, their specific contributions remain untested. Quantifying systematically the expression and organization of these scaffolding components in left versus right MHb terminals could directly test whether the left side's lower P_r stems from subtle architectural divergences in the active zone. Single-cell transcriptomics, super-resolution imaging, and targeted proteomic analyses could help pinpoint the molecular architecture responsible for lateralization. Additionally, investigating whether post-translational modifications, such as phosphorylation states or differential local signaling cascades, contribute to hemispheric specialization may yield deeper mechanistic

insights. Understanding these molecular determinants would provide a more comprehensive picture of how subtle biochemical gradients translate into meaningful functional asymmetries in emotional circuits.

4.6.2 Extending investigations beyond fear to other emotional states

This work focuses on fear conditioning and the recall of aversive memories, but the MHb-IPN pathway's role may extend beyond fear related behaviors. It is possible that lateralized synaptic properties could also influence how organisms respond to other emotional states, such as anxiety, reward processing, or stress resilience. Future experiments could incorporate paradigms that test anxiolytic behaviors, motivational tasks, or social interactions to determine whether the observed asymmetry generalizes to a broader spectrum of affective and cognitive processes. By expanding beyond fear, we may uncover principles of hemispheric specialization in subcortical circuits and gain a more holistic understanding of the MHb-IPN pathway's multifaceted contributions to emotional regulation.

4.6.3 Translational potential for understanding lateralized circuit dysfunctions

Dysregulation of fear responses and emotional processing underlies numerous psychiatric conditions, including anxiety disorders, post-traumatic stress disorder, and mood disorders (Ressler and Mayberg 2007; Pitman et al. 2012). If lateralized synaptic properties contribute to the fine-tuning of emotional responses, then pathological disruptions to this balance could lead to abnormal fear generalization or impaired extinction of aversive memories. Investigating whether lateralization is altered in animal models of psychopathology, or examining post-mortem human tissue for molecular asymmetries, could inform translational research.

In addition, identifying pharmacological or genetic tools that selectively target the molecular components of lateralized synapses might open new avenues for therapeutic intervention. Manipulating the balance of left-right MHb signaling or the potency of $GABA_BR$-mediated facilitation could help restore appropriate emotional responses in individuals suffering from excessive fear or anxiety.

4.7 *Conclusions*

This study embarks several conclusions; First, the discovery of lateralized synaptic function in the MHb-IPN pathway challenges the conventional view that the MHb is a bilaterally uniform structure in mammals. Second, the demonstration that the left MHb terminals exhibiting lower basal P_r yet showing greater $GABA_BR$-mediated potentiation (being uniquely excitatory), highlights the complexity of synaptic modulation in this pathway. Such a synaptic configuration equips the left

MHb with a dynamic gain control mechanism, enabling it to swiftly increase synaptic output and strength under conditions requiring a precise and adaptive fear response. Third, showing that unilateral inhibition or knocking out $GABA_BR$ in the left MHb, link the synaptic lateralization to a behavioral outcome, highlighting how such synapse level asymmetries can confer functional advantages to organisms to efficiently distinguish among the salient and threatening cues and respond accordingly.

Finally, this work opens new avenues for future research: Determining the molecular mechanisms of MHb lateralization and its formation from a developmental aspect: Examining whether the MHb asymmetry plays a role in different behaviors. With the advanced technology, it might be feasible to harness knowledge of this laterality for clinical research and treatment of stress, anxiety related disorders.

By uncovering lateralized synaptic mechanism in the MHb-IPN pathway, this dissertation adds a new dimension to the study of fear and emotion, underscoring the intricate interplay between molecular specialization, hemispheric differences and adaptive behavior.

References

Ables, Jessica L., Kwanghoon Park, and Inés Ibañez-Tallon. 2023. "Understanding the Habenula: A Major Node in Circuits Regulating Emotion and Motivation." *Pharmacological Research: The Official Journal of the Italian Pharmacological Society* 190 (106734): 106734.

Ackermann, Frauke, Clarissa L. Waites, and Craig C. Garner. 2015. "Presynaptic Active Zones in Invertebrates and Vertebrates." *EMBO Reports* 16 (8): 923–38.

Agetsuma, Masakazu, Hidenori Aizawa, Tazu Aoki, Ryoko Nakayama, Mikako Takahoko, Midori Goto, Takayuki Sassa, et al. 2010. "The Habenula Is Crucial for Experience-Dependent Modification of Fear Responses in Zebrafish." *Nature Neuroscience* 13 (11): 1354–56.

Aizawa, Hidenori, Isaac H. Bianco, Takanori Hamaoka, Toshio Miyashita, Osamu Uemura, Miguel L. Concha, Claire Russell, Stephen W. Wilson, and Hitoshi Okamoto. 2005. "Laterotopic Representation of Left-Right Information onto the Dorso-Ventral Axis of a Zebrafish Midbrain Target Nucleus." *Current Biology : CB* 15 (3): 238–43.

Aizawa, Hidenori, Midori Goto, Tomomi Sato, and Hitoshi Okamoto. 2007. "Temporally Regulated Asymmetric Neurogenesis Causes Left-Right Difference in the Zebrafish Habenular Structures." *Developmental Cell* 12 (1): 87–98.

Aizawa, Hidenori, Megumi Kobayashi, Sayaka Tanaka, Tomoki Fukai, and Hitoshi Okamoto. 2012. "Molecular Characterization of the Subnuclei in Rat Habenula." *The Journal of Comparative Neurology* 520 (18): 4051–66.

Allen, Heather N., Harley J. Bobnar, and Benedict J. Kolber. 2021. "Left and Right Hemispheric Lateralization of the Amygdala in Pain." *Progress in Neurobiology* 196 (101891): 101891.

Arimura, Daigo, Kei Shinohara, Yukari Takahashi, Yae K. Sugimura, Mariko Sugimoto, Tomokazu Tsurugizawa, Keishi Marumo, and Fusao Kato. 2019. "Primary Role of the Amygdala in Spontaneous Inflammatory Pain-Associated Activation of Pain Networks - A Chemogenetic Manganese-Enhanced MRI Approach." *Frontiers in Neural Circuits* 13 (October): 58.

Atluri, P. P., and W. G. Regehr. 1996. "Determinants of the Time Course of Facilitation at the Granule Cell to Purkinje Cell Synapse." *The Journal of*

Neuroscience: The Official Journal of the Society for Neuroscience 16 (18): 5661–71.

Atwood, Harold L., and Shanker Karunanithi. 2002. "Diversification of Synaptic Strength: Presynaptic Elements." *Nature Reviews. Neuroscience* 3 (7): 497–516.

Bacaj, Taulant, Dick Wu, Xiaofei Yang, Wade Morishita, Peng Zhou, Wei Xu, Robert C. Malenka, and Thomas C. Südhof. 2013. "Synaptotagmin-1 and Synaptotagmin-7 Trigger Synchronous and Asynchronous Phases of Neurotransmitter Release." *Neuron* 80 (4): 947–59.

Barth, K. Anukampa, Adam Miklosi, Jenny Watkins, Isaac H. Bianco, Stephen W. Wilson, and Richard J. Andrew. 2005. "Fsi Zebrafish Show Concordant Reversal of Laterality of Viscera, Neuroanatomy, and a Subset of Behavioral Responses." *Current Biology: CB* 15 (9): 844–50.

Bassetti, Davide. 2022. "Keeping the Balance: GABAB Receptors in the Developing Brain and Beyond." *Brain Sciences* 12 (4): 419.

Béhuret, Sébastien, Charlotte Deleuze, and Thierry Bal. 2015. "Corticothalamic Synaptic Noise as a Mechanism for Selective Attention in Thalamic Neurons." *Frontiers in Neural Circuits* 9 (December): 80.

Benarroch, Eduardo E. 2012. "GABAB Receptors: Structure, Functions, and Clinical Implications." *Neurology* 78 (8): 578–84.

Betke, Katherine M., Christopher A. Wells, and Heidi E. Hamm. 2012. "GPCR Mediated Regulation of Synaptic Transmission." *Progress in Neurobiology* 96 (3): 304–21.

Bettler, Bernhard, and Jim Yu-Hsiang Tiao. 2006. "Molecular Diversity, Trafficking and Subcellular Localization of GABAB Receptors." *Pharmacology & Therapeutics* 110 (3): 533–43.

Bhandari, Pradeep, David Vandael, Diego Fernández-Fernández, Thorsten Fritzius, David Kleindienst, Cihan Önal, Jacqueline Montanaro, et al. 2021. "GABAB Receptor Auxiliary Subunits Modulate Cav2.3-Mediated Release from Medial Habenula Terminals." *ELife* 10 (April): 1–28.

Bianco, Isaac H., and Stephen W. Wilson. 2009. "The Habenular Nuclei: A Conserved Asymmetric Relay Station in the Vertebrate Brain." *Philosophical Transactions of the Royal Society of London. Series B, Biological*

Sciences 364 (1519): 1005–20.

Bliss, T. V., and G. L. Collingridge. 1993. "A Synaptic Model of Memory: Long-Term Potentiation in the Hippocampus." *Nature* 361 (6407): 31–39.

Boulanger, Lisa M. 2004. "MHC Class I in Activity-Dependent Structural and Functional Plasticity." *Neuron Glia Biology* 1 (3): 283–89.

Bowery, N. 1989. "GABAB Receptors and Their Significance in Mammalian Pharmacology." *Trends in Pharmacological Sciences* 10 (10): 401–7.

Bowery, N. G. 1993. "GABAB Receptor Pharmacology." *Annual Review of Pharmacology and Toxicology* 33: 109–47.

Bowery, N. G., and D. A. Brown. 1997. "The Cloning of GABA(B) Receptors." *Nature*.

Bowery, N. G., D. R. Hill, A. L. Hudson, A. Doble, D. N. Middlemiss, J. Shaw, and M. Turnbull. 1980. "(-)Baclofen Decreases Neurotransmitter Release in the Mammalian CNS by an Action at a Novel GABA Receptor." *Nature* 283 (5742): 92–94.

Bromberg-Martin, Ethan S., and Okihide Hikosaka. 2011. "Lateral Habenula Neurons Signal Errors in the Prediction of Reward Information." *Nature Neuroscience* 14 (9): 1209–16.

Broussard, Gerard Joey, Yajie Liang, Marina Fridman, Elizabeth K. Unger, Guanghan Meng, Xian Xiao, Na Ji, Leopoldo Petreanu, and Lin Tian. 2018. "In Vivo Measurement of Afferent Activity with Axon-Specific Calcium Imaging." *Nature Neuroscience* 21 (9): 1272–80.

Bühler, Anja, and Matthias Carl. 2021. "Zebrafish Tools for Deciphering Habenular Network-Linked Mental Disorders." *Biomolecules* 11 (2): 324.

Calver, A. R., C. H. Davies, and M. Pangalos. 2002. "GABA(B) Receptors: From Monogamy to Promiscuity." *Neuro-Signals* 11 (6): 299–314.

Carrasquillo, Yarimar, and Robert W. Gereau 4th. 2007. "Activation of the Extracellular Signal-Regulated Kinase in the Amygdala Modulates Pain Perception." *The Journal of Neuroscience: The Official Journal of the Society for Neuroscience* 27 (7): 1543–51.

———. 2008. "Hemispheric Lateralization of a Molecular Signal for Pain Modulation in the Amygdala." *Molecular Pain* 4 (June): 24.

Cetin, Ali, Shoji Komai, Marina Eliava, Peter H. Seeburg, and Pavel Osten. 2006. "Stereotaxic Gene Delivery in the Rodent Brain." *Nature Protocols* 1 (6): 3166–73.

Chalifoux, Jason R., and Adam G. Carter. 2011. "GABAB Receptor Modulation of Voltage-Sensitive Calcium Channels in Spines and Dendrites." *The Journal of Neuroscience: The Official Journal of the Society for Neuroscience* 31 (11): 4221–32.

Chater, Thomas E., and Yukiko Goda. 2014. "The Role of AMPA Receptors in Postsynaptic Mechanisms of Synaptic Plasticity." *Frontiers in Cellular Neuroscience* 8 (November): 401.

Chebib, M., and G. A. Johnston. 1999. "The 'ABC' of GABA Receptors: A Brief Review." *Clinical and Experimental Pharmacology & Physiology* 26 (11): 937–40.

Choi, Jung-Hwa, Erik R. Duboue, Michelle Macurak, Jean-Michel Chanchu, and Marnie E. Halpern. 2021. "Specialized Neurons in the Right Habenula Mediate Response to Aversive Olfactory Cues." *ELife* 10 (December). https://doi.org/10.7554/eLife.72345.

Choquet, Daniel, and Antoine Triller. 2013. "The Dynamic Synapse." *Neuron* 80 (3): 691–703.

Citri, Ami, and Robert C. Malenka. 2008. "Synaptic Plasticity: Multiple Forms, Functions, and Mechanisms." *Neuropsychopharmacology : Official Publication of the American College of Neuropsychopharmacology* 33 (1): 18–41.

Concha, M. L., and S. W. Wilson. 2001. "Asymmetry in the Epithalamus of Vertebrates." *Journal of Anatomy* 199 (Pt 1-2): 63–84.

Concha, Miguel. 2016. "An Evolutionary Perspective on Habenular Asymmetry in Humans." *Journal of Neurology and Neuromedicine* 1 (8): 44–50.

Concha, Miguel L., Isaac H. Bianco, and Stephen W. Wilson. 2012. "Encoding Asymmetry within Neural Circuits." *Nature Reviews. Neuroscience* 13 (12): 832–43.

Contestabile, A., and B. A. Flumerfelt. 1981. "Afferent Connections of the Interpeduncular Nucleus and the Topographic Organization of the Habenulo-Interpeduncular Pathway: An HRP Study in the Rat." *The Journal of Comparative Neurology* 196 (2): 253–70.

Contestabile, A., L. Villani, A. Fasolo, M. F. Franzoni, L. Gribaudo, O. Oktedalen,

and F. Fonnum. 1987. “Topography of Cholinergic and Substance P Pathways in the Habenulo-Interpeduncular System of the Rat. An Immunocytochemical and Microchemical Approach.” *Neuroscience* 21 (1): 253–70.

Corballis, Michael C. 2014. “Left Brain, Right Brain: Facts and Fantasies.” *PLoS Biology* 12 (1): e1001767.

Corcoran, Kevin A., and Gregory J. Quirk. 2007. “Recalling Safety: Cooperative Functions of the Ventromedial Prefrontal Cortex and the Hippocampus in Extinction.” *CNS Spectrums* 12 (3): 200–206.

Cull-Candy, S., S. Brickley, and M. Farrant. 2001. “NMDA Receptor Subunits: Diversity, Development and Disease.” *Current Opinion in Neurobiology* 11 (3): 327–35.

Cull-Candy, Stuart G., and Daniel N. Leszkiewicz. 2004. “Role of Distinct NMDA Receptor Subtypes at Central Synapses.” *Science's STKE : Signal Transduction Knowledge Environment* 2004 (255): re16.

Cull-Candy, Stuart, Leah Kelly, and Mark Farrant. 2006. “Regulation of Ca2+-Permeable AMPA Receptors: Synaptic Plasticity and Beyond.” *Current Opinion in Neurobiology* 16 (3): 288–97.

Dao, Dang Q., Erika E. Perez, Yanfen Teng, John A. Dani, and Mariella De Biasi. 2014. “Nicotine Enhances Excitability of Medial Habenular Neurons via Facilitation of Neurokinin Signaling.” *The Journal of Neuroscience : The Official Journal of the Society for Neuroscience* 34 (12): 4273–84.

Davies, C. H., and G. L. Collingridge. 1993. “The Physiological Regulation of Synaptic Inhibition by GABAB Autoreceptors in Rat Hippocampus.” *The Journal of Physiology* 472 (December): 245–65.

Davis, M., and P. J. Whalen. 2001. “The Amygdala: Vigilance and Emotion.” *Molecular Psychiatry* 6 (1): 13–34.

Dingledine, R., K. Borges, D. Bowie, and S. F. Traynelis. 1999. “The Glutamate Receptor Ion Channels.” *Pharmacological Reviews* 51 (1): 7–61.

Djebari, Souhail, Guillermo Iborra-Lázaro, Sara Temprano-Carazo, Irene Sánchez-Rodríguez, Mauricio O. Nava-Mesa, Alejandro Múnera, Agnès Gruart, José M. Delgado-García, Lydia Jiménez-Díaz, and Juan D. Navarro-López. 2021. “G-Protein-Gated Inwardly Rectifying Potassium (Kir3/GIRK)

Channels Govern Synaptic Plasticity That Supports Hippocampal-Dependent Cognitive Functions in Male Mice." *The Journal of Neuroscience : The Official Journal of the Society for Neuroscience* 41 (33): 7086–7102.

Dobrunz, L. E., and C. F. Stevens. 1997. "Heterogeneity of Release Probability, Facilitation, and Depletion at Central Synapses." *Neuron* 18 (6): 995–1008.

Dreosti, Elena, Nuria Vendrell Llopis, Matthias Carl, Emre Yaksi, and Stephen W. Wilson. 2014. "Left-Right Asymmetry Is Required for the Habenulae to Respond to Both Visual and Olfactory Stimuli." *Current Biology: CB* 24 (4): 440–45.

Duboué, Erik R., Elim Hong, Kiara C. Eldred, and Marnie E. Halpern. 2017. "Left Habenular Activity Attenuates Fear Responses in Larval Zebrafish." *Current Biology: CB* 27 (14): 2154-2162.e3.

Facchin, Lucilla, Harold A. Burgess, Mahmud Siddiqi, Michael Granato, and Marnie E. Halpern. 2009. "Determining the Function of Zebrafish Epithalamic Asymmetry." *Philosophical Transactions of the Royal Society of London. Series B, Biological Sciences* 364 (1519): 1021–32.

Fanselow, Michael S., and Andrew M. Poulos. 2005. "The Neuroscience of Mammalian Associative Learning." *Annual Review of Psychology* 56: 207–34.

Fore, Stephanie, Fabrizio Palumbo, Robbrecht Pelgrims, and Emre Yaksi. 2018. "Information Processing in the Vertebrate Habenula." *Seminars in Cell & Developmental Biology* 78 (June): 130–39.

Fowler, Christie D., and Paul J. Kenny. 2014. "Nicotine Aversion: Neurobiological Mechanisms and Relevance to Tobacco Dependence Vulnerability." *Neuropharmacology* 76 Pt B (0 0): 533–44.

Frahm, Silke, Beatriz Antolin-Fontes, Andreas Görlich, Johannes-Friedrich Zander, Gudrun Ahnert-Hilger, and Ines Ibañez-Tallon. 2015. "An Essential Role of Acetylcholine-Glutamate Synergy at Habenular Synapses in Nicotine Dependence." *ELife* 4 (December): e11396.

Gabriel, Christopher J., Zachary Zeidler, Benita Jin, Changliang Guo, Caitlin M. Goodpaster, Adrienne Q. Kashay, Anna Wu, et al. 2022. "BehaviorDEPOT Is a Simple, Flexible Tool for Automated Behavioral Detection Based on Markerless Pose Tracking." *ELife* 11 (August). https://doi.org/10.7554/eLife.74314.

Gassmann, Martin, and Bernhard Bettler. 2012. "Regulation of Neuronal GABA(B) Receptor Functions by Subunit Composition." *Nature Reviews. Neuroscience* 13 (6): 380–94.

Gazzaniga, M. S. 2000. "Cerebral Specialization and Interhemispheric Communication: Does the Corpus Callosum Enable the Human Condition?" *Brain : A Journal of Neurology* 123 (Pt 7) (July): 1293–1326.

Geisler, Stefanie, and Michael Trimble. 2008. "The Lateral Habenula: No Longer Neglected." *CNS Spectrums* 13 (6): 484–89.

Goto, Kazuhiro, and Isao Ito. 2017. "The Asymmetry Defect of Hippocampal Circuitry Impairs Working Memory in B2-Microglobulin Deficient Mice." *Neurobiology of Learning and Memory* 139 (March): 50–55.

Gugliemotti, V., and L. Fiorino. 1998. "Asymmetry in the Left and Right Habenulo-Interpeduncular Tracts in the Frog." *Brain Research Bulletin* 45 (1): 105–10.

Güntürkün, Onur, and Sebastian Ocklenburg. 2017. "Ontogenesis of Lateralization." *Neuron* 94 (2): 249–63.

Haller, Corinne, Emilio Casanova, Matthias Müller, Claire-Marie Vacher, Rejan Vigot, Thierry Doll, Samuel Barbieri, Martin Gassmann, and Bernhard Bettler. 2004. "Floxed Allele for Conditional Inactivation of the GABAB(1) Gene: GABAB(1)Conditional Allele in Mice." *Genesis (New York, N.Y.: 2000)* 40 (3): 125–30.

Hamada, Hiroshi, Chikara Meno, Daisuke Watanabe, and Yukio Saijoh. 2002. "Establishment of Vertebrate Left-Right Asymmetry." *Nature Reviews. Genetics* 3 (2): 103–13.

Han, Jeong Seok, and Volker Neugebauer. 2004. "Synaptic Plasticity in the Amygdala in a Visceral Pain Model in Rats." *Neuroscience Letters* 361 (1–3): 254–57.

Han, Sung, Matthew Soleiman, Marta Soden, Larry Zweifel, and Richard D. Palmiter. 2015. "Elucidating an Affective Pain Circuit That Creates a Threat Memory." *Cell* 162 (2): 363–74.

Han, Yunyun, Pascal S. Kaeser, Thomas C. Südhof, and Ralf Schneggenburger. 2011. "RIM Determines Ca^{2}+ Channel Density and Vesicle Docking at the Presynaptic Active Zone." *Neuron* 69 (2): 304–16.

Hashikawa, Yoshiko, Koichi Hashikawa, Mark A. Rossi, Marcus L. Basiri, Yuejia Liu, Nathan L. Johnston, Omar R. Ahmad, and Garret D. Stuber. 2020. "Transcriptional and Spatial Resolution of Cell Types in the Mammalian Habenula." *Neuron* 106 (5): 743-758.e5.

Herkenham, M., and W. J. Nauta. 1977. "Afferent Connections of the Habenular Nuclei in the Rat. A Horseradish Peroxidase Study, with a Note on the Fiber-of-Passage Problem." *The Journal of Comparative Neurology* 173 (1): 123–46.

Herry, Cyril, and Joshua P. Johansen. 2014. "Encoding of Fear Learning and Memory in Distributed Neuronal Circuits." *Nature Neuroscience* 17 (12): 1644–54.

Hikosaka, Okihide. 2010. "The Habenula: From Stress Evasion to Value-Based Decision-Making." *Nature Reviews. Neuroscience* 11 (7): 503–13.

Hnasko, Thomas S., and Robert H. Edwards. 2012. "Neurotransmitter Corelease: Mechanism and Physiological Role." *Annual Review of Physiology* 74: 225–43.

Hobin, Jennifer A., Ki A. Goosens, and Stephen Maren. 2003. "Context-Dependent Neuronal Activity in the Lateral Amygdala Represents Fear Memories after Extinction." *The Journal of Neuroscience : The Official Journal of the Society for Neuroscience* 23 (23): 8410–16.

Hollmann, M., M. Hartley, and S. Heinemann. 1991. "Ca2+ Permeability of KA-AMPA--Gated Glutamate Receptor Channels Depends on Subunit Composition." *Science (New York, N.Y.)* 252 (5007): 851–53.

Hong, Elim, Kirankumar Santhakumar, Courtney A. Akitake, Sang Jung Ahn, Christine Thisse, Bernard Thisse, Claire Wyart, Jean-Marie Mangin, and Marnie E. Halpern. 2013. "Cholinergic Left-Right Asymmetry in the Habenulo-Interpeduncular Pathway." *Proceedings of the National Academy of Sciences of the United States of America* 110 (52): 21171–76.

Hsu, Yun-Wei A., Lynne Tempest, Lely A. Quina, Aguan D. Wei, Hongkui Zeng, and Eric E. Turner. 2013. "Medial Habenula Output Circuit Mediated by A5 Nicotinic Receptor-Expressing GABAergic Neurons in the Interpeduncular Nucleus." *The Journal of Neuroscience: The Official Journal of the Society for Neuroscience* 33 (46): 18022–35.

Huganir, Richard L., and Roger A. Nicoll. 2013. "AMPARs and Synaptic Plasticity: The Last 25 Years." *Neuron* 80 (3): 704–17.

Hüsken, Ulrike, Heather L. Stickney, Gaia Gestri, Isaac H. Bianco, Ana Faro, Rodrigo M. Young, Myriam Roussigne, et al. 2014. "Tcf7l2 Is Required for Left-Right Asymmetric Differentiation of Habenular Neurons." *Current Biology: CB* 24 (19): 2217–27.

Ichijo, Hiroyuki, and Tomoko Toyama. 2015. "Axons from the Medial Habenular Nucleus Are Topographically Sorted in the Fasciculus Retroflexus." *Anatomical Science International* 90 (4): 229–34.

Isaac, John T. R., Michael C. Ashby, and Chris J. McBain. 2007. "The Role of the GluR2 Subunit in AMPA Receptor Function and Synaptic Plasticity." *Neuron* 54 (6): 859–71.

Jackman, Skyler L., and Wade G. Regehr. 2017. "The Mechanisms and Functions of Synaptic Facilitation." *Neuron* 94 (3): 447–64.

Ji, Guangchen, and Volker Neugebauer. 2009. "Hemispheric Lateralization of Pain Processing by Amygdala Neurons." *Journal of Neurophysiology* 102 (4): 2253–64.

Ji, Jinzhao, and Stephen Maren. 2007. "Hippocampal Involvement in Contextual Modulation of Fear Extinction." *Hippocampus* 17 (9): 749–58.

Johansen, Joshua P., Christopher K. Cain, Linnaea E. Ostroff, and Joseph E. LeDoux. 2011. "Molecular Mechanisms of Fear Learning and Memory." *Cell* 147 (3): 509–24.

Kaeser, Pascal S., Lunbin Deng, Yun Wang, Irina Dulubova, Xinran Liu, Josep Rizo, and Thomas C. Südhof. 2011. "RIM Proteins Tether Ca2+ Channels to Presynaptic Active Zones via a Direct PDZ-Domain Interaction." *Cell* 144 (2): 282–95.

Kaeser, Pascal S., and Wade G. Regehr. 2014. "Molecular Mechanisms for Synchronous, Asynchronous, and Spontaneous Neurotransmitter Release." *Annual Review of Physiology* 76: 333–63.

Kapp, B. S., R. C. Frysinger, M. Gallagher, and J. R. Haselton. 1979. "Amygdala Central Nucleus Lesions: Effect on Heart Rate Conditioning in the Rabbit." *Physiology & Behavior* 23 (6): 1109–17.

Katz, B., and R. Miledi. 1965. "THE MEASUREMENT OF SYNAPTIC DELAY, AND THE TIME COURSE OF ACETYLCHOLINE RELEASE AT THE NEUROMUSCULAR JUNCTION." *Proceedings of the Royal Society of*

London. Series B, Biological Sciences 161 (February): 483–95.

———. 1967a. "The Timing of Calcium Action during Neuromuscular Transmission." *The Journal of Physiology* 189 (3): 535–44.

———. 1967b. "Ionic Requirements of Synaptic Transmitter Release." *Nature* 215 (5101): 651.

Katz, Bernard. 1969. *The Release of Neural Transmitter Substances*.

Kaupmann, K., K. Huggel, J. Heid, P. J. Flor, S. Bischoff, S. J. Mickel, G. McMaster, et al. 1997. "Expression Cloning of GABA(B) Receptors Uncovers Similarity to Metabotropic Glutamate Receptors." *Nature* 386 (6622): 239–46.

Kawahara, Aiko, Shotaro Kurauchi, Yuko Fukata, José Martínez-Hernández, Terumi Yagihashi, Yuya Itadani, Rui Sho, et al. 2013. "Neuronal Major Histocompatibility Complex Class I Molecules Are Implicated in the Generation of Asymmetries in Hippocampal Circuitry." *The Journal of Physiology* 591 (19): 4777–91.

Kawakami, Ryosuke, Alice Dobi, Ryuichi Shigemoto, and Isao Ito. 2008. "Right Isomerism of the Brain in Inversus Viscerum Mutant Mice." *PloS One* 3 (4): e1945.

Kawakami, Ryosuke, Yoshiaki Shinohara, Yuichiro Kato, Hiroyuki Sugiyama, Ryuichi Shigemoto, and Isao Ito. 2003. "Asymmetrical Allocation of NMDA Receptor Epsilon2 Subunits in Hippocampal Circuitry." *Science* 300 (5621): 990–94.

Kennedy, M. B. 2000. "Signal-Processing Machines at the Postsynaptic Density." *Science (New York, N.Y.)* 290 (5492): 750–54.

Kim, Uhnoh, and Su-Youne Chang. 2005. "Dendritic Morphology, Local Circuitry, and Intrinsic Electrophysiology of Neurons in the Rat Medial and Lateral Habenular Nuclei of the Epithalamus." *The Journal of Comparative Neurology* 483 (2): 236–50.

Kohl, Michael M., Olivia A. Shipton, Robert M. Deacon, J. Nicholas P. Rawlins, Karl Deisseroth, and Ole Paulsen. 2011. "Hemisphere-Specific Optogenetic Stimulation Reveals Left-Right Asymmetry of Hippocampal Plasticity." *Nature Neuroscience* 14 (11): 1413–15.

Koppensteiner, Peter, Pradeep Bhandari, Cihan Önal, Carolina Borges-Merjane,

Elodie Le Monnier, Utsa Roy, Yukihiro Nakamura, et al. 2024. “GABAB Receptors Induce Phasic Release from Medial Habenula Terminals through Activity-Dependent Recruitment of Release-Ready Vesicles.” *Proceedings of the National Academy of Sciences of the United States of America* 121 (8): e2301449121.

Koppensteiner, Peter, Riccardo Melani, and Ipe Ninan. 2017. “A Cooperative Mechanism Involving Ca2+-Permeable AMPA Receptors and Retrograde Activation of GABAB Receptors in Interpeduncular Nucleus Plasticity.” *Cell Reports* 20 (5): 1111–22.

Krashes, Michael J., Shuichi Koda, Chianping Ye, Sarah C. Rogan, Andrew C. Adams, Daniel S. Cusher, Eleftheria Maratos-Flier, Bryan L. Roth, and Bradford B. Lowell. 2011. “Rapid, Reversible Activation of AgRP Neurons Drives Feeding Behavior in Mice.” *The Journal of Clinical Investigation* 121 (4): 1424–28.

Krnjević, K. 1974. “Chemical Nature of Synaptic Transmission in Vertebrates.” *Physiological Reviews*, April. https://doi.org/10.1152/physrev.1974.54.2.418.

Kulik, Akos, Kazuhiko Nakadate, Gábor Nyíri, Takuya Notomi, Barbara Malitschek, Bernhard Bettler, and Ryuichi Shigemoto. 2002. “Distinct Localization of GABA(B) Receptors Relative to Synaptic Sites in the Rat Cerebellum and Ventrobasal Thalamus.” *The European Journal of Neuroscience* 15 (2): 291–307.

Kullmann, D. M. 2000. “Spillover and Synaptic Cross Talk Mediated by Glutamate and GABA in the Mammalian Brain.” *Progress in Brain Research* 125: 339–51.

Kusick, Grant F., Morven Chin, Sumana Raychaudhuri, Kristina Lippmann, Kadidia P. Adula, Edward J. Hujber, Thien Vu, M. Wayne Davis, Erik M. Jorgensen, and Shigeki Watanabe. 2020. “Synaptic Vesicles Transiently Dock to Refill Release Sites.” *Nature Neuroscience* 23 (11): 1329–38.

Lammel, Stephan, Byung Kook Lim, Chen Ran, Kee Wui Huang, Michael J. Betley, Kay M. Tye, Karl Deisseroth, and Robert C. Malenka. 2012. “Input-Specific Control of Reward and Aversion in the Ventral Tegmental Area.” *Nature* 491 (7423): 212–17.

Lawson, Rebecca P., Ben Seymour, Eleanor Loh, Antoine Lutti, Raymond J. Dolan, Peter Dayan, Nikolaus Weiskopf, and Jonathan P. Roiser. 2014. “The Habenula Encodes Negative Motivational Value Associated with Primary Punishment in Humans.” *Proceedings of the National Academy of Sciences of*

the United States of America 111 (32): 11858–63.

LeDoux, J. E. 2000. "Emotion Circuits in the Brain." *Annual Review of Neuroscience* 23: 155–84.

Lee, E. H., and S. L. Huang. 1988. "Role of Lateral Habenula in the Regulation of Exploratory Behavior and Its Relationship to Stress in Rats." *Behavioural Brain Research* 30 (3): 265–71.

Lee, Hyun Woo, Soo Hyun Yang, Jin Yong Kim, and Hyun Kim. 2019. "The Role of the Medial Habenula Cholinergic System in Addiction and Emotion-Associated Behaviors." *Frontiers in Psychiatry / Frontiers Research Foundation* 10 (FEB): 100.

Levin, Michael. 2005. "Left-Right Asymmetry in Embryonic Development: A Comprehensive Review." *Mechanisms of Development* 122 (1): 3–25.

Lima, Leandro B., Debora Bueno, Fernanda Leite, Stefani Souza, Luciano Gonçalves, Isadora C. Furigo, Jose Donato Jr, and Martin Metzger. 2017. "Afferent and Efferent Connections of the Interpeduncular Nucleus with Special Reference to Circuits Involving the Habenula and Raphe Nuclei." *The Journal of Comparative Neurology* 525 (10): 2411–42.

Liu, Siqiong June, and R. Suzanne Zukin. 2007. "Ca2+-Permeable AMPA Receptors in Synaptic Plasticity and Neuronal Death." *Trends in Neurosciences* 30 (3): 126–34.

Luo, Fujun, and Thomas C. Südhof. 2017. "Synaptotagmin-7-Mediated Asynchronous Release Boosts High-Fidelity Synchronous Transmission at a Central Synapse." *Neuron* 94 (4): 826-839.e3.

Lüscher, Christian, and Paul A. Slesinger. 2010. "Emerging Roles for G Protein-Gated Inwardly Rectifying Potassium (GIRK) Channels in Health and Disease." *Nature Reviews. Neuroscience* 11 (5): 301–15.

Malenka, Robert C., and Mark F. Bear. 2004. "LTP and LTD: An Embarrassment of Riches." *Neuron* 44 (1): 5–21.

Malinow, Roberto, and Robert C. Malenka. 2002. "AMPA Receptor Trafficking and Synaptic Plasticity." *Annual Review of Neuroscience* 25 (March): 103–26.

Maren, S. 2001. "Neurobiology of Pavlovian Fear Conditioning." *Annual Review of Neuroscience* 24: 897–931.

Maren, Stephen, K. Luan Phan, and Israel Liberzon. 2013. “The Contextual Brain: Implications for Fear Conditioning, Extinction and Psychopathology.” *Nature Reviews. Neuroscience* 14 (6): 417–28.

Maren, Stephen, and Gregory J. Quirk. 2004. “Neuronal Signalling of Fear Memory.” *Nature Reviews. Neuroscience* 5 (11): 844–52.

Mathis, Alexander, Pranav Mamidanna, Kevin M. Cury, Taiga Abe, Venkatesh N. Murthy, Mackenzie Weygandt Mathis, and Matthias Bethge. 2018. “DeepLabCut: Markerless Pose Estimation of User-Defined Body Parts with Deep Learning.” *Nature Neuroscience* 21 (9): 1281–89.

Matsumoto, Masayuki, and Okihide Hikosaka. 2007. “Lateral Habenula as a Source of Negative Reward Signals in Dopamine Neurons.” *Nature* 447 (7148): 1111–15.

McLaughlin, Ian, John A. Dani, and Mariella De Biasi. 2017. “The Medial Habenula and Interpeduncular Nucleus Circuitry Is Critical in Addiction, Anxiety, and Mood Regulation.” *Journal of Neurochemistry* 142 Suppl 2 (Suppl 2): 130–43.

Meye, Frank J., Mariano Soiza-Reilly, Tamar Smit, Marco A. Diana, Martin K. Schwarz, and Manuel Mameli. 2016. “Shifted Pallidal Co-Release of GABA and Glutamate in Habenula Drives Cocaine Withdrawal and Relapse.” *Nature Neuroscience* 19 (8): 1019–24.

Miyazawa, Yuta, Yukari Takahashi, Ayako M. Watabe, and Fusao Kato. 2018. “Predominant Synaptic Potentiation and Activation in the Right Central Amygdala Are Independent of Bilateral Parabrachial Activation in the Hemilateral Trigeminal Inflammatory Pain Model of Rats.” *Molecular Pain* 14 (January): 1744806918807102.

Morley, B. J. 1986. “The Interpeduncular Nucleus.” *International Review of Neurobiology* 28: 157–82.

Murphy, C. A., A. M. DiCamillo, F. Haun, and M. Murray. 1996. “Lesion of the Habenular Efferent Pathway Produces Anxiety and Locomotor Hyperactivity in Rats: A Comparison of the Effects of Neonatal and Adult Lesions.” *Behavioural Brain Research* 81 (1–2): 43–52.

Myers, K. M., and M. Davis. 2007. “Mechanisms of Fear Extinction.” *Molecular Psychiatry* 12 (2): 120–50.

Namboodiri, Vijay Mohan K., Jose Rodriguez-Romaguera, and Garret D. Stuber. 2016. "The Habenula." *Current Biology: CB* 26 (19): R873–77.

Nath, Tanmay, Alexander Mathis, An Chi Chen, Amir Patel, Matthias Bethge, and Mackenzie Weygandt Mathis. 2019. "Using DeepLabCut for 3D Markerless Pose Estimation across Species and Behaviors." *Nature Protocols* 14 (7): 2152–76.

Neher, Erwin, and Takeshi Sakaba. 2008. "Multiple Roles of Calcium Ions in the Regulation of Neurotransmitter Release." *Neuron* 59 (6): 861–72.

Neugebauer, Volker, and Weidong Li. 2003. "Differential Sensitization of Amygdala Neurons to Afferent Inputs in a Model of Arthritic Pain." *Journal of Neurophysiology* 89 (2): 716–27.

Neugebauer, Volker, Weidong Li, Gary C. Bird, and Jeong S. Han. 2004. "The Amygdala and Persistent Pain." *The Neuroscientist: A Review Journal Bringing Neurobiology, Neurology and Psychiatry* 10 (3): 221–34.

Newpher, Thomas M., and Michael D. Ehlers. 2008. "Glutamate Receptor Dynamics in Dendritic Microdomains." *Neuron* 58 (4): 472–97.

Nishikawa, T., D. Fage, and B. Scatton. 1986. "Evidence for, and Nature of, the Tonic Inhibitory Influence of Habenulointerpeduncular Pathways upon Cerebral Dopaminergic Transmission in the Rat." *Brain Research* 373 (1–2): 324–36.

Nonaka, Shigenori, Hidetaka Shiratori, Yukio Saijoh, and Hiroshi Hamada. 2002. "Determination of Left-Right Patterning of the Mouse Embryo by Artificial Nodal Flow." *Nature* 418 (6893): 96–99.

Ocklenburg, Sebastian, Julian Packheiser, Judith Schmitz, Noemi Rook, Onur Güntürkün, Jutta Peterburs, and Gina M. Grimshaw. 2018. "Hugs and Kisses - The Role of Motor Preferences and Emotional Lateralization for Hemispheric Asymmetries in Human Social Touch." *Neuroscience and Biobehavioral Reviews* 95 (December): 353–60.

Okada, Y., S. Nonaka, Y. Tanaka, Y. Saijoh, H. Hamada, and N. Hirokawa. 1999. "Abnormal Nodal Flow Precedes Situs Inversus in Iv and Inv Mice." *Molecular Cell* 4 (4): 459–68.

Okamoto, Hitoshi, Masakazu Agetsuma, and Hidenori Aizawa. 2012. "Genetic Dissection of the Zebrafish Habenula, a Possible Switching Board for

Selection of Behavioral Strategy to Cope with Fear and Anxiety." *Developmental Neurobiology* 72 (3): 386–94.

Okamoto, Hitoshi, and Hidenori Aizawa. 2013. "Fear and Anxiety Regulation by Conserved Affective Circuits." *Neuron*. Cell Press.

Okamoto, Hitoshi, Bor-Wei Cherng, Haruna Nakajo, Ming-Yi Chou, and Masae Kinoshita. 2021. "Habenula as the Experience-Dependent Controlling Switchboard of Behavior and Attention in Social Conflict and Learning." *Current Opinion in Neurobiology* 68 (June): 36–43.

Paoletti, Pierre, Camilla Bellone, and Qiang Zhou. 2013. "NMDA Receptor Subunit Diversity: Impact on Receptor Properties, Synaptic Plasticity and Disease." *Nature Reviews. Neuroscience* 14 (6): 383–400.

Pape, Hans-Christian, and Denis Pare. 2010. "Plastic Synaptic Networks of the Amygdala for the Acquisition, Expression, and Extinction of Conditioned Fear." *Physiological Reviews* 90 (2): 419–63.

Parajuli, Laxmi Kumar, Chikako Nakajima, Akos Kulik, Ko Matsui, Toni Schneider, Ryuichi Shigemoto, and Yugo Fukazawa. 2012. "Quantitative Regional and Ultrastructural Localization of the Ca(v)2.3 Subunit of R-Type Calcium Channel in Mouse Brain." *The Journal of Neuroscience: The Official Journal of the Society for Neuroscience* 32 (39): 13555–67.

Paxinos, George, and Keith B. J. Franklin. 2019. *Paxinos and Franklin's the Mouse Brain in Stereotaxic Coordinates*. Academic Press.

Pin, Jean-Philippe, and Bernhard Bettler. 2016. "Organization and Functions of MGlu and GABA Receptor Complexes." *Nature* 540 (7631): 60–68.

Pinard, Audrée, Riad Seddik, and Bernhard Bettler. 2010. "GABAB Receptors: Physiological Functions and Mechanisms of Diversity." *Advances in Pharmacology (San Diego, Calif.)* 58: 231–55.

Pinheiro, Paulo S., and Christophe Mulle. 2008. "Presynaptic Glutamate Receptors: Physiological Functions and Mechanisms of Action." *Nature Reviews. Neuroscience* 9 (6): 423–36.

Pitman, Roger K., Ann M. Rasmusson, Karestan C. Koenen, Lisa M. Shin, Scott P. Orr, Mark W. Gilbertson, Mohammed R. Milad, and Israel Liberzon. 2012. "Biological Studies of Post-Traumatic Stress Disorder." *Nature Reviews. Neuroscience* 13 (11): 769–87.

Plant, Karen, Kenneth A. Pelkey, Zuner A. Bortolotto, Daiju Morita, Akira Terashima, Chris J. McBain, Graham L. Collingridge, and John T. R. Isaac. 2006. "Transient Incorporation of Native GluR2-Lacking AMPA Receptors during Hippocampal Long-Term Potentiation." *Nature Neuroscience* 9 (5): 602–4.

Qin, C., and M. Luo. 2009. "Neurochemical Phenotypes of the Afferent and Efferent Projections of the Mouse Medial Habenula." *Neuroscience* 161 (3): 827–37.

Quirk, Gregory J., and Devin Mueller. 2008. "Neural Mechanisms of Extinction Learning and Retrieval." *Neuropsychopharmacology : Official Publication of the American College of Neuropsychopharmacology* 33 (1): 56–72.

Rajalu, Mathieu, Thorsten Fritzius, Lisa Adelfinger, Valerie Jacquier, Valerie Besseyrias, Martin Gassmann, and Bernhard Bettler. 2015. "Pharmacological Characterization of GABAB Receptor Subtypes Assembled with Auxiliary KCTD Subunits." *Neuropharmacology* 88 (January): 145–54.

Regan, Jennifer C., Miguel L. Concha, Myriam Roussigne, Claire Russell, and Stephen W. Wilson. 2009. "An Fgf8-Dependent Bistable Cell Migratory Event Establishes CNS Asymmetry." *Neuron* 61 (1): 27–34.

Regehr, Wade G. 2012. "Short-Term Presynaptic Plasticity." *Cold Spring Harbor Perspectives in Biology* 4 (7): a005702.

Ren, Jing, Chang Qin, Fei Hu, Jie Tan, Li Qiu, Shengli Zhao, Guoping Feng, and Minmin Luo. 2011. "Habenula 'Cholinergic' Neurons Co-Release Glutamate and Acetylcholine and Activate Postsynaptic Neurons via Distinct Transmission Modes." *Neuron* 69 (3): 445–52.

Ren, Yuqi, Yang Liu, Sanduo Zheng, and Minmin Luo. 2022. "KCTD8 and KCTD12 Facilitate Axonal Expression of GABAB Receptors in Habenula Cholinergic Neurons." *The Journal of Neuroscience: The Official Journal of the Society for Neuroscience* 42 (9): 1648–65.

Ressler, Kerry J., and Helen S. Mayberg. 2007. "Targeting Abnormal Neural Circuits in Mood and Anxiety Disorders: From the Laboratory to the Clinic." *Nature Neuroscience* 10 (9): 1116–24.

Rizo, Josep, and Christian Rosenmund. 2008. "Synaptic Vesicle Fusion." *Nature Structural & Molecular Biology* 15 (7): 665–74.

Robins, Andrew, and Lesley J. Rogers. 2002. “Limb Preference and Skeletal Asymmetry in the Cane Toad, Bufo Marinus (Anura: Bufonidae).” *Laterality* 7 (3): 261–75.

Rudy, J. W., N. C. Huff, and P. Matus-Amat. 2004. “Understanding Contextual Fear Conditioning: Insights from a Two-Process Model.” *Neuroscience and Biobehavioral Reviews* 28 (7): 675–85.

Sadler, Katelyn E., Neal A. McQuaid, Abigail C. Cox, Marissa N. Behun, Allison M. Trouten, and Benedict J. Kolber. 2017. “Divergent Functions of the Left and Right Central Amygdala in Visceral Nociception.” *Pain* 158 (4): 747–59.

Salas, Ramiro, Renea Sturm, Jim Boulter, and Mariella De Biasi. 2009. “Nicotinic Receptors in the Habenulo-Interpeduncular System Are Necessary for Nicotine Withdrawal in Mice.” *The Journal of Neuroscience : The Official Journal of the Society for Neuroscience* 29 (10): 3014–18.

Salin, P. A., M. Scanziani, R. C. Malenka, and R. A. Nicoll. 1996. “Distinct Short-Term Plasticity at Two Excitatory Synapses in the Hippocampus.” *Proceedings of the National Academy of Sciences of the United States of America* 93 (23): 13304–9.

Sanderson, Jennifer L., Jessica A. Gorski, and Mark L. Dell’Acqua. 2016. “NMDA Receptor-Dependent LTD Requires Transient Synaptic Incorporation of Ca^{2+}-Permeable AMPARs Mediated by AKAP150-Anchored PKA and Calcineurin.” *Neuron* 89 (5): 1000–1015.

Schneggenburger, R., A. C. Meyer, and E. Neher. 1999. “Released Fraction and Total Size of a Pool of Immediately Available Transmitter Quanta at a Calyx Synapse.” *Neuron* 23 (2): 399–409.

Schoch, Susanne, Pablo E. Castillo, Tobias Jo, Konark Mukherjee, Martin Geppert, Yun Wang, Frank Schmitz, Robert C. Malenka, and Thomas C. Südhof. 2002. “RIM1alpha Forms a Protein Scaffold for Regulating Neurotransmitter Release at the Active Zone.” *Nature* 415 (6869): 321–26.

Schulz, P. E., E. P. Cook, and D. Johnston. 1994. “Changes in Paired-Pulse Facilitation Suggest Presynaptic Involvement in Long-Term Potentiation.” *The Journal of Neuroscience : The Official Journal of the Society for Neuroscience* 14 (9): 5325–37.

Shaye, Hamidreza, Andrii Ishchenko, Jordy Homing Lam, Gye Won Han, Li Xue, Philippe Rondard, Jean-Philippe Pin, Vsevolod Katritch, Cornelius Gati,

and Vadim Cherezov. 2020. “Structural Basis of the Activation of a Metabotropic GABA Receptor.” *Nature* 584 (7820): 298–303.

Shepherd, Jason D., and Richard L. Huganir. 2007. “The Cell Biology of Synaptic Plasticity: AMPA Receptor Trafficking.” *Annual Review of Cell and Developmental Biology* 23: 613–43.

Shibata, H., T. Suzuki, and M. Matsushita. 1986. “Afferent Projections to the Interpeduncular Nucleus in the Rat, as Studied by Retrograde and Anterograde Transport of Wheat Germ Agglutinin Conjugated to Horseradish Peroxidase.” *The Journal of Comparative Neurology* 248 (2): 272–84.

Shin, Lisa M., Scott L. Rauch, and Roger K. Pitman. 2006. “Amygdala, Medial Prefrontal Cortex, and Hippocampal Function in PTSD.” *Annals of the New York Academy of Sciences* 1071 (July): 67–79.

Shinohara, Yoshiaki, Hajime Hirase, Masahiko Watanabe, Makoto Itakura, Masami Takahashi, and Ryuichi Shigemoto. 2008. “Left-Right Asymmetry of the Hippocampal Synapses with Differential Subunit Allocation of Glutamate Receptors.” *Proceedings of the National Academy of Sciences of the United States of America* 105 (49): 19498–503.

Shinohara, Yoshiaki, Aki Hosoya, and Hajime Hirase. 2013. “Experience Enhances Gamma Oscillations and Interhemispheric Asymmetry in the Hippocampus.” *Nature Communications* 4 (1): 1652.

Shipton, Olivia A., Mohamady El-Gaby, John Apergis-Schoute, Karl Deisseroth, David M. Bannerman, Ole Paulsen, and Michael M. Kohl. 2014. “Left-Right Dissociation of Hippocampal Memory Processes in Mice.” *Proceedings of the National Academy of Sciences of the United States of America* 111 (42): 15238–43.

Sierra-Mercado, Demetrio, Jr, Kevin A. Corcoran, Kelimer Lebrón-Milad, and Gregory J. Quirk. 2006. “Inactivation of the Ventromedial Prefrontal Cortex Reduces Expression of Conditioned Fear and Impairs Subsequent Recall of Extinction.” *The European Journal of Neuroscience* 24 (6): 1751–58.

Song, Da, Deheng Wang, Qinghu Yang, Tianyi Yan, Zhe Wang, Yan Yan, Juan Zhao, et al. 2020. “The Lateralization of Left Hippocampal CA3 during the Retrieval of Spatial Working Memory.” *Nature Communications* 11 (1): 2901.

Soria-Gómez, Edgar, Arnau Busquets-Garcia, Fei Hu, Amine Mehidi, Astrid Cannich, Liza Roux, Ines Louit, et al. 2015. “Habenular CB1 Receptors

Control the Expression of Aversive Memories." *Neuron* 88 (2): 306–13.

Südhof, Thomas C., and Robert C. Malenka. 2008. "Understanding Synapses: Past, Present, and Future." *Neuron* 60 (3): 469–76.

Südhof, Thomas C., and Josep Rizo. 2011. "Synaptic Vesicle Exocytosis." *Cold Spring Harbor Perspectives in Biology* 3 (12). https://doi.org/10.1101/cshperspect.a005637.

Supp, D. M., M. Brueckner, M. R. Kuehn, D. P. Witte, L. A. Lowe, J. McGrath, J. Corrales, and S. S. Potter. 1999. "Targeted Deletion of the ATP Binding Domain of Left-Right Dynein Confirms Its Role in Specifying Development of Left-Right Asymmetries." *Development (Cambridge, England)* 126 (23): 5495–5504.

Sutherland, R. J. 1982. "The Dorsal Diencephalic Conduction System: A Review of the Anatomy and Functions of the Habenular Complex." *Neuroscience and Biobehavioral Reviews* 6 (1): 1–13.

Swanson, L. W., and W. M. Cowan. 1979. "The Connections of the Septal Region in the Rat." *The Journal of Comparative Neurology* 186 (4): 621–55.

Tabata, Toshihide, and Masanobu Kano. 2006. "GABA(B) Receptor-Mediated Modulation of Glutamate Signaling in Cerebellar Purkinje Cells." *Cerebellum (London, England)* 5 (2): 127–33.

Thanawala, Monica S., and Wade G. Regehr. 2013. "Presynaptic Calcium Influx Controls Neurotransmitter Release in Part by Regulating the Effective Size of the Readily Releasable Pool." *The Journal of Neuroscience : The Official Journal of the Society for Neuroscience* 33 (11): 4625–33.

Tong, Rudi, Nigel J. Emptage, and Zahid Padamsey. 2020. "A Two-Compartment Model of Synaptic Computation and Plasticity." *Molecular Brain* 13 (1): 79.

Tovote, Philip, Jonathan Paul Fadok, and Andreas Lüthi. 2015. "Neuronal Circuits for Fear and Anxiety." *Nature Reviews. Neuroscience* 16 (6): 317–31.

Ukai, Hikari, Aiko Kawahara, Keiko Hirayama, Matthew Julian Case, Shotaro Aino, Masahiro Miyabe, Ken Wakita, et al. 2017. "PirB Regulates Asymmetries in Hippocampal Circuitry." *PloS One* 12 (6): e0179377.

Vallortigara, Giorgio, and Lesley J. Rogers. 2005. "Survival with an Asymmetrical Brain: Advantages and Disadvantages of Cerebral Lateralization." *The Behavioral and Brain Sciences* 28 (4): 575–89; discussion 589-633.

Viswanath, Humsini, Asasia Q. Carter, Philip R. Baldwin, David L. Molfese, and Ramiro Salas. 2013. "The Medial Habenula: Still Neglected." *Frontiers in Human Neuroscience* 7 (JAN): 931.

Vyleta, Nicholas P., Carolina Borges-Merjane, and Peter Jonas. 2016. "Plasticity-Dependent, Full Detonation at Hippocampal Mossy Fiber-CA3 Pyramidal Neuron Synapses." *ELife* 5 (October). https://doi.org/10.7554/eLife.17977.

Wotjak, Carsten T. 2019. "Sound Check, Stage Design and Screen Plot - How to Increase the Comparability of Fear Conditioning and Fear Extinction Experiments." *Psychopharmacology* 236 (1): 33–48.

Xu, Chunpeng, Yanfei Sun, Xuewei Cai, Tingting You, Hongzhe Zhao, Yang Li, and Hua Zhao. 2018. "Medial Habenula-Interpeduncular Nucleus Circuit Contributes to Anhedonia-Like Behavior in a Rat Model of Depression." *Frontiers in Behavioral Neuroscience* 12 (October): 238.

Xu, Jun, Tomoyuki Mashimo, and Thomas C. Südhof. 2007. "Synaptotagmin-1, -2, and -9: Ca(2+) Sensors for Fast Release That Specify Distinct Presynaptic Properties in Subsets of Neurons." *Neuron* 54 (4): 567–81.

Yamaguchi, Takashi, Teruko Danjo, Ira Pastan, Takatoshi Hikida, and Shigetada Nakanishi. 2013. "Distinct Roles of Segregated Transmission of the Septo-Habenular Pathway in Anxiety and Fear." *Neuron* 78 (3): 537–44.

Zhang, Guang-Wei, Li Shen, Wen Zhong, Ying Xiong, Li I. Zhang, and Huizhong W. Tao. 2018. "Transforming Sensory Cues into Aversive Emotion via Septal-Habenular Pathway." *Neuron* 99 (5): 1016-1028.e5.

Zhang, Juen, Lubin Tan, Yuqi Ren, Jingwen Liang, Rui Lin, Qiru Feng, Jingfeng Zhou, et al. 2016. "Presynaptic Excitation via GABAB Receptors in Habenula Cholinergic Neurons Regulates Fear Memory Expression." *Cell* 166 (3): 716–28.

Zucker, Robert S., and Wade G. Regehr. 2002. "Short-Term Synaptic Plasticity." *Annual Review of Physiology* 64: 355–405.